Sina Maria Lystvet

Emergent properties of protein-gold nanoconstructs for biomedical applications

Thesis for the degree of Philosophiae Doctor

Trondheim, March 2013

Norwegian University of Science and Technology
Faculty of Natural Sciences and Technology
Department of Chemical Engineering

NTNU – Trondheim
Norwegian University of
Science and Technology

NTNU
Norwegian University of Science and Technology

Thesis for the degree of Philosophiae Doctor

Faculty of Natural Sciences and Technology
Department of Chemical Engineering

© Sina Maria Lystvet

ISBN 978-82-471-4247-9 (printed version)
ISBN 978-82-471-4248-6 (electronic version)
ISSN 1503-8181

Doctoral theses at NTNU, 2013:75

Printed by Skipnes Kommunikasjon as

Preface

This thesis is submitted in partial fulfillment of the requirements for the degree of Philosophiae Doctor (Ph.D.) at the Norwegian University of Science and Technology (NTNU) and consists of five papers. The work presented here was mainly carried out at the Ugelstad laboratory at the Department of Chemical Engineering, between March 2009 and March 2013, and was financed by research and development funds from NTNU. My main supervisor has been Associate Professor Wilhelm Robert Glomm, and my co-supervisors were Ph.D. Sondre Volden and Associate Professor Øyvind Halskau Jr.

I completed my Master of Science degree at NTNU in December 2008, and was accepted as a graduate student at the Ugelstad laboratory, department of chemical engineering, in March 2009. My main project during the Ph.D. period has been to make bionanomaterials from proteins and gold nanoconstructs (such as gold nanoparticles and gold nanoclusters), and then study their spectroscopic properties and interfacial activities. The aim was to make bionanomaterials which can be used within medical research.

This thesis begins with a chapter about the motivation behind the project. Following a short theoretical background regarding proteins, gold, and their uses in medicine, comes a chapter about the different experimental techniques employed in the work presented here. The theoretical introduction is followed by a results and discussion chapter, that presents the five appended papers. The thesis ends with concluding remarks and future perspectives.

Acknowledgements

Completing a Ph.D. is a lot of hard work and I sincerely believe that no one is able to get this far without the help and support from others. There are many that deserve a big thank you, and one of them is Ph.D. Anders Riise Moen. If he had not told me about this project back in December 2008 and encouraged me to talk to Wilhelm, I would probably never have known about this opportunity, and I might not have started my Ph.D. studies at all. Thank you Wilhelm for easily convincing a fed up Master student, who recently had sworn to never start a Ph.D. project, that this was a cool project that I just had to join. And most of all I thank you for actually making the project awesome and for your great motivational skills. Sondre has been my "go to man" whenever I had a losing fight with the instrumentation in the lab, or any other problem for that matter. With their professional input and discussions, and by being the positive and encouraging people that they are, Wilhelm, Sondre and Øyvind have been great supervisors during these last four years.

Thank you, Professor Johan Sjöblom for including me in all the social events at the Ugelstad laboratory, and for providing us with a well-equipped laboratory. A big thank you goes out to all my former and present colleagues at the Ugelstad laboratory for nice talks in both science and for fun.

I also owe a great thank you to my friends and family, especially my parents, for always having faith in me. The only thing my parents ever required from me was to always do my best, and I think that got me pretty far.

The one that deserve the biggest thank you of all is Thor. Thank you for all your support in all ways possible, and for understanding that a grumpy Sina can most of the time be made happy again with some nice food, a bit of rest, and a big hug. You are the best.

Abstract

Bionanomaterials are exciting materials with applications both in diagnostics and treatment of a broad spectrum of diseases. Binding to colloidal structures, such as gold nanoparticles (AuNPs), is known to affect protein conformation. Such alterations in conformation can potentially alter the function and bio-invasiveness of the biopolymer. This implies that a better understanding of the structure/function relationship of proteins can be achieved by deliberately altering protein conformation by modifying them with gold nanoparticles. The acquired protein-gold nanoconstructs may then achieve protein-like properties, gold-like properties, a bit of both, or even brand new properties. A better understanding of the relationship between structure and function for proteins is important because several diseases, such as Alzheimer's disease, sickle cell anemia, and some types of cancers, are due to errors in protein folding. Lately, the interest for fluorescent protein-stabilized gold nanoclusters (AuNCs) has increased. AuNCs introduce fluorescent probes simultaneously as protein conformation can be altered. Gold nanoconstructs (AuNPs, AuNCs, or mixtures of the two) present the ability to stabilize and study protein folding intermediates that would otherwise be too unstable to study.

In this thesis, several proteins modified by gold-nanoconstructs, such as AuNPs and AuNCs, have been studied. The aim has been to investigate whether it is possible to combine proteins and gold to make new materials with properties not present in either constituent alone. In this thesis such properties are often referred to as "emergent properties". Of the proteins studied, alpha-lactalbumin (aLa) has been the main focus, because of its link to Human Alpha-lactalbumin Made LEthal to Tumor cells (HAMLET), and its bovine analogue BAMLET. Both of which are promising candidates as anti cancer therapeutic agents.

A palette of optical techniques such as UV-vis and fluorescence spectroscopy, ζ-potential measurements, dynamic light scattering, and circular dichroism were used to characterize gold nanoconstructs, protein-gold nanoconstructs and concomitant changes in protein conformation. Additionally, the size of gold nanoconstructs were studied with scanning transmission electron microscopy. Langmuir- and Gibbs monolayers studies,

Brewster Angle Microscopy, Digital Video Imaging and Atomic Force Microscopy were used to observe changes in interfacial activity as well as ability to induce film miscibility for the new constructs. Trypan blue assays were used to study the protein-gold nanoconstructs' ability to induce cell death in cancer cell samples.

The results showed that protein-AuNPs possess membrane affinity properties not seen for any single constituents alone. Bionanomaterials with protein-stabilized AuNCs or AuNPs provide for an inherent optical marker that can be used for imaging and diagnostics. These bionanomaterials also provided a tunability in protein structure, which can be used to understand more about the protein structure/function relationship. Depending on the synthesis-protocol used for the formation of protein-gold nanoconstructs, it was possible to make small (~8 Au atoms, Au_8) and large (~25 Au atoms, Au_{25}) protein-stabilized AuNCs, AuNPs stabilized by covalently bound protein-AuNCs, and even to manipulate hydrophobic and hydrophilic properties of the resulting protein-gold nanoconstructs. Langmuir studies of hydrophilic aLa-gold nanoconstructs showed that the protein-gold nanoconstruct induced increased lipid interaction as compared to native aLa. For this reason, cell-viability studies of native bovine aLa, hydrophilic bovine aLa-gold nanoconstructs and BAMLET were compared. The results were very promising as the hydrophilic aLa-gold nanoconstructs showed an ability to kill cancer cells close to the efficiency of BAMLET.

List of publications

Paper I

Sina M. Lystvet, Sondre Volden, Masahiro Yasuda, Øyvind Halskau, and Wilhelm R. Glomm

Emergent membrane-affecting properties of BSA-gold nanoparticle constructs

Nanoscale, **2011**, 3, (4), p. 1788-1797

Paper II

Sina M. Lystvet, Sondre Volden, Øyvind Halskau, and Wilhelm R. Glomm

Immobilization onto gold nanoparticles alters α-lactalbumin interaction with pure and mixed phospholipid monolayers

Soft Matter, **2011**, 7, (24), p. 11501-11509

Paper III

Sina M. Lystvet, Sondre Volden, Gurvinder Singh, Masahiro Yasuda, Øyvind Halskau, and Wilhelm R. Glomm

Tunable photophysical properties, conformation and function of nanosized protein-gold constructs

RSC Advances, **2013**, 3, (2), p. 482-495

Paper IV

Sondre Volden, Sina M. Lystvet, Øyvind Halskau, and Wilhelm R. Glomm

Generally applicable procedure for *in situ* formation of fluorescent protein-gold nanoconstructs

RSC Advances, **2012**, 2, (31), p. 11704 - 11711

Paper V
Sina M. Lystvet, Sondre Volden, Gurvinder Singh, Ida Marie Rundgren, Hanzhen Wen, Øyvind Halskau, and Wilhelm R. Glomm
Anticancer activity from gold-alpha-lactalbumin nanoconstructs?
The Journal of Physical Chemistry C, **2013**, 117, (5), p. 2230-2238

Additional publications

Staining an cytotoxicity of transferrin-gold nanoconstructs on brain cancer cells
Sondre Volden, Birgitte H. McDonagh, Sina M. Lystvet, Gurvinder Singh, Marit-Helen G. Ese, Mikael Lindgren, Ionna Sandvig, Axel Sandvig, and Wilhelm R. Glomm
Manuscript in preparation

Polymer nanoparticles for protein extraction
Masahiro Yasuda, Sina M. Lystvet, Sondre Volden, and Wilhelm R. Glomm
Manuscript in preparation

Invited talks

Presentation at NKS (Norwegian Chemical Society) Trondheim
Name of presentation: Proteiner + gull = nanomedisin?
(Eng.: Proteins + gold = nanomedicine) (45 minutes)
Date: October 23rd 2012.
Location: NTNU, Gløshaugen.

Presentation at the Department of Biophysics, NTNU
Name of presentation: Old proteins - new tricks (30 minutes)
Date: September 18th 2012.
Location: NTNU, Gløshaugen.

Presentation at the autumn seminar for NBS (Norwegian Biochemical Society)
Name of presentation: Old proteins - new tricks (15 minutes)
Date: November 24th 2011
Location: NTNU, Gløshaugen.

Posters and conference contributions

Poster at The French-Norwegian Interdisciplinary Symposium on Nano and Micro Frontiers in Biology and Medicine
Name of presentation: Interactions between BSA-gold nanoparticle constructs and a phospholipid monolayer
Authors: Sina M. Lystvet, Sondre Volden, Øyvind Halskau, and Wilhelm R. Glomm
Date: August 31st - September 2nd 2009
Location: Department of Biomedicine, UiB, Bergen

Popular science communication

TV performance
Program: Schrödingers katt (Eng.: Schrödingers cat) (NRK1)
Name of presentation: Min doktorgrad (Eng.: My Ph.D.) (1.5 minutes)
Date: September 6th 2012.
http://www.nrk.no/nett-tv/klipp/864672/ (fast forward to 22.30)

Article in GEMINI
Name of article: Gull for kroppen (Eng.: Gold for the body)
Magazine: GEMINI, number 2, June 2012, p. 20-23
http://www.ntnu.no/gemini/2012-02/20-23.htm

Competition: Forsker Grand Prix - Trondheim 2011
Name of presentation: Gamle proteiner - nye triks. (Eng.: Old proteins - new tricks)
(4 + 6 minutes)
Comment: I was voted number three out of ten.
Date: September 29th 2011.
Location:Byscenen, Trondeim.
The presentation can be found on the NRK2 web pages
http://tv.nrk.no/serie/kunnskapskanalen/mdfp17003611/12-02-2012
(fast forward 33:24 to and 01:12:11)

Outreach

Barneuniversitetet (Eng.: Childrens university)
Name of presentation: Gamle proteiner - nye triks
(Eng.: Old proteins - new tricks) (1 hour)
Descripton: Presentation about proteins and gold for kids ages 8 to 12. The presentation also included live experiments.
Location: Trondheim folkebibliotek
Date: April 14th 2012

Researchers night - 2011
Stand: Lag ditt eget gull. (Eng.: Make your own gold)
Description: High school students were invited to make their own colloidal gold, while I explained its potential applicability.
Date: September 23rd 2011
Location: NTNU, Gløshaugen.

Presentations for students
Descripton: Presentations of the colloid- and polymer chemistry group (Ugelstad group) to second grade students at NTNU, as well as to high school students.
Date: On several occasions.
Location: NTNU, Gløshaugen.

Most important abbreviations

AFM = Atomic Force Microscopy
aLa = Alpha-lactalbumin
AuNP = Gold nanoparticle
AuNC = Gold nanocluster
BAM = Brewster Angle Microscopy
BSA = Bovine serum albumin
CD = Circular dichroism
Emergent properties = New properties found in the bionanomaterial, which are not found for the single constituents.
Gold nanoconstructs = AuNPs, AuNCs, or mixtures thereof.
λ_{em} = Emission wavelength (nm)
λ_{ex} = Excitation wavelength (nm)
LYZ = Lysozyme
MG = Molten Globule
Protein-gold nanoconstructs = Protein-stabilized gold nanoconstructs
STEM = Scanning transmission electron microscopy
TCAA = Hydrogen tetrachloroaurate(III) x $3H_2O$
TCSPC = Time-correlated single-photon counting
Trp = Tryptophan
UV-vis = Ultra violet-visual

Contents

1. Motivation

Bionanotechnology is a rapidly advancing field within medical research and includes different proteins and other biomacromolecules combined with different types of nanomaterials. Such materials can be metal or polymer nanoparticles, nanowires, carbon nanotubes, metal nanoclusters and more.[1–3] Their small sizes provide these materials with unique optical, chemical and physical properties not seen for larger materials, making bionanomaterials highly suited for e.g. bioimaging, biosensors, X-ray contrast, targeted drug delivery, cancer treatment and diagnostics.[2–13] The choice of nanomaterials for this thesis have been restricted to gold nanoparticles and nanoclusters. This selection is based on the optical properties of nano-sized gold, which enables the use of simple analyzing techniques, the fact that proteins can easily be conjugated to gold, and good biocompatibility.

Proteins are involved in many physiological processes, such as muscle structure, regulation of blood sugar level, digestion of food, transportation of oxygen and transfer of important signals (e.g. neurological signals). Some times proteins are over- or underexpressed, incorrectly post-translationally modified, or misfolded. This may have serious consequences. For example, genetically-caused underexpression of the tumor suppressing protein p53 make people predisposed to cancer and can cause development of several independent tumors in a variety of tissues.[14] Protein misfolding and aggregation are connected to several diseases like Alheimerz's disease and other neurodegenerative disorders, as well as complicating the administration of therapeutic proteins.[15,16] A better understanding of the connection between the protein fold and the subsequent consequences can aid in the development of better therapeutics and diagnostic tools.[16] Important information about this connection can be elucidated by studying the altered protein conformation in bionanomaterials.

This thesis aims to contribute to an enhanced understanding of the structure/function relationship by using gold nanoparticles (AuNPs) and gold nanoclusters (AuNCs) as folding templates for a selection of proteins. Additionally, it is likely that the protein-gold nanoconstructs themselves can be used both for diagnostics and treatment. Examples of such use are transport of drugs over the cell membrane, and optical probes in bioimaging.

2. Proteins

The purpose of this chapter is to provide some basic background information about proteins. Such knowledge is important to achive a proper understanding of what happens with proteins when they are conjugated to gold nanoconstructs.

2.1 Protein structure

Proteins are made up by long polypeptide chains (primary structure, Figure 2.1 a) of L-α-amino acids combined uniquely for each type of protein.[17]

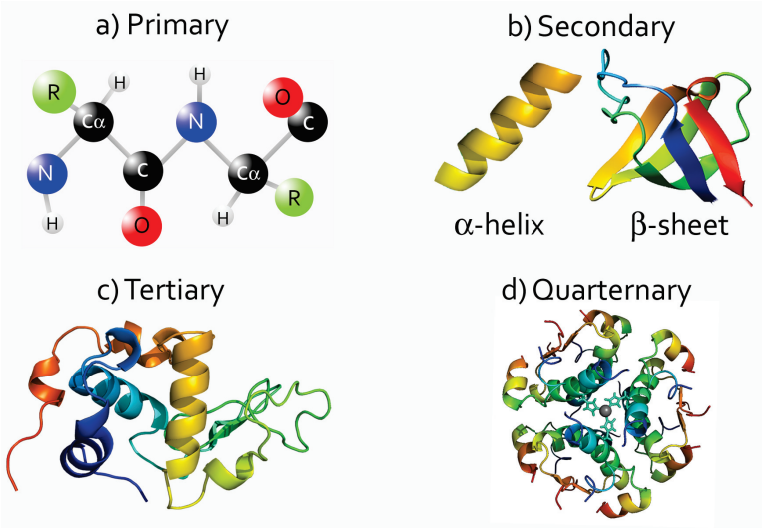

Figure 2.1: (a) A small section of the primary structure. R = amino acid side chain. (b) Examples of motifs of secondary structure. (c) Tertiary structure of aLa. (d) Quaternary structure of insulin hexamer (adapted from Michael Tyka).[18]

The polypeptide chain can coil itself into secondary structure motifs connected by loops and turns (Figure 2.1 b). The secondary structure α-helices are formed when one amino acid residue (n) forms a hydrogen bond with the amino acid four residues ahead (n+4),

while β-sheets are formed due to H-bonds between longer strands of the peptide laying either parallel, anti-parallel, or a mixture of these, to each other. β-sheets are normally more hydrophobic than α-helices.[17,19] While α-helices and β-sheets are the most well known, other secondary structure motifs exists as well, such as the 3_{10}-helix. In a 3_{10}-helix amino acid residue n and n+3 are connected.[20] The secondary structure motifs are spatially ordered into a tertiary structure (illustrated by alpha-lactalbumin (aLa) in Figure 2.1 c) dependent on type of protein and the surrounding media. For globular, water soluble proteins the secondary structure will bend and fold in such a way that the hydrophobic groups will be buried inside the interior of the protein, away from water, while the hydrophilic groups will turn outwards. The protein structure is stabilized by hydrogen bonds, van der Waals forces, and disulfide bridges. A disruption of the tertiary structure can deactivate the protein, decrease protein activity or even change the protein function.[17,21,22] The active form of several proteins, e.g. insulin and haemoglobin, consists of several tertiary structured polypeptide chains linked together to a quaternary structure, as illustrated by insulin in Figure 2.1 d.[17]

2.1.1 Molten globules

Traditionally, there has been a perception that a protein only can exist as either a set of folded conformations or a set of unfolded conformations, depending on the surrounding conditions. These conformations were assumed to be strictly separated by energy barriers.[21] The assumption was that in the native state the proteins coil up in compact, rigid structures, while the denatured state is flexible. However, in the early 1980's the molten globular (MG) state was discovered.[23] MG states have no defined three-dimensional structure, but they are compact and have secondary structure content, often reported to be similar to that of the native protein.[24] The presence of a stable MG state give the proteins a greater ability to flip and bend when interacting with interfaces.

One of the most studied MG-state forming proteins is aLa.[23,25,26] Human alpha-lactalbumin is an important whey protein in breast milk, where it is a part of the lactose synthase protein complex.[27] By binding to a galactosyltransferase protein, aLa alters the specificity of the galactosyltransferase from N-acetyl-D-glucosamine to glucose, and enables lactose synthesis. This milk protein contains an α- and a β-domain, separated by a deep cleft.[28] Four α-helices and two 3_{10}-helices constitute α-domain, while the β-domain is built up by one 3_{10}-helix, a series of loops and an antiparallel β-sheet.[28] Flexible, MG-forming aLa is structurally very similar to the rigid protein lysozyme (LYZ), which has the same genetic origin.[29] Dependent on species, lysozyme differs much in amino acid

sequence but the 3D-structure is always very similar. The lysozyme structure is rich in α-helices, and especially two domains separated by a polysaccharide binding cleft is conserved between the different species.[30] The α-helices are mainly found in the largest domain, while the smaller one consists of β-sheets. The best conserved structural motifs in lysozyme is the central α-helix containing the acid catalyst glutamic acid, and the β-hairpin close to the catalytic site.[30] If the helices and sheets in aLa and LYZ are disrupted, protein conformation and function might be altered.

2.2 Protein function

There are many different types of proteins and the variation in function is large. Some proteins are important for structure and support (e.g. myosin in muscles and fibrin in blood clots), others are important for signaling (e.g. somatotropin, which is a growth hormone), transport (e.g. haemoglobin transports oxygen) and protection (e.g. antibodies detect pathogens).[17] To better understand how some of these proteins function, different models have been developed. Enzymes are proteins that catalyzes the transformation of one or more substrates into one or more products. Due to high activation energy, some of these reactions would never take place without proteins as catalyzers. The two main models used to explain protein-substrate interactions is the lock-and-key-model and the induced-fit model (Figure 2.2).[17] The lock-and-key model (Figure 2.2 a) depicts the

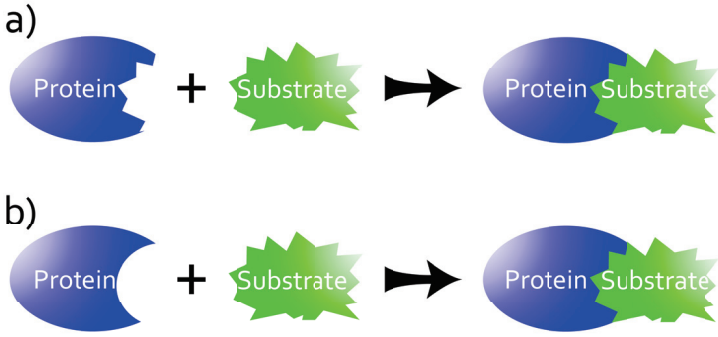

Figure 2.2: The main models for how proteins (enzymes) interact with their substrates. (a) Lock-and-key model. (b) Induced-fit model.

substrate as a key that fits perfectly into the protein lock, and is mostly used to describe rigid proteins. Several proteins are partly or even almost completely without secondary

structure motifs. These proteins are better explained by the induced-fit model, in which the protein is believed to be more flexible and able to adapt to the shape of the substrate (Figure 2.2 b). Several proteins might be best explained by an intermediate of these two models.

2.3 Protein structure/function relationship

If the active sites are blocked, or the protein is structurally altered, the substrate might be hindered from interacting properly with the protein and the product will not be formed.[17] Small structural alterations in flexible proteins might influence the protein function less than for more rigid proteins, as the former may twist and bend so that the substrate still fits.

There are several factors that can alter the tertiary structure of a protein, e.g. mutations in the amino acid sequence, pH, temperature, polarity of the solvent, and adsorption to interfaces.[17,19,20] Changes in temperature and pH can disrupt hydrogen bonds, van der Waals interactions and electrostatic bonds, thus making the protein unfold and potentially reduce its activity. Changes in pH can also lead to decreased activity as the charge of amino acids is altered. This is especially important if the charge is altered in the active site. To keep track of which changes might occur as the pH, temperature, and solvent polarity changes, or amino acids are replaced, it helps to divide the amino acids into different groups. How this is done varies, but one example is given in Table 2.1.

Table 2.1: An example of how to divide the amino acids in different groups dependent on functionalities.[20] Charge signs of the charged amino acids at neutral pH are given in brackets.

Hydrophobic	**Charged**	**Polar**
Glycine	Aspartic acid [-]	Serine
Alanine	Glutamic acid [-]	Threonine
Valine	Lysine [+]	Tyrosine
Phenylalanine	Arginine [+]	Histidine
Proline		Cysteine
Methionine		Asparagine
Isoleucine		Glutamine
Leucine		Tryptophan

Mutations in the DNA sequence can cause changes in the protein structure.[31] Alterations in stop and start codons can have very severe consequences, as the peptide sequence then can be very different from what was intended. Smaller mutation can lead to an exchange of single amino acids. Dependent on the location of the amino acid within the

protein, and what type of amino acids are exchanged, the consequences of the mutations varies. An alteration of the amino acid sequence in the active site of the protein can be more severe than if the exchange happens in a non-important part of the protein. Changing one amino acid with a similar amino acid (like exchanging glycine with alanine) would have little effect, while exchanging amino acids with opposite charge or different hydrophobicity can have severe consequences for the protein folding.[20] One example is sickle-cell anemia caused by hydrophilic glutamic acid in the β-globin chain of haemoglobin being replaced by hydrophobic valine. This error makes the haemoglobin aggregate, and less elastic and charactersitic sickle shaped red blood cells are formed.[20] Sickle cell-anemia results in poor oxygen transportation, vessel occlusion and ischemia. However, the disease has the benefit of imparting malaria resistance, hence being most common in regions in Africa where malaria is widespread. Moreover, the different secondary structural motifs in proteins (see section 2.1, page 2 for details) have varying rigidity.[17,19,20] The random coil is very flexible, and any problems due to alterations of amino acids in this type of region, is likely to be overcome by the coils ability to twist and bend. The α-helices are more structured, due to interactions between amino acid residues that are close to one another in the primary structure.[19] Thus, a change in structure in the α-helix is more severe than changes in the random coil. The transformation from normal erythrocytes to sickle-cells is due to structural changes in α-helices found in globin folds in haemoglobin.[20] β-sheets are even more structured than α-helices because they also interact with amino acids that are further away in the primary structure.[20] Thus, changes in the β-sheets may have more severe effects on protein structure and function than changes in α-helices.

In ailments such as Alzheimer's disease, Parkinson's disease and other neurodegenerative dementia, one of the major problems is the time-dependent convertion of α-helices into intermolecular β-sheet assemblies of intrinsically unfolded proteins. This misfolding exposes hydrophobic groups that are normally buried in the interior of the protein, and makes the proteins aggregate and form large arrangements of proteins called prefibrils. These are stabilized by intermolecular β-sheets (Figure 2.3). The prefibrils are belived to be neurotoxic by themselves, but also take part in neurotoxic amyloid plaque formation.[15,16,32–34] The amyloid plaques deposit on neurons in the brain, prohibiting crucial nerve signals from passing through. The consequences can be reduced cognitive abilities, reduced movement control, reduced learning ability, and memory loss.[15,33] A better understanding of how the reduced dimensionality at interfaces act as folding templates can aid the development of early diagnostic tools or efficient therapeutics for such protein misfolding diseases.[16,35–37]

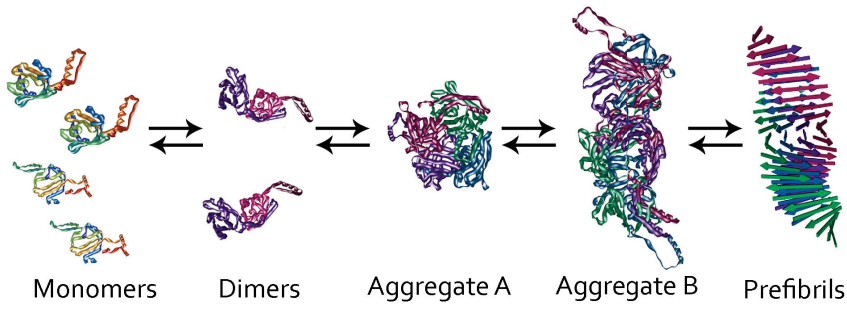

Figure 2.3: Monomeric proteins are destabilized, made conformationally labile and form dimers. The dimers are then aggregated into tetramers. The aggregation continues and intermolecular β-sheets are formed. The prefibrils can evolve further to fibrils, and form amyloid plaques. Adapted from Giurleo.[32]

While structural changes in proteins often can be harmful, there are some exceptions. One example of this is Human Alpha-lactalbumin Made LEthal to Tumor cells (HAMLET). This oleic acid stabilized non-native form of the protein is known to kill cancer cells, while sparing healthy mature cells.[21,38]

2.4 HAMLET - conformationally modulated aLa for use in medicine

Several types of materials and molecules can be used to alter protein conformation or function to create constructs which can be used in medical research. HAMLET is an example of how combining substances can produce surprising results; the oleic acid becomes solubilized and deliverable, while the polypeptide chain may expose motifs hidden in the folded protein that are disruptive to the cell in combination with the stress from the oleic acid.

HAMLET is formed when human alpha-lactalbumin is complexed with several oleic acid molecules. The complex is able to induce cell death in tumor cells, but not in healthy cells.[21] HAMLET causes DNA fragmentation in the nucleus and also interacts with mitochondria and other organelles in the cell.[38–41] The interaction with mitochondria causes release of cytochrome c and thus induce activation of the caspase cascade.[42,43] Caspases are proteolytic enzymes that target and destroy specific proteins, such as proteins that are supposed to maintain the cell.[17] In the caspase cascade a series of caspases are activated, and by destroying vital proteins they are essential for apoptosis.

In the complex, calsium depleted aLa (type III) is held in a molten globular form by oleic acid.[21,44] Svensson *et al.*[45] showed in 2003 that aLa unfolding is a requirement to form HAMLET and necessary, but not sufficient to cause apoptosis. Despite that Ca^{2+}-bound aLa (type I) cannot be converted to HAMLET, they also found that oleic acid probably stabilizes the altered conformation without interfering with the Ca^{2+} site.[21,45] This early study implies that both the protein and the oleic acid is necessary to form the HAMLET-complex. From the mid 1990's to the present, a lot of effort has been put down in studying how HAMLET function, and which component is the most important one. This led to two main explanation models for HAMLET. One where the protein simply is a carrier of the fatty acids, and that the fatty acids are what kills the cells. And another where it is the conformational changes in aLa that enables HAMLET to enter cells and cause cell death, while oleic acid is just a stabilizer to keep the protein in the correct folding state.

Permyakov *et al.*[41] have made oleic acid complexes with bovine β-lactoglobulin and pike parvalbumin, and compared their ability to kill *Streptococcus pneumoniae* and human epidermoid larynx carcinoma (HEp-2) with HAMLET. In their study they point out that the human aLa part of the HAMLET can be exchanged with aLa from bovine, equine, porcine, or caprine and still cause cell death.[41] These proteins have 76 - 79% structural similarities with human aLa. Oleic acid modified equine lysozyme is also found to induce cell death.[46] This could imply that oleic acid is more improtant to the HAMLET effect, than aLa. Earlier studies also show that the exchange of oleic acid C18:1 with C16 or C20 *cis*-oleic acids makes the complex less active, or not active at all.[40,41,44] Moreover, in the studies by Permyakov *et al.*[41] β-lactoglobulin and pike parvalbumin complexed with oleic acid kill both *Streptococcus pneumoniae* and HEp-2 more efficiently than HAMLET. Half of the human epidermoid larynx carcinoma cells are killed at ~200 μM oleic acid, which is similar to when the protein-oleic acid complexes are present.

These studies show the importance of oleic acid, but there are also studies on similar effects caused by other fatty acids. Tuei *et al.*[47] modifed human and bovine serum albumin (HSA and BSA) with several types of fatty acids and then tested the cell-viability. This study show that HSA/BSA modified with palmitate and stearate induce more cell death than when modified with oleate. Which implies that the fatty acid does not need to be oleic acid, and that saturated fatty acids have a more severe effect on cell-viability than unsaturated ones.

The protein might not need to be aLa, and the conformational stabilizer might not need to be oleic acid, but several researchers have proposed that the whole protein-fatty acid complex is important to target cancer cells and cause apoptosis. Lišková *et al.*[48]

have done studies with β-lactoglobulin and sodium oleate which show that the degree of apoptosis is dependent on the concentration of sodium oleate, but not the concentration of β-lactoglobulin. However, they also show that the trends in cytotoxicity for BAMLET and the β-lactoglobulin-sodium oleate complex varies between different types of cell lines. This suggests that the protein part of the complexes is important for interaction with different types of cells, and contributes to the total cytotoxicity. Moreover, HAMLET possesses membrane affecting properties enabling disruption of vesicle- and model cell membranes. This kind of membrane interaction is not seen for native aLa or constitutively unfolded Cys-Ala aLa mutants.[49] This suggest that aLa must be stabilized with e.g. oleic acid to achieve the membrane affecting properties observed for HAMLET.[21,45,49] Membrane interaction or disruption of the membrane could be an initial step in killing the cells. When vesicles are made from intact tumor cells the interaction seemes to be selective to specific patches, but HAMLET is not transported into synthetic membrane vesicles.[40,49] This can indicate that cellular uptake of HAMLET occurs via specific interaction between the construct and reseptors at cancer cell surfaces, and may be the reason why HAMLET affect cancer cells more than healthy cells. Several studies also imply that both the protein and the fatty acid are needed for HAMLET to specifically enter cancer cells and kill them.[27,50–52]

It might be that HAMLET dissociates inside the cell or in the membrane, and it is difficult to know if the further events are caused by the whole HAMLET complex, aLa, or oleic acid. Thus, further studies on the HAMLET mechanisms are required. To fully be able to utilize HAMLET and similar constructs as anticancer agents, it must be understood how HAMLET is able to select cancer cells over healthy cells, how the construct enters the cells, and how it induces cell death. Independent of mechanism, HAMLET is able to reduce both skin papilloma and bladder cancer,[40,53,54] and the bovine version of HAMLET (BAMLET) possesses many of the same properties as HAMLET.[49]

3. Gold nanoparticles and gold nanoclusters

Carbon nanotubes, polymer particles, mesoporous silica particles, magnetic nanoparticles (e.g. iron oxide) and other metal nanoparticles are all examples of conformation-modulating nanomaterials that can be used to alter protein structure.[11–13] For the study presented here, gold nanoconstructs were chosen as modulating tools because they have optical properties (localized surface plasmon resonance (LSPR) for gold nanoparticles (AuNPs) and fluorescence for gold nanoclusters (AuNCs)) that allow for the introduction of an optical marker at the same time as the protein conformation can be changed. Their optical properties can also be used for characterization of the constructs.[55–60] AuNPs have high chemical stability and can be easily coated with several different organic compounds e.g. carboxylic acids, amines and proteins (see e.g. review by Glomm and references therein).[7] Finally, by varying the reaction conditions protein-gold nanoconstructs can be made in a wide range of sizes and shapes, allowing for tunability of the protein conformational changes.[7,56–58,61,62] This chapter addresses an introduction to optical properties of AuNPs and AuNCs, followed by potential use of such constructs in medicine. To be able to display LSPR in UV-vis spectroscopy, the constructs must be $\geq$ 3 nm. Based on the limit for LSPR the assumption that the size of AuNC < 3 nm $\leq$ AuNP is used to distinguishing between the two types of gold nanoconstructs here. In some systems AuNC and AuNPs coexist.

3.1 Optical properties of gold nanoparticles

When gold nanoparticles interact with light, effects like light absorbance and light scattering are enhanced due to the free electrons in the metal.[9] Different sizes and shapes of gold nanoparticles scatter and absorb light at different wavelengths, and due to the nice colors that occur, AuNPs have been used for centuries to stain glass[61] Gold nanoparticles can also quench fluorescence as they absorb the resonance energy emitted from fluorescent species.[63] This is a distance-dependent phenomenon that occurs when the emission spec-

tra of a donor overlaps with the absorbance spectra of an acceptor.[63] Small gold nanoparticles absorb light around 520 nm and appear red, while larger particles color aqueous suspensions purple. These effects are due to localized surface plasmon resonance, which is a phenomenon where incident light makes the conduction-band electrons collectively oscillate around the nanoparticle core. This happens when the frequency of the incident light matches the frequency of the surface electrons.[9] The phenomenon is described in Figure 3.1

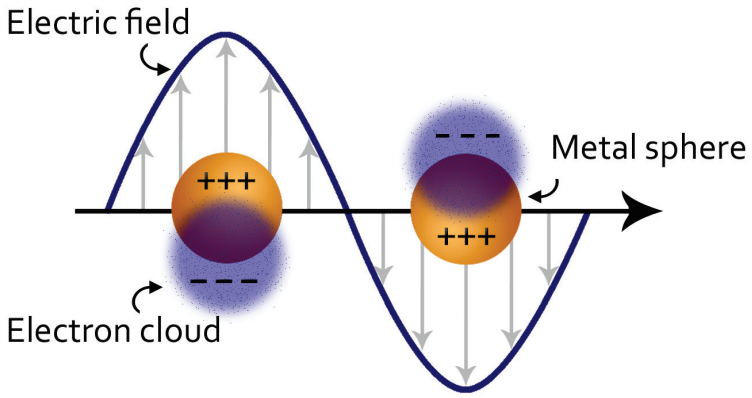

Figure 3.1: Collective oscillation of negative electrons around the positive metal core occur when the frequency of the incident light matches the frequency of the conduction-band electrons and results in localized surface plasmon resonance (LSPR)[6]

Frequency and intensity of Rayleigh and Mie scattering for gold nanoparticles are highly enhanced due to the LSPR.[9] Mie scattering is the scattering of electromagnetic radiation by a spherical nanoparticle, and occurs when the wavelength of the incident light is larger or the same size as the nanoparticle which it interacts with.[64,65] The Mie theory can be applied to both absorbing and nonabsorbing particles. If the particle diameter is smaller than the wavelength of the light (approximately $\lambda/10$), Rayleigh scattering occurs, and if the particle is larger than the wavelength of the incident light, the scatter is called Rayleigh-Gans-Debye scattering.[65] For the Rayleigh scattering theory to be applied, the particles must be nonabsorbing and non-interacting. This theory is thus best suited for gasses and aerosols, and is used to explain the color of the sky.[65,66] While Rayleigh scattering is isotropic and scatters light in all directions, Mie-scattering is anisotropic and in the forward direction.[65,67] Since the size, shape, coating and environment of the AuNPs affect the LSPR, UV-vis spectroscopy can be used to study macromolecule (e.g. polymers and proteins) adsorption onto the AuNPs, and to study the stability of the system.[55,68–71] Shift of LSPR is often discussed within the frames of the Mie-Drude theory. The Drude

model describes the transport properties of electrons in metals (see Figure 3.2), and enables the interfacial properties of the metal to be interpreted from changes in absorption of light.[69]

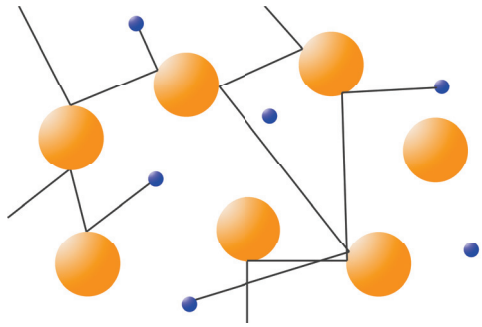

Figure 3.2: The Drude model describe electrical conduction by electrons that bounce between the larger, rather immobile, positive ions in a crystal lattice.

This model describes how the free electrons experience damping due to the positive lattice and applied electromagnetic field. The Drude model can be described by eq. 3.1.[72]

$$\varepsilon(\omega) = 1 - \frac{\omega_p^2}{\omega^2 + i\gamma\omega} \tag{3.1}$$

Here, γ is the damping constant, i is the imaginary number $\sqrt{-1}$, ω is the angular frequency, ω_p is the plasmon frequency and ε is the complex dielectric function. The Drude model is based on the fact that large shifts in the absorption spectra of metal sols can be observed when changes are made in the double-layer (two parallell layers of charge) at the interface between the metal particle and solvent.[69] This happens whenever the environment at the particle surface is altered.

By solving the Maxwell's equation with respect to electromagnetic light interacting with small metalic spheres, Gustav Mie explained in the early 1900's how the colors of metal colloid suspensions are dependent on the absorbance and scattering of incident light.[60,69] When the Mie-solution is applied to the Drude model, the Mie-Drude theory can be used to predict changes in LSPR. If the size of the gold core is kept constant, the equation for the Mie-Drude theory can be simplified, as shown in eq. 3.2.[60,69,73]

$$\sigma_{ext} = 4\chi Im\left\{\frac{(\varepsilon_s - \varepsilon_0)(\varepsilon_m + 2\varepsilon_s) + (1-\phi)(\varepsilon_m - \varepsilon_s)(\varepsilon_0 + 2\varepsilon_s)}{(\varepsilon_s + 2\varepsilon_0)(\varepsilon_m + 2\varepsilon_s) + (1-\phi)(2\varepsilon_s - 2\varepsilon_0)(\varepsilon_m - \varepsilon_s)}\right\} \tag{3.2}$$

σ_{ext} is the extinction cross section per particle, Im means that the imaginary solution of the following part should be applied, ε_s is the optical dielectric function of the shell

layer, ε_m is that of the gold core, and ε_0 that of the solvent. ϕ is the volume fraction of the shell layer, and χ is the size parameter (given in eq. 3.3).

$$\chi = \frac{2\pi R \varepsilon_0^{1/2}}{\lambda} \tag{3.3}$$

Here, R is the coated particle radius and λ is the wavelength of incident light. Eq. 3.2 and eq. 3.3 describes how light absorbance is dependent on particle size, solvent refractive index, interparticle distance, stabilizing ligand shell (type and thickness) and core charge state. Based on these parameters the Mie-Drude theory is used to predict or explain how much light is absorbed.[68] When the solvent and the size of AuNPs are kept constant any changes observed must be due to the stabilizing ligand shell (e.g. proteins) and/or the core charge state.[68] To observe these changes with UV-vis spectroscopy, eq. 3.2 can be simplified to eq. 3.4.

$$EC(M^{-1} \cdot cm^{-1}) = \frac{\sigma_{ext}(3 \cdot 10^{-3})V_m}{4(2.303R)} \tag{3.4}$$

Here, EC is the actual extinction coefficient of the particle and is not concentration dependent, and V_m is the molar volume of gold (~10.4 cm^3/mol).

When the distance between gold nanparticles decreases, as when aggregation occurs, near-field coupling is induced and a distinct red shift and a broadening of the LSPR band are observed in the absorbance spectra.[55,71] If the line shape of the UV-vis absorption spectra is not significantly altered upon protein adsorption the protein-gold nanoparticles have likely remained as single colloids rather than dense flocs. However, protein adsorption on AuNPs will always lead to a change in the dielectric function of the nanoparticle resulting in a shift of the LSPR band,[68–70] thus giving a good indication about whether proteins are adsorbed or not, and whether the system is stable.

3.2 Optical properties of gold nanoclusters

AuNPs are large enough to have a big cloud of electrons surrounding them, and this is needed to create the LSPR effect. However, when the size is reduced to nanoclusters, the energy levels become more discrete, and the LSPR is lost.[74] AuNCs have molecular-like HOMO-LUMO bandgap openings and the electronic transitions here are smaller in size than the Fermi wavelength.[75,76] This causes AuNCs consistent of a "magic number" of atoms to luminesce.[59,74–76] A "magic number" of atoms is when the clusters have an amount of "free" electrons that match the spherical shell closing number.[61] The spherical

shell closing number is to clusters, what filled valence shells are to atoms, and typical "magic numbers" are n = 8, 11, 13, 18, 22, 25, 28, and more.[57,61] While many protein solutions are more or less colorless when exposed to UV-light at ~365 nm, AuNCs have a strong fluorescent color (see Figure 3.3). The presence of AuNPs can reduce the fluorescence observed from AuNCs due to energy transfer from AuNCs to AuNPs.

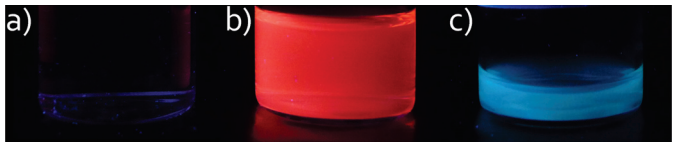

Figure 3.3: Images of protein and protein-gold nanoconstruct solutions illuminated with UV-light (λ_{ex} = 365 nm). (a) BSA in buffer, (b) BSA-gold nanoclusters in buffer, (c) Transferrin-gold nanoclusters, also in buffer.

AuNCs can be studied with steady-state fluorescence.[57] When excited with a light source with λ_{ex} = 370 nm, earlier studies have concluded that small protein-stabilized gold nanoclusters (8 Au atoms, Au_8) emit at λ_{em} = 450 nm, while larger nanoclusters (25 Au atoms, Au_{25}) show emission at λ_{em} = 685 nm.[57] When λ_{ex} = 450 nm small AuNCs are not excited, but larger AuNCs are. By choosing higher excitation wavelengths, it is thus possible to study fluorescence from larger AuNCs, exclusively.

3.3 Use of nano-sized gold in medicine

Gold in many shapes and sizes has been used for medical purposes for centuries, and is well incorporated in traditional Chinese medicine.[4] Gold teeth are in the upper size range of gold constructs used in medicine. Teeth made of gold are possible because gold is nontoxic, in addition to not being prone to oxidation in air or water. At the other end of the size range, gold ions have been used for 80 years to treat rheumatoid arthritis.[77] This section will mainly focus on gold in the size range corresponding to nanoparticles and nanoclusters. It is important to keep in mind that when gold nanoconstructs are used in medicine, some of the observed effects can be due to the molecules conjugated to gold, and not necessarily gold itself.[4] In some cases the gold and coating combined have properties which are not observed for any of the constituents alone. The nano-size itself imparts gold nanoconstructs with unique properties. Their chemistry and physical properties often deviate significantly from both atomic behaviour as well as bulk behaviour. If the particles are smaller than ~200 nm they can enter cells through endocytosis, and if they are smaller than ~40 nm they can even enter the cell nucleus.[7] For uptake from

the vasculature, the diameter must be less than 70 nm.[7,78] The small size makes the gold nanoparticles less affected by gravity, and thus less susceptible to sedimentation.[65] Moreover, small colloids have large surface areas compared to their size, thus many of the physical and chemical properties of these colloids are linked to their surface properties.[65] The surface chemistry of AuNPs allow for functionalization with several different compounds, such as polymers, DNA, proteins, and others. Thus, modified AuNPs can be tailored to different environments and tasks.[7,8] By combining AuNPs or AuNCs with different biological macromolecules, like proteins or peptides, it might be possible to make new bionanomaterials with emergent properties that can aid in medical research.

3.3.1 Gold nanoparticles in medicine

The unique optical properties of AuNPs and their ability to adsorb organic compounds and alter protein conformation have made these colloids much studied for intracellular delivery.[7,79–82] Gold nanoparticles can carry proteins, siRNA, DNA, peptides as well as small organic compounds and penetrate into individual cells.[79–81,83–85] Transport of such molecules into cells may be important for treatment and diagnostics of e.g. cancer, and AuNPs can be cost-efficient and safe alternatives to traditional viral vectors.[81] The siRNAs are potential promising therapeutic candidates, as they can be used to silence disease-causing genes.[84,86] To be able to silence genes, siRNA must enter the nucleus without being degraded during transport.[86,87] Layer-by-layer modified AuNPs have proven to be well suited vectors for safe transport of siRNA.[84,85,87] The AuNPs are functionalized with a hydrophilic polymer (e.g. poly(ethylene glycol)), then the siRNA is linked to this initial polymer layer, before another layer of polymer (this polymer can be the same as the first one) is added to create a protective layer around the whole construct.[84,85,87] By using gold nanoparticles as scaffolds for proteins and other biomolecules, the optical properties of nanosized gold can be used as a diagnostic tool to track the nanoparticle construct and the surronding physicochemical environment. When using immunogold electron microscopy, specific antigens are detected and their location can be visualized by antibodies modified with colloidal gold.[4] Due to the enhanced permeability and retention effect in tumors, AuNPs in the size range 10-100 nm often accumulate in tumor tissues, and the light scattering properties of AuNPs can thus be used for imaging of cancer cells.[9,13] To improve studies of cells using different types of microscopy, BSA-AuNPs are modified with a variety of polypetides. This enhances cellular uptake and improves the chance of the AuNPs reaching the nucleus.[80] For spherical AuNPs excitation of LSPR occur using light in the visible region. This light is not able to penetrate deep into the skin, but if the

shape of the nanoparticles is altered to e.g. rods, near infrared light can collectively oscillate electrons to induce photothermal properties. Cancer cells can then be killed through hyperthermia while the effects on non-targeted cells are minimal.[13]

Modified AuNPs can be used for much more than diagnosis of cancer. They can also be used for diagnosis of syphilis, sensing of narcotics, antidoping tests, pregnancy tests, and more.[88,89]

Gold nanoconstructs at the size-border between AuNPs and AuNCs can be used as X-ray contrast agents.[10] In Figure 3.4 1.9 nm gold nanoconstructs as contrast agent for X-ray, is compared to traditional iodine contrast agent (Omnipaque). Gold provides higher contrast at lower X-ray dosages than iodine, and due to slower clearance rate, images can be collected over a longer peroide of time.

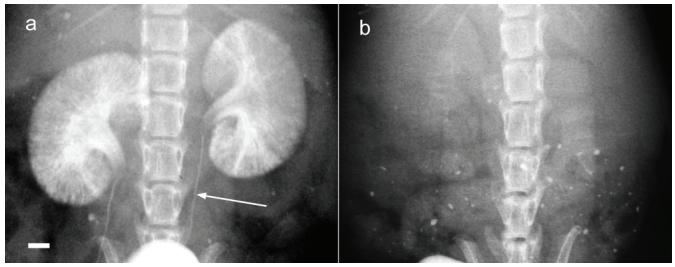

Figure 3.4: X-ray image obtained 60 minutes after intravenous injection with (a) 1.9 nm gold-nanoconstructs and (b) iodine contrast agent.[10]

Despite the extensive research on biomolecules conjugated to AuNPs for drug delivery and diagnostic purposes, little is known about how the adsorption prosess alters conformation and function of e.g. proteins.[83]

3.3.2 Protein-gold nanoclusters in medicine

Gold nanoclusters do not possess the same plasmonic properties as gold nanoparticles but they do, however, present fluorescent properties.[56,57,74] This is described in more details in section 5.5, page 31. AuNCs can be stabilized by polymers, peptides, DNA, thiols, etc. (see review by Shiang *et al.*[74] and references therein). Studies on protein-stabilized AuNCs so far have used the proteins only as AuNC stabilizer, and articles published on the medical applications of protein-AuNCs have hitherto mainly focused on the properties of the gold itself.[56,57,74,90,91] Recently published results by Chen *et al.*[90] show how lysozyme-AuNCs can be used to detect glutathione, which can be an indicator of brain damage and other diseases, in a single drop of blood. The sensing of glutathione is

based on the fact that it quenches fluorescence from AuNCs.[90] Quenching of AuNC fluorescence can also be used for sensing IgG (antibodies connected to breast cancer), and several other proteins as well.[74] Hu *et al.*[92] have used BSA-AuNCs to detect trypsin by studying the alteration of fluorescence as the protease digests BSA. This technique can be used to measure elevated levels of proteases, which may be connected to neurodegenerative diseases, cancer and inflammations. Acute myeloid leukaemia can be discovered at an earlier stage by using flow cytometric detection of BSA-AuNCs conjugated with CD33 mono-clonal antibodies to detect CD33 myeloid antigens.[75] Protein-AuNCs can also be used for cellular imaging.[5,74] Zhang *et al.*[93] have used BSA-AuNCs to develop a fluorescence imaging technique to detect altered levels of serum proteins. Their aim was to find a method to distinguish healthy people from people with liver diseases. This new method for sensing serum proteins is 7-14 times more sensitive than traditional methods. Folic acid conjugated BSA-AuNCs have been tested and proved promising for cancer imaging.[76] Guével *et al.*[94] have made very stable BSA-AuNCs by covering them with silica, and it is likely that these constructs can be used to image lung cancer. Other protein-AuNCs have also showed promising results for tumor imaging and therapy as well.[91] The protein-AuNCs can be conjugated with antibodies to specifically find cancer cells, and then their fluorescence can be utilized to image tumors.

The relatively new field of probing protein-AuNCs for medical use is expanding rapidly. So far most of the studies are done on BSA-stabilized AuNCs and few other proteins have been studied for this purpose. Most of the studies focus on how the fluorescent properties of the AuNCs can be used in diagnostics and targeted drug delivery, and few focus on how protein conformation and function are altered.

4. Protein modification with gold nanoconstructs

The two main methods for manipulating proteins with gold presented here are protein adsorption onto gold nanoparticles, and formation of gold nanoclusters within the protein, both with subsequent changes in protein conformation (Figure 4.1). The following chapter deals with how these bionanomaterials can be utilized for medical purposes.

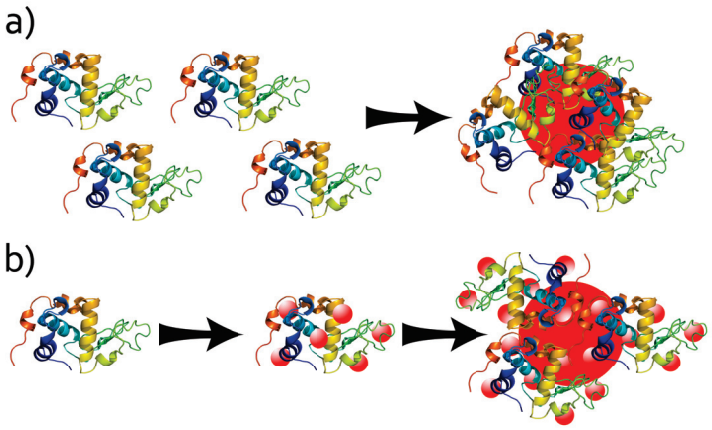

Figure 4.1: (a) Modification of proteins using AuNPs. (b) Modification of proteins using AuNCs. In some cases modification of proteins with AuNCs leads to formation of protein-AuNC stabilized AuNPs.

4.1 Protein adsorption onto gold nanoparticles

There are several studies on the adsorption of polypeptides onto gold surfaces.[3,83,87,95–97] Adsorption to surfaces and interfaces can occur either through weak electrostatic, van der Waals and hydrophobic forces (physisorption), or through strong electrostatic interactions and covalent bonds (chemisorption). Physisorption is normally characterized by

high adsorption rates and the formation of multilayers, while chemisorption normally is characterized by lower adsorption rates resulting in monolayer formation.[7] When proteins adsorb onto gold nanoparticles they have to go through a three-step procedure: 1 - transport toward the surface through diffusion or convection, 2 - attachment to the surface, and 3 - spreading on the surface (see Figure 4.2 a).[96,98]

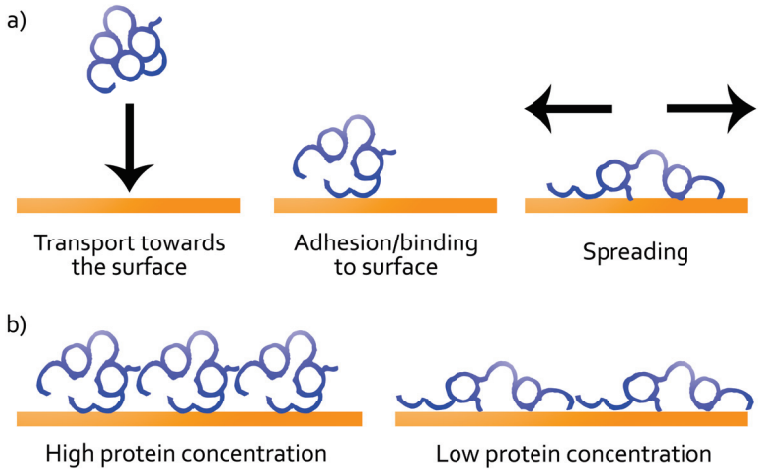

Figure 4.2: (a) The process of adsorption of proteins onto surfaces are divided into: 1 - transport towards the surface, 2 - binding to the surface, and 3 - spreading on the surface. (b) Degree of protein unfolding at the interface depends on protein concentration.[96]

If the last step in the adsorption prosess leads to exposure of hydrophobic- or functional groups, the spreading could lead to denaturation of the protein.[7] Depending on the type of interaction, curvature of the surface and reaction conditions in general, different conformational changes can occur. Partial unfolding of water-soluble globular proteins may lead to exposure of more hydrophobic groups, which can induce increased interfacial activity. Despite the fact that proteins are often immobilized by adsorption onto different materials, the full picture of how adsorption might alter protein conformation and function is still unclear.

As a protein adsorbs to a surface, several sub-processes occur with the protein and the adsorbent. These are defined as; (i) changes in hydration states of the adsorbent and the protein surface, (ii) redistribution of charged groups, both chemical (medium change for transferred ions) and electrical (overlap of electric fields), and (iii) rearrangements in protein structure. For the latter, the structural stability of the protein molecule comprises an important parameter.[99] As has been shown by e.g. Glomm *et al.*,[96] the properties of the adsorbed layer, such as adsorbed amount, layer thickness and adlayer flexibility, can

also be tuned through control of the deposition kinetics (Figure 4.2 b, page 19). This can be controlled through variations in protein concentration, flow-rate and pressure. As the protein concentration increases, each protein will have less time to spread (step 3 in Figure 4.2 a) before more proteins arrive through steps 1 and 2. In other words, at low protein concentrations (or low pressures/flow-rates) the proteins can spread more at the surface than what they may under higher protein concentrations, pressures or flow-rates. Size and coating of the gold nanoparticle, temperature, pH, solvent (type and ionic strength), surface curvature, type of particle and choice of protein are other possible variables.

Larger particles have less curvature than smaller ones, which might lead to differences in available surface area as well. Earlier studies indicate that small nanoparticles promote retention of native-like protein structure, while larger nanoparticles tend to give more spreading and unfolding.[1,100,101] However, there are also examples of the opposite effects occurring.[102]

Stable gold nanoparticles in suspensions are not bare but covered with a stabilizing agent such as citrate or other ligands. This means that normally two adsorption hypothesis must be concidered: the electrostatic hypothesis and the displacement hypothesis.[7] The electrostatic hypothesis involves pH-dependent attraction between charged groups in the passivating layer on the AuNP surface and oppositely charged groups in the adsorbant, while the displacement hypothesis involves displacement of the passivating layer. For proteins, amino groups from lysine and thiol groups from cysteine can interact directly with the gold surface.[7,13,103,104] There are many ways to synthesize AuNPs, such as disintegration of gold nanorods or reduction of gold salts using reducing agents or radiation.[105–108] The gold nanoparticles used in papers I and II are initially citrate stabilized. They are bought commercialy and synthesized as described by Turkevich.[105] In this method, sodium citrate reduces hydrogen tetrachloroaurate(III) at 100 °C to form uniform and stable AuNPs. In addition to be the reducing agent, citrate also functions as a passivating and stabilizing agent of the AuNPs formed. A study by Brewer *et al.*[95] concluded that when citrate is present, BSA binds electrostatically to the citrate layer on the gold surfaces. In addition, adsorption behavior studies of eight different proteins onto citrate-covered AuNPs concluded that binding of proteins occur through charged patches on the protein and the adsorbent, fitting with the electrostatic hypothesis.[96] Moreover, the global charge of the protein is less important, provided that the proteins have local positive patches that can interact with the negatively charged citrate at a given pH. Since the amino acids have different pK_a-values, the hydrophobic and electrostatic forces can be manipulated by adjusting pH in the bulk solution.

Several issues can occur when gold nanoparticles are used to modify proteins: 1 - The

structural changes in the protein can be larger than desired. In general this is manifested as low tunability in the degree of unfolding. 2 - Normally more than one protein adsorb to each AuNP, making any observed chemical and physical properties dependent on the whole construct, not the individual protein. 3 - The total size of the construct can be too large for cellular uptake (~100-200 nm, dependent on uptake method), and thereby preventing usage of the construct as a drug vector.

4.2 Protein modification using gold nanoclusters

Many of the obstacles when using AuNPs to modify proteins can be surpassed by using smaller modifying entities such as AuNCs. The definition of gold nanoclusters varies between research fields,[56–58,61] but in this thesis gold nanoclusters are defined to be made up from a few atoms to tens of atoms, and having diameters less than 3 nm.

In theory, the size of the gold nanoconstructs can be tuned from nanoclusters to nanoparticles by varying the concentration of reducing agent and gold precursor. The reducing agent can either be the amino acid residues themselves, or an added reducing agent.[56,57] Varying reaction time or the temperature can also influence the type of protein-gold nanoconstructs formed. The wide range of possible protein-gold nanoconstructs allows for controlled protein-modification, and it might be possibile to study to what extent protein conformation may change before the protein function is compromised. Such studies can improve the understanding of protein misfolding diseases such as Alzheimer's disease. Also, AuNCs are fluorescent, and an inherent optical marker can be of great benefit for diagnostic purposes.

In HAMLET-research it is difficult to know if the conformational changes of the protein causes the anti-cancer properties, or if the protein simply transports oleic acid (section 2.4, page 7). In HAMLET, oleic acid is reversibly bound to aLa, and the construct might dissociate. However, in aLa-AuNCs, the conformation modulating entity would be covalently bound to aLa. Thus, any observed effects must be due to the whole construct as such.

Earlier studies on protein-gold nanoclusters have mainly focused on the synthesis of the gold nanoclusters and the fluorescent properties of the gold,[56–58] but few have studied the conformational and functional changes in the protein. How the synthesis of gold nanoclusters whithin the protein affects proteins with different properties is also scarcely studied. Even the study by Chen *et al.*,[90] where lysozyme-Au_8 constructs were used to detect glutathione (section 3.3.2, page 16), focused on the properties of the AuNC, not on the altered structure of lysozyme. In this thesis, both the structural changes in the protein,

as well as the resulting optical properties of the protein-gold nanoconstructs formed have been taken into consideration. The protein-gold nanoconstructs are also studied to see if they have any emergent properties not found in either protein or gold alone. The AuNCs also allow for a different method for modifying proteins as compared to adsorption onto AuNPs.

4.3 Toxicity of gold nanoparticles

The increased use of gold nanoparticles in medicine gives rise to a demand for an increased knowledge about potential toxicity of AuNP-constructs. In 2005 Connor *et al.*[109] published results showing that AuNPs can be taken up by human cells without inducing cytotoxic effects. However, it is known that nanoparticles behave differently than both their bulk and atomic counterparts, and that they are likely to interact with biological systems (e.g. biomolecules such as proteins and lipids) in ways currently not understood.[110,111] Toxicology of AuNPs is very complex. A study performed by Uboldi *et al.*,[112] shows that the concentration of contaminants, such as excess sodium citrate, on the surface of gold nanoparticles can be important for inducing cytotoxicity *in vitro*, but not for the uptake of AuNPs in human ATII-like cell lines. Recently Choi *et al.*[113] published *in vitro* results with serum protein-coated citrate-reduced AuNPs causing apoptosis in human lung adenocarcinoma cells. The cell death show some concentration dependence (0-60 μg/ml), but no difference between 24h and 72h exposure was observed. At the maximum concentration of AuNPs approximately 50% of the cells died. Moreover, increased negative charge of the AuNPs seems to be more lethal than a lower charge. In an *in vivo* study using AuNPs as X-ray contrast agents in mice, the AuNPs were found to be non-toxic.[10] However, zebra fish experience alteration of genome composition and dysfunction at a sub-cellular level after being fed with low dosage (36-106 ng gold/fish/day) of gold nanoparticles.[114] Earlier studies on mice also show that intravenously administered citrate-covered AuNPs accumulate in the liver, lungs, spleen, kidneys, heart and stomach.[115] The distribution of AuNPs in the mice is dependent on the particle size, and the smallest (15 nm) AuNPs tested were found in all the mentioned organs. The concentration in the brain was also quite high. However, Sonavane *et al.*[115] only studied the distribution of the introduced gold, not how the present gold affected the mice.

Some of the above results are conflicting, and to get a full picture of the toxicity of AuNPs, more *in vitro* and *in vivo* experiments are needed. The toxicity of gold nanoparticles is probably dependent on size and shape of the particle, the species and charge of the coating layer, purity of the suspension, concentration, and means of administration

(through the skin, through inhalation, intravenously, etc.).

4.4 Toxicity of gold nanoclusters

In recent years, the interest for using gold nanoclusters for medical applications has increased, and just as for gold nanoparticles, the knowledge of their toxicity is at present inadequate. Since the use of AuNCs for medical research is a much younger field than similar use of AuNPs, possible toxic effects from AuNCs are even less known. In several cases, AuNCs are used as fluorescent probes to determine the concentration of different target species in blood samples, such as glutathione,[90] serum proteins,[93] trypsin,[92] and CD33 myeloid antigens.[75] In these cases, the AuNCs are never actually introduced to the body, making potential toxicity less essential. However, if the AuNCs are to be used to image tissues or as therapeutics, the toxicology is of great importance. A study by Wang *et al.*,[4] shows that when the AuNC concentration is kept below 500 nM their gold nanoclusters do not reduce cell-viability. This is very promising for using AuNCs as fluorescent probes, since biocompatibility is of great importance for medical usage. Furthermore, Chen *et al.*[91] have made BSA-AuNCs conjugated with methionine (Met). The Met is added to increase specificity toward cancer cells. The BSA-AuNC-Met are labeled with either MPA (MPA is a fluorescent hydrophilic derivative of indocyanine green made by Chen *et al.*) or DOX (Doxorubicin, an anti-cancer drug). BSA-AuNC, BSA-AuNC-Met, and BSA-AuNC-Met-MPA are tested in cell-viability studies using both healthy cells and different cancer cell-lines. Even at high dosages of the three constructs (1 mM), 80% of the cells survived. *In vivo* studies in mice also show low toxicity of the AuNC constructs.[91] Chen *et al.* observed some discoloration of the liver due to BSA-AuNC, but the other constructs showed no harmful effects on the mice. The *in vivo* studies also shows that Met-labeled constructs targeted cancer cells instead of healthy cells. The uptake efficiency also vary between the different types of cancer tumors. *In vivo* studies with the DOX-modified constructs showed that BSA-AuNC-Met-DOX is taken up more in cancer cells than in healthy cells, and kill cancer cells more efficiently than pure DOX does. Moreover, BSA-AuNC-Met-DOX uptake in healthy cells is less than what is observed for pure DOX. In short, Chen *et al.* has created a non-toxic protein-AuNC construct which can be used to image tumors safely (BSA-AuNC-Met-MPA), and a AuNC-cancer drug construct (BSA-AuNC-Met-DOX) that is more selective towards cancer cells, as well as being more efficient as a cancer therapeutic, than the original drug. As for AuNPs, the toxicity of AuNCs is probably highly dependent on the conjugated species, concentration, and route of administration.

5. Experimental techniques

This chapter provides some theory, and brief descriptions of the experimental techniques most relevant to the work presented in this thesis.* The description of the different techniques are focused on their specific use for the presented work, not necessarily their general use.

5.1 UV-vis spectroscopy

Ultra violet-visual light (UV-vis) spectroscopy is one of the most basic characterization techniques and can provide information about gold nanoconstructs, protein-gold nanoconstructs, adsorption, protein concentration and protein activity. The method is based on different species (chromophores) absorbing light at different wavelengths depending on the type of energy transition occurring. Molecules in solutions can contain several chromophores, and several transitions are possible, but $\pi \rightarrow \pi*$ is the most common.[116]

UV-vis measurements are often used to determine concentration of proteins in solution via the Beer-Lambert law (eq. 5.1).[117]

$$A = log\left(\frac{I_0}{I}\right) = \varepsilon cl \tag{5.1}$$

Equation 5.1 shows that the absorbance (A) is proportional to the sample concentration (c) in $^{mol}/_{L}$. At the given wavelength the molar extinction coefficient (ε) is a measure of how strongly the compound absorbs. I_0 is the light intensity before the light has passed through the sample, and I is the light intensity afterwards.

Shift in the UV-vis absorption maxima can be used to study induced changes in certain systems, such as changes in the micro-environment for proteins as the protein fold is altered.[117,118] The changes can e.g. be differences in the solvent polarity (solvatochromism), or the viscosity of the system (rigidochromism).[119] Protein UV-absorbance is mainly due to Trp, for which absorbance is very environment dependent. A blue shift in

*The AFM and STEM studies were executed by Ph.D. Gurvinder Singh, while Ida Maria Rundgren and Hanzhen Wen performed the cell-viability studies.

absorbance spectra indicates a more polar environment for Trp, while a red shift indicates more non-polar surroundings.[117] When proteins unfold in water, a blue shift is normally observed.[118]

Due to AuNPs strong absorption band, caused by LSPR (see section 3.1, page 10), UV-vis spectroscopy can also be used to prove the presence of gold nanoparticles, and to characterize them. Changes in this absorption band can be used to observe protein adsorption onto AuNPs.[7,72,120] As polypeptides adsorb onto AuNPs the absorbance maxima shifts to higher wavelengths (red shift).[55] This can normally be observed by the naked eye, as such a shift will cause the suspension to appear more purple in color. If aggregates are formed, the line shape will broaden as well.[55]

Protein adsorption onto gold can also be measured through changes in size and ζ-potential, by using dynamic light scattering (DLS).

5.2 Dynamic light scattering

The size distribution of nanoparticles in suspension can be measured by dynamic light scattering (DLS). When light hits small particles, the light will be scattered in different directions, with different intensities and different degrees of polarization in all directions, and this can be detected by a detector placed at a specific angle with respect to the incident beam.[66,67] The emerging pattern is dependent on both the refractive index of the particle, solvent, as well as the particle size.[67] An illustration of the scattering pattern is given in Figure 5.1.

Browninan motions of the particle cause the intensity of the scattered light to fluctuate over time, and an autocorrelation function can be made. The autocorrelation function C(s,t_d) models the decay between the highest intensity value $\overline{[i(s,0)]^2}$ and its lowest asymptotic value $[\bar{i}(s)]^2$ as a function of delay time (t_d) (see Figure 5.2).[65,121] This function decays exponentially with the time delay.[121] The exponential delay is dependent on the particles diffusion coefficients, which in turn can be used to find the particle's hydrodynamic diameter using the Stokes-Einstein relationship (eq. 5.2).[65,121] For eq. 5.2 to be valid, the particle is assumed to be spherical and solid.

$$D = \frac{k_B T}{6\pi\eta R_H} \tag{5.2}$$

Here, D is the self diffusion coefficient of the particle, k_B is the Boltzmanns' constant, T is temperature, R_H is the hydrodynamic radius of the particle, and η is the viscosity of the suspension fluid.

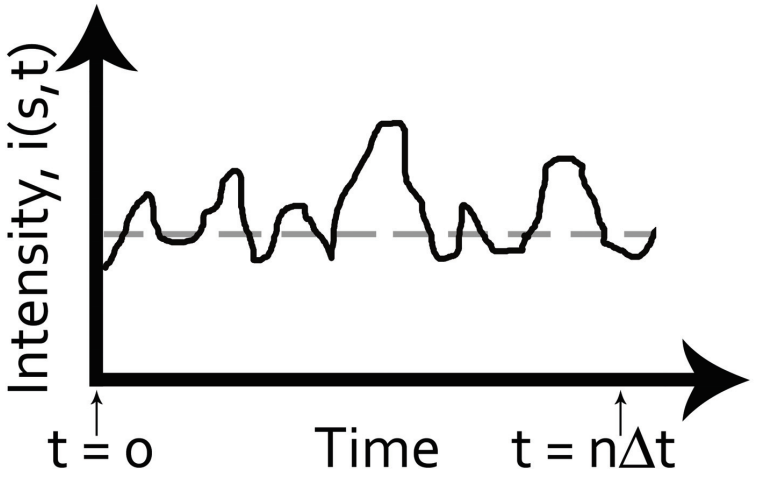

Figure 5.1: Illustration of the intensity of scattered light with time. The intensity fluctuates around an average value.

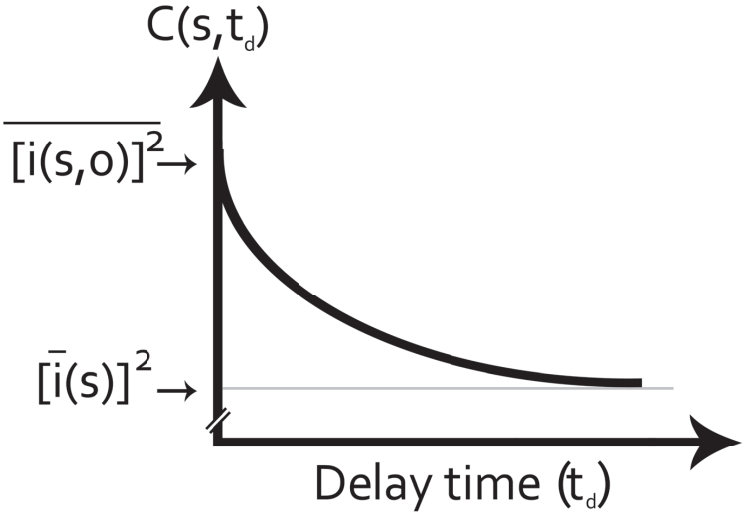

Figure 5.2: Schematic illustration of the variation of the autocorrelation C(s,t_d) with delay time t_d. Adapted from Hiemenz.[65]

DLS can be used to measure sizes of particles in the range from ~2 nm to ~1 μm. Here, DLS was used to confirm adsorption of proteins on AuNPs, introduction of AuNCs inside proteins, and to observe if aggregation of these constructs occured. All these events will lead to an increase in the measured size. DLS allows for rapid size measurements with little sample preparations. However, it is important to be aware that DLS measurements have some limitations regarding accuracy. DLS can only measure very dilute samples or samples that scatter light weakly, which is not necessarily true for gold nanoparticles.[65,122] AuNPs with 60 nm diameter actually scatters light 200-300 times more than polystyrene beads of similar size.[123] Depending on the size of AuNPs studied, it is also important to choose the detection angle with care. (Not all instruments allow for an adjustment of the detection angle.) Small particles scatter little light in the forward direction, while larger AuNPs and aggregates scatter little light backwards and in the 90° angle, but much in the forward direction.[66,123] This is especially important to keep in mind if the suspension is expected to be polydisperse. Khlebtsov has written a paper about the benefits and drawbacks of using DLS for AuNP studies, like the appearance of false peaks, and also provide some solutions to problems that can occur.[124] Furthermore, the Stokes-Einstein relationship assumes that the particles are solid and spherical,[121] which is not always true for proteins. Many of the samples studied here contained proteins, or gold nanoconstrucst covered with proteins. Moreover, accurate calculations of size from DLS require monodisperse suspensions.[67,121] Since solutions rarely are monodisperse, different numerical algorithms are needed to fit the data, and it is important to choose the correct one to achieve the correct size.[121] Some examples of models that can be used are the general purpose (GP) analysis algorithm or the multiple narrow peak (MNP) algorithm. The latter was mostly used here.

Despite these obstacles, DLS-measurements provide more than sufficient information about particle/aggregation state for the work presented here as the method was not used to measure exact size. Rather, DLS was used to observe changes in size upon protein adsorption onto gold, or modification of proteins with AuNCs. DLS also provided for a quick check to study the stability of the samples, such as potential aggregation. DLS is often used to study the stability of protein-gold conjugates. Jans *et al.*[123] have used the changes in size observed through DLS to study the interaction between protein A-gold nanoparticles with IgG, and Hermanson have explained how DLS can be used to study protein stabilization of citrate covered AuNPs.[123,125] Gold nanoparticles have also been used as DLS probes in detection of arsenic,[126] and for cancer biomarker detection.[127]

Dynamic light scattering can also be used to find the charge of nanoparticles by measuring the ζ-potential.

5.3 Zeta-potential

The goal of the ζ-potential measurements was mainly to confirm protein adsorption onto gold nanoparticles, alterations in protein structure when modified with different gold species, and to monitor system stability.

The electrophoretic mobility is a measure of the speed at which charged particles travel as they move from one electrode to an other when exposed to an electric field, and can be used to calculate the ζ-potential.[128] When a particle moves in the electric field, there will be a slipping plane between the particle and the surrounding solution, creating an electrical potential relative to the bulk solution. This electrical potential is the definition of the ζ-potential.[128] The slipping layer is normally at, or just outside, the Stern layer (see Figure 5.3).

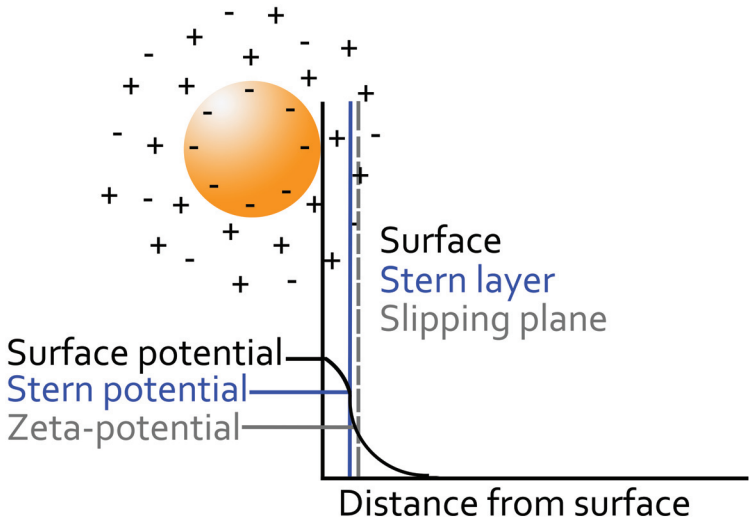

Figure 5.3: Schematic illustration of the ζ-potential (adapted from Stenius[128])

As proteins adsorb onto gold nanoparticles, or when proteins are modified with gold nanoclusters, the charge profile of the constructs will change. ζ-potential measurements are often used to characterize AuNPs after particle synthesis or after adsorption of adlayers.[95,115,129] A high charge, i.e. |25|-|30| mV, normally implies a higher colloidal stability due to electrostatic repulsion. To get information about system stability, it is also possible to observe if the ζ-potential changes over time. The Helmholtz-Smoluchowski equation (eq. 5.3) is the most common to calculate the ζ-potential.

$$\zeta = \frac{u_E \eta}{\varepsilon_0 \varepsilon_r} \tag{5.3}$$

Here, ζ is the zeta-potential, u_E is the electrophoretic mobility, η is the viscosity, ε_0 is the permittivity of free space, and ε_r is the dielectric constant of the dispersion medium. However, this equation is only valid if the thickness of the double layer is thin enough as compared to the particle radius.[65,128] The ratio between the particle radius and the thickness of the double layer is often designated as κa. High κa values is designated to imply thin double layers, and the Helmholtz-Smoluchowski equation (eq. 5.3) can be used. However, if the double layer is thick compared to the particle radius, the Hückel equation (eq. 5.4) should be used instead.

$$\zeta = \frac{3 u_E \eta}{2\varepsilon} \tag{5.4}$$

Here, ε is the dielectric constant, which equals ε_0 times ε_r in eq. 5.3. Both the size of the particles, and the ionic strength of the solution can change κa. Normally, larger particles in polar media can be explained by the Helmholtz-Smoluchowski equation, and smaller particles in non-polar media can be explained by the Hückel equation.[65] Here small particles in polar media were used, which means that these systems cannot be adequately explained by either of the equations. In addition, the fact that the ionic strength of the solution can change the κa, makes the ζ-potentials measured inaccurate for high saline samples such as buffer solutions. However, these issues can be surpassed. The difference between eq. 5.3 and eq. 5.4 is a factor of 1.5, and by using the same equation for all measurements the acquired results are comparable. The Helmholtz-Smoluchowski equation was used for all samples in this study. The aim with the ζ-potential measurements was to observe differences in the system before and after proteins were manipulated with gold. For all samples that were directly compared, the ionic strength was constant. Since only relative values were of interest, small inaccuracies in ζ-potential were not deemed to represent a problem.

5.4 Scanning transmission electron microscopy

The accuracy of size estimation of gold nanoparticles using UV-vis and DLS can be system dependent, meaning that the results can vary with e.g. concentrations and choise of solvent. For this reason, scanning transmission electron microscopy (STEM) was used to determine the exact size of the AuNPs formed during synthesis of protein-gold nanoconstructs (papers III and V).

When measuring STEM, the beam from an electron gun (Figure 5.4) is first focused and partially demagnified through two condenser lenses, before a final objective lense provides more demagnification.[130] The point of demagnification is to form an atomic-scale probe at the sample. Aberrations from the objective lens dominate the optical system, so to avoid blurring of the probe an objective aperture is adjusted so that the impact of the aberrations is reduced. The scan coils are used to scan the probe over the sample. The occurring scattering pattern can be detected in several different ways. Here, bright field detection was used. In this mode only transmitted electrons which are scattered from the sample at low angles compared to the optic axis, are detected.[130] The final image is created as the scattered signals are plotted as a function of the probe position. For more information about STEM, please refer to Nellist, Wall, and Browning.[130–132]

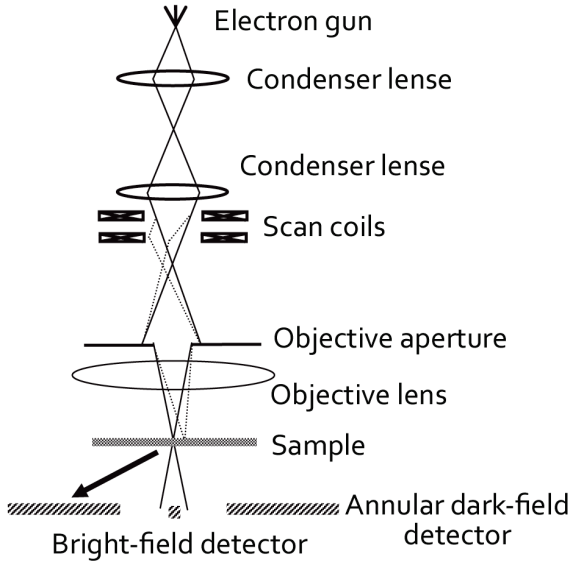

Figure 5.4: STEM instrumentation shown schematically. Adapted from Nellist.[130]

5.5 Steady-state fluorescence

Although UV-vis, ζ-potential measurements and DLS size measurements can be used to confirm protein adsorption onto AuNPs, they reveal little about the conformational changes in the adsorbed layer or the conformational changes in proteins as they are manipulated with AuNCs. Conformational changes can be studied using fluorescence, which is the emission of light from the singlet excited state (S). Singlet state means that the

electron in the exited state is paired (opposite spin) with the electron in the ground state, resulting in a zero net electronic spin. Phosphorescence, which is another type of luminescence, occurs from the triplet excited state (T).[63] The processes that take place between absorption and emission of light are normally illustrated by Jablonski diagrams (Figure 5.5).

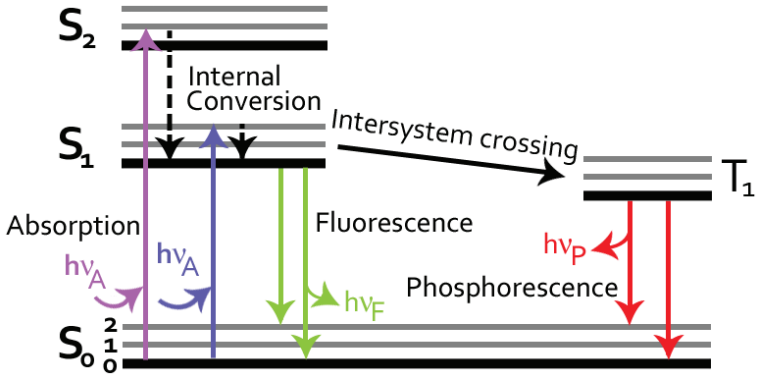

Figure 5.5: Example of a Jablonski diagram. Adapted from Lakowicz[63]

Fluorophores are usually excited to a higher vibrational level of S_1 or S_2 (Figure 5.5), and then rapidly relaxed to the lowest vibrational level of S_1. After this internal conversion, the fluorophore can either return to S_0 and fluoresce, or undergo an intersystem crossing to T_1. As seen from Figure 5.5 the energy of the emission is less than the absorption energy. This is called a Stokes shift and can be influenced by solvent effects, changes in viscosity, excited-state reactions, complex formation and energy transfer.

Here, steady-state fluorescence was used to confirm the formation of AuNCs, estimate AuNC size based on size-dependent shifts in emission, and estimate relative relationship between small and large AuNCs when AuNCs of several different sizes were made. This technique was also used to study changes in protein conformation, when proteins were manipulated with AuNCs or AuNPs. Both intrinsic and extrinsic fluorophores were used to study these conformational changes.

The aromatic amino acids tryptophan (Trp), tyrosine (Tyr), and phenylalanine (Phe) are all intrinsic fluorophores in proteins. However, when λ_{ex} = 295 nm the emission observed is mainly caused by Trp. Trp is well suited to study conformational changes, because its emission is highly sensitive to its local environment.[63] Blue shifts in Trp emission reveal a more hydrophobic environment (buried inside the protein/shielded from polar solvent), while red shifts indicate more hydrophilic surroundings (directed towards water/polar solvent). As proteins adsorb onto gold, or gold nanoclusters are formed within

the protein, electron or energy transfers from protein to gold result in quenching of the Trp emission, and a decrease in fluorescence intensity. With only one Trp present the emission spectrum is simple to interpret, but different proteins have different numbers of Trp. The Trps can be present in different environments depending on where in the proteins they are located. This makes the interpretation of Trp emission for protein-gold nanoclusters complex. Emission maxima of Trp is dependent on the environment surrounding it, and a shift in emission maxima is usually due to conformational changes such as unfolding. But a decrease in intensity can be due to both energy transfer to the gold species, and quenching as Trp-residues get more exposed to the solvent. Some of these interpretation challenges can be elucidated by adding an extrinsic probe. In papers I and II 1-anilino-8-naphthalene sulfonate (ANS), which is commonly used to study protein conformational changes,[133–138] was used for this task. ANS is weakly or non-fluorescent in water, while exposure to a less polar environment results in an increased quantum yield of the probe, as well as a shift of the emission profile. When the protein unfolds, the emission from ANS will decrease as the fluorophore goes from being associated with hydrophobic patches on the protein, to being more exposed to water.[63] Here, ANS was used to study protein unfolding upon adsorption onto AuNPs, but it was not possible to use ANS in studies with AuNCs because ANS and AuNCs are exited at the same wavelength (λ_{ex} = 370 nm), and small AuNCs also emitt at the same wavelength as ANS (around 450-470 nm). ANS can also be an energy donor, so that the ANS emission is quenched by the large AuNCs (acceptor).

Steady-state fluorescence can also be used to estimate the approximate size and abundance of gold nanoclusters. As explained in section 3.2, page 13, AuNCs consistent of a "magic number" of atoms, fluoresce when exited at 370 nm.[57] Small AuNCs then emit at λ_{em} ~450 nm, while larger nanoclusters (25 Au atoms, Au_{25}) show emission at λ_{em} ~685 nm. The emission wavelength is dependent on the size of the AuNCs, and the fluorescence intensity will be dependent on the cluster concentration.

A steady-state spectrum is an average of the time-resolved phenomena over the intensity decay of the sample.[63] Some information is lost in this averaging process, but this can be regained by time-resolved measurements, such as time-correlated single-photon counting (TCSPC). One example where TCSPC provides information lost in steady-state measurements, is when two Trps have different lifetimes, but are difficult to separate in an steady-state emission spectrum.

5.6 Time-correlated single-photon counting

Time-correlated single-photon counting (TCSPC) was used to gain more information about the conformational changes in proteins, when manipulated with different gold nanoconstructs.

The main information gained from TCSPC are lifetimes (T) and populations (B), which can be calculated from the decay fit shown in eq. 5.5.[139]

$$Y(t) = \sum_{i=1}^{N} A_i e^{-k_i t} \tag{5.5}$$

Here, Y(t) is the decay over time, A_i is the amplitude/fraction/population, k_i is the rate constant for each component, respectively, and N is the total number of luminescent contributers. A decay fit would look similar to that shown in Figure 5.6.

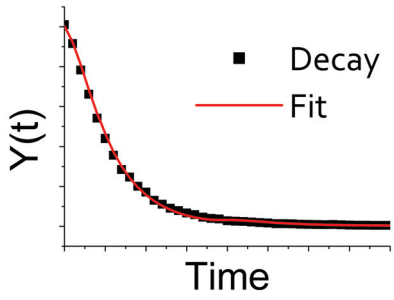

Figure 5.6: Example of fitted TCSPC decay as function of time.

Trp has a long lifetime when buried inside the hydrophobic interior of the protein and a short lifetime if close to a quencher, for example water. Thus, changes in lifetime, and population distribution between the lifetimes if more than one is observed, give information about the local environment of the Trp-residues. If the lifetime decreases, it is plausible that the protein has unfolded, exposing normally shielded Trp to water. Sometimes the lifetimes stay the same, and only the populations change. If the population changes in favor of the shortest lifetime, this too implies that more Trp is exposed to quencher and can imply unfolding.[140] If the lifetimes become longer, or the population of the longest lifetime increases, this indicates that more Trp is shielded from quencher and can be a sign of aggregation. Aggregation or flocculation would bury Trp that is on the surface of the folded protein inside larger protein aggregates or flocs, shielding the Trp from water. When a protein contains more than one Trp, the lifetimes obtained does not

necessarily represent each singular Trp-residue, but are gained from a mathematical fit of the decay curve (Figure 5.6).[63,139] BSA and aLa contain 3 Trps each, while LYZ contains 5 Trps, but for most of the proteins studied here, two lifetimes were obtained from the mathematical fit and precautions were taken as the data was interpreted. Even though interpretation sometimes must be done with care, TCSPC provide important information and the method is easy to use. A schematic overview of TCSPC electronics is given in Figure 5.7.

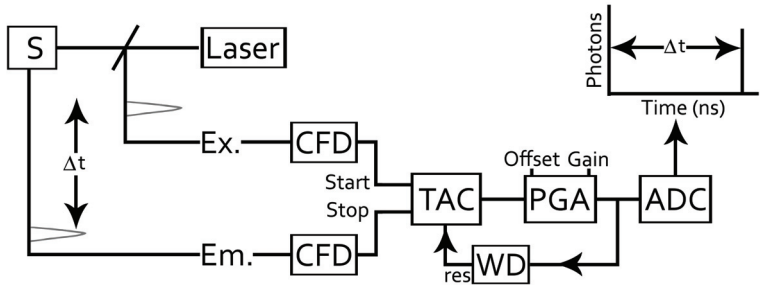

Figure 5.7: Schematic overview of the electronic set-up for TCSPC. Adapted from Lakowicz.[63]

A light emitting diode (LED) sends out pulses that excite the sample. As the pulse leaves the light source, a signal is passed through a constant function discriminator (CFD) which accurately measures when the pulse arrives (starts the stop watch). The signal is then converted to voltage by the time-to-amplitude converter (TAC), which starts a voltage ramp. The ramp is stopped as a single photon is detected in the CDF which sends a stop signal to the TAC (stops the stop watch). The voltage is linear to time, and is amplified by a programmable gain amplifier (PGA) and converted to a number using an analog-to-digital converter (ADC). A window discriminator (WD) suppresses the signal if it is outside the accepted voltage range. This is to reduce false readings. As the name time-correlated single-photon counting implies, the photons are counted rather than measured. The TAC needs to be reset to zero each time, and to avoid problems with premature arrivals of photons the procedure is often done in reverse mode. The voltage ramp is started in the TAC when the emitted photon enters, and stopped when the second excited photon arrives.[63]

5.7 Circular dichroism

Different types of fluorescence provide for indirect information about changes in conformation as proteins are manipulated with gold nanoconstructs, but reveal little about whether it is the secondary or only the tertiary structure that is altered. Circular dichroism (CD) can be used to gain more details about the conformational changes in the protein.

The principle behind CD-measurements is that compounds containing structural asymmetry, like chiral compounds and proteins, absorb right- and left circularly polarized light to different extents.[141] When the difference in absorption coefficients for the left- and the right circularly polarized light is given as a function of the incident light, a CD spectrum is created.[142] Compounds with no regular structure will result in zero CD signal. Figure 5.8 shows an example of left circularly polarized light.

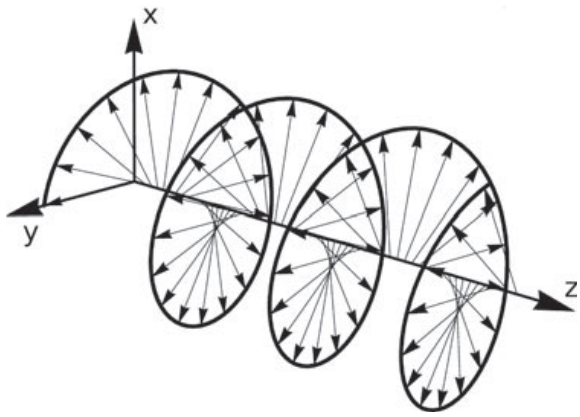

Figure 5.8: Left circularly polarized light. The light propagates in the z-direction and the electrical field vectors rotate in the x-y plane. (Reprinted with permission from Professor Furche.[142])

CD measurements in the far-UV region (< 250 nm) provides information about the secondary structure of the protein.[143] Alterations in protein conformation, such as random disorder or transformation of α-helixes into β-sheets, can be observed as changes in recorded the CD-spectra.[144,145] The ratio between signal intensities at 200/220 nm was also studied to make sure that observed spectral changes were actually due to alterations in protein conformation, not attenuation of the signal by the presence of gold nanoconstructs.

5.8 Langmuir-trough studies

One of the major goals of this study was to obtain constructs that could be candidates for targeted drug delivery. For such constructs, interfacial activity and lipid interactions are important properties. Langmuir-trough studies, and additional techniques connected to this technique, were the main methods used to study interfacial activity.

Films at an air-water surface formed by water insoluble species, such as lipids, are called Langmuir monolayer films. Water soluble species (e.g. many proteins) form films called Gibbs monolayers.[146,147] Langmuir phospholipid monolayer films at air-water surfaces are well established model systems for biological membranes, mimicking the interface between phospholipids and the surrounding aqueous media.[148–151] Combined with other techniques, these model systems can be used to study the composition and distribution of lipids in mixed lipid films, and how additives affect this distribution and film morphology.[152–154] Here, Langmuir-trough experiments were used to study air-water surface activity of native proteins, gold nanoparticles and protein-gold nanoconstructs. Interfacial interactions with phospholipid films were studied for the same species. Both equilibrium measurements and compression/decompression isotherms were obtained with this technique.

There are several ways to execute Langmuir experiments, and in this study both the Injected method (Figure 5.9 a and b) and the Subphase method (Figure 5.9 c and d) were used for introduction of proteins and other species to the trough.[148] For both methods

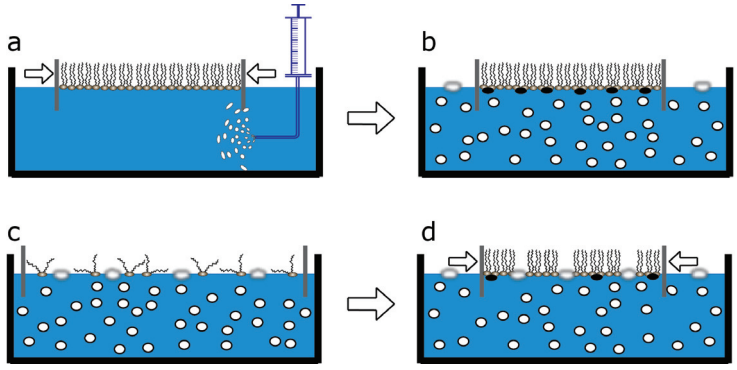

Figure 5.9: The upper panel (a and b) illustrates the Injected method, and the lower panel (c and d) illustrates the Subphase method.

the subphase is poured into the trough, and then the surfactant (dissolved in an organic solvent, usually $CHCl_3$) is spread on top. The choice of spreading agent can influence on the Langmuir isotherms obtained, and it is important that the spreading solvent solvates

the lipid well, does not mix with the subphase, and evaporates quickly.[155] The barriers can be moved to control the molecular arrangement and orientation at the surface. A Wilhelmy plate or a paper probe is used to monitor the surface pressure. When the Subphase method (Figure 5.9 c and d) is used to study the interaction between proteins in subphase and lipid films, the protein is already dissolved in the subphase when the lipid is spread on top. Thus, amphiphilic proteins will already be present at the surface as the lipid is introduced, and a mixed protein-lipid film can be formed. This mixed film can be avoided by using the Injected method (Figure 5.9 a and b), wherein the lipid is spread on a protein free subphase, and the protein is introduced first after the lipid film is compressed to the desired degree. The different ways of introducing the protein can have severe effect on the results achieved.[148] In addition to introduction protocol, adjustments of the physicochemical properties of the subphase, such as pH, temperature and ionic strength, can affect the results. For most of the studies here, phosphate buffers at pH 7.4 were used to mimic physiological conditions.

To interpret the data from Langmuir monolayer experiments it is helpful to know the different phase transitions which might occur during film compressions (see Figure 5.10). As a rigid film is compressed, such as phospholipid monolayers, the surface pressure will

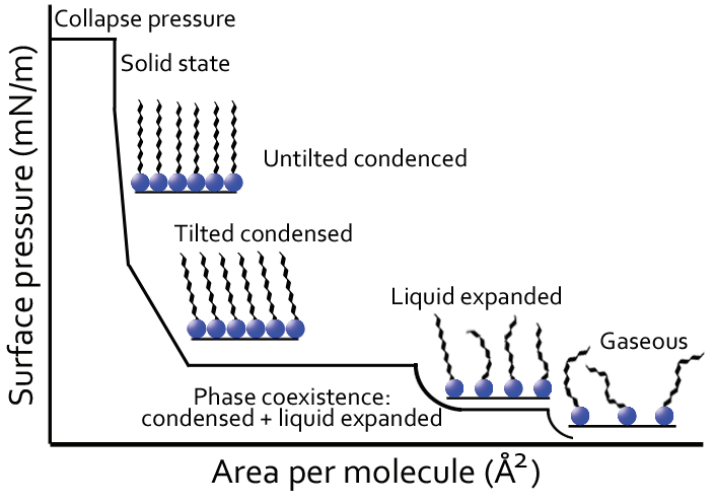

Figure 5.10: A generalized isotherm of a Langmuir monolayer. (Adapted from Kaganer[151])

increase rapidly. If the film is less rigid, or contains water soluble species, the surface pressure increases more slowly. This behavior is quite common for proteins. Interactions between proteins and lipids can be studied by observing changes in the compressibility of the mixed film compared to pure systems. Langmuir monolayer studies provide informa-

tion about film behavior, but it is difficult to understand exactly how lipids and proteins are distributed in the film. To obtain insight into film miscibility, the films can be studied with different types of microscopy directly at the interface or after being transferred to a solid surface.

5.8.1 Langmuir depositions

Two ways of transferring films from the air-water surface to solid surfaces are Langmuir-Blodgett (LB) and Langmuir-Schaefer (LS) depositions (Figure 5.11). Both types of depositions have advantages and drawbacks. The LB method can be used to make sequential deposistions and the transfer number can be calculated. The disadvantage is that the presence of solvent in the deposited layer can cause film runoff from the substrate. This is avoided in the LS deposition, but then it is not possible to make sequential depositions, and the transfer number is not known. Langmuir-Blodgett depositions were studied with Digital Video Microscopy, and Langmuir-Schaefer depositions were studied with Atomic Force Microscopy.

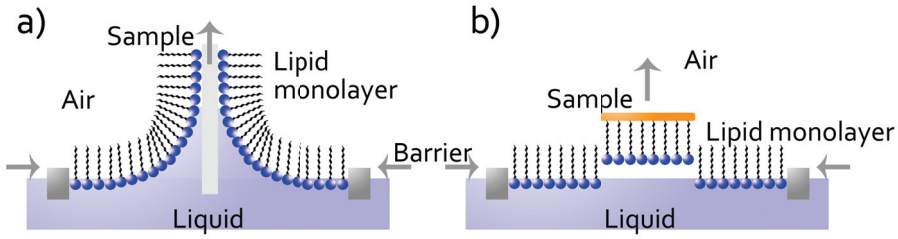

Figure 5.11: (a) Langmuir-Blodgett deposition and (b) Langmuir-Schaefer deposition.

To avoid any of the problems due to tranfer onto a solid surface, the film can be studied directly at the interface using Brewster Angle Microscopy (BAM).

5.9 Brewster Angle Microscopy

To obtain a visual understanding of distribution of lipids and proteins in the film, Brewster Angle Microscopy (BAM) was used. Examples of BAM images are given in Figure 6.2, page 45. The Brewster Angle (53° for water) is dependent on the refractive index of the system, and at this angle incident plane-polarized light is not reflected.[156] At the beginning of the Langmuir experiment, the laser light source and the camera is adjusted to the Brewster Angle of the subphase, and a completely dark image is achived. Lipids

and proteins change the refractive index and reflect light. The brightness of the different areas in the picture will then vary with film density and type of molecules in the sample area, making it possible to distinguish between different samples. In Figure 6.2, page 45 the lipids are seen as a dense, darker areas with bright spots, while the proteins are seen as light gray areas.

5.10 Digital Video Microscopy

The Langmuir-Blodgett depositions were studied using Digital Video Microscopy birefringence. The aim was to study whether the lipids formed liquid crystalline phases, and if protein-AuNPs could break up these structures. A liquid crystalline phase is defined as having short-range disorder but some distinct ordering over larger distances, with a liquid-like state of the alkyl chains.[146] When studying the sample through cross-polarized light, isotropic structures will result in a black image while anisotropic liquid crystals result in bright images (see paper I for an example).[146]

5.11 Atomic Force Microscopy

The Langmuir-Schaefer depositions made of protein or protein-gold nanoconstructs interacting with a lipid film, can be studied further using Atomic Force Microscopy (AFM). AFM is a high-resolution type of scanning probe microscopy at the level of atomic-resolution characterization.[157] A schematic presentation of the AFM set-up is shown in Figure 5.12.

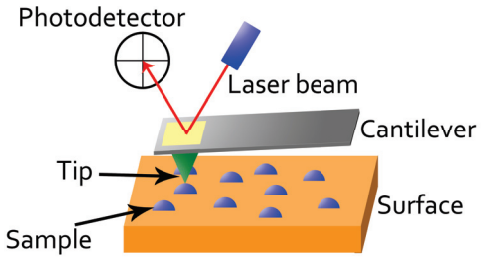

Figure 5.12: A reflected laser beam reports changes in cantilever positon to a photodetector while moving across the surface of the substrate. Adapted from Kada *et al.*[158]

The measurements can be done in three different modes; contact mode, noncontact mode, or tapping mode.[157] The latter was used for the measurements presented in paper

V. In the contact mode the tip of the cantilever is in contact with the sample, measuring interaction forces, while for the noncontact mode the cantilever is moved slightly away from the sample while oscillating at/near its natural resonance frequency. The tapping mode contains aspects from both of the other techniques: the tip of the cantilever oscillates near its natural resonance frequency and is for a minimal amount of time allowed to impact with the sample.[157] The point of the tapping mode is to keep the tip close enough to the sample surface to detect short range forces without sticking to it, and can be used to measure soft samples that are difficult to measure with the contact mode. In tapping mode a piezoelectric actuator makes the cantilever vibrate with specific amplitude (20-100 nm). When the tip gets close to the surface, interaction forces will reduce the amplitude of this oscillation. An optical system detects this alteration, and generates a signal that makes the piezoelectric element adjust so that a constant distance between cantilever and sample surface (and thus constant amplitude) is maintained.[157] The changes in the vertical position of the tip is expressed as a function of its lateral position, and this information is then used to generate the AFM image. In addition to measuring topography, AFM can be used to study elasticity, hardness, adhesion and surface charge densities.[159] For further information about AFM and it's use in biochemistry see papers by Jalili *et al.*,[157] Gan,[160] Kada *et al.*,[158] and Gadegaard.[161]

5.12 Cell-viability studies

To test if the aLa-gold nanoconstructs made had HAMLET-/BAMLET-like cancer cell killing efficiency, the cell-viability of HeLa cells in the prescence of aLa, BAMLET, aLa-gold nanoconstructs, and other possible interferrents were tested in a trypan blue assay. In this assay dead cells are dyed blue, while living cells remain unstained (Figure 5.13).[162–164] After incubation the number of blue cells were counted using confocal microscopy.

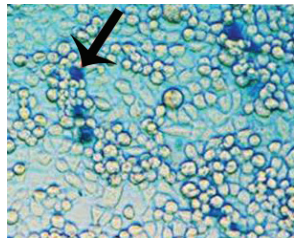

Figure 5.13: Typan blue colors dead cells, while live cells remain unstained.[164]

6. Results and discussion

In this chapter the main highlights from papers I-V are written together, beginning with proof of concept, via manipulation of different proteins using a variety of gold nanoconstructs, and ending with a protein-gold nanoconstruct exhibiting similar mortality rates towards cancer cells as BAMLET. Each section corresponds to the paper with the same name in List of publications.

Bovine serum albumin (BSA) was chosen for the first study because it is readily available and, despite the big difference in molecular weight compared to aLa, BSA has many structural and physiological resemblances to alpha-lactalbumin (aLa).

6.1 Emergent membrane-affecting properties of BSA-gold nanoparticle constructs

Nanoscale, **2011**, 3, (4), p. 1788-1797

Because of their optical and biological properties, protein-coated gold nanoparticles are often studied for potential use in bioimaging and targeted drug delivery.[4,7,10,79–85] It is also known that adsorption onto interfaces may alter protein-conformation.[83,165] The main focus of paper I was to investigate how the adsorption of BSA onto gold nanoparticles with different curvatures would alter BSA conformation, and properties such as interfacial activity. BSA was adsorbed onto both 30 nm and 80 nm citrate covered gold nanoparticles, and protein-AuNPs were studied with UV-vis spectroscopy, ζ-potential measurements, steady-state and time-resolved fluorescence. Langmuir monolayer studies (both Subphase method and Injected method) accompanied by Brewster Angle Microscopy (BAM), Langmuir-Blodgett deposition and Digital Video Microscopy (DVM) were used to investigate differences in phospholipid monolayer interactions for protein-gold nanoparticles compared with native protein.

While UV-vis spectroscopy and ζ-potential measurements confirmed protein adsorption, these techniques revealed little about the degree of unfolding. Therefore, unfolding

was studied using steady-state (Figure 6.1) and TCSPC (Table 6.1) fluorescence techniques.

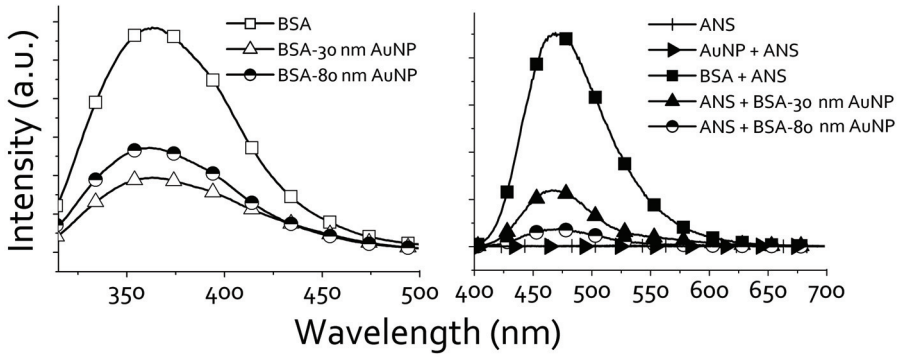

Figure 6.1: (a) Steady-state Trp fluorescence of BSA and BSA-AuNPs (λ_{ex} = 295 nm). (b) Steady-state fluorescence of samples with ANS (λ_{ex} = 388 nm)

The decrease in Trp fluorescence intensity for BSA (Figure 6.1 a), when adsorbed onto AuNPs, can be both due to protein unfolding, which exposes Trp to water and quenches the signal, and energy transfer from Trp emission to AuNPs absorption. Also for samples containing 1-anilino-8-naphthalene sulfonate (ANS) (Figure 6.1 b), there was a AuNP-size dependent loss of intensity. This can mean that BSA unfolded more on the larger particles, pushing the ANS from the hydrophobic interior of the protein towards the hydrophilic solvent. ANS is a lot less fluorescent in a hydrophilic environment than in a hydrophobic one.

Table 6.1: Fluorescence lifetimes and corresponding populations of BSA, BSA-AuNPs and samples with added ANS. T = lifetimes in nanoseconds (ns), B = populations in %[a]

	T1 (ns)	**B1** (%)	**T2 (ns)**	**B2 (%)**	χ^2
Protein-gold nanoparticles (λ_{ex} = 280 nm)					
BSA	4.0	23 ± 4	7.1	77 ± 4	0.86
BSA + 30 nm AuNP	3.8	32 ± 3	7.1	68 ± 3	1.21
BSA + 80 nm AuNP	3.7	30 ± 4	6.9	70 ± 4	1.11
ANS and protein-gold nanoparticles (λ_{ex} = 370 nm)					
BSA	4.7	6 ± 1	18.5	94 ± 1	0.99
BSA + 30 nm AuNP	5.7	8.4 ± 0.1	19.0	91.6 ± 0.1	1.00
BSA + 80 nm AuNP	6.6	11.4 ± 0.6	19.1	88.7 ± 0.6	0.98

[a] For aqueous ANS the lifetime in nanoseconds was $T1 = 5.4 \pm 0.8$, $T2 = 18 \pm 2$, and $T3 = 0.27$ with the corresponding populations $B1 = 8 \pm 1$, $B2 = 12 \pm 2$, and $B3 = 80 \pm 2$, respectively.

Table 6.1 (upper panel) shows that for intrinsic fluorescence there was no significant

changes in lifetimes for the BSA-AuNPs compared to the free protein. However, the relative population (B1) of the short lifetime (T1) increased (see Table 6.1). The total available AuNP-surface area was lower in the 80 nm AuNP suspensions than for the 30 nm suspensions, but both of the protein-AuNPs had similar lifetime populations. To achieve this, BSA must have unfolded more on the larger AuNPs than on the smaller ones. This is in agreement with the studies by Kane *et al.*[1] For ANS fluorescence in the lower panel in Table 1 the short lifetime (T1) increases progressively upon adsorption onto AuNPs and with increasing particle size, whereas the longer lifetime (T2) remained unchanged for all three systems. The small increase in T1 may be due to close packing of BSA on the AuNP surfaces, which is expected to increase with increasing core diameter. The increase in B1 with increasing particle diameter can be caused by a higher degree of protein unfolding and a subsequent exposure of ANS to water. All in all, the steady-state fluorescence data combined with the TCSPC data imply that BSA unfolded more on the larger particles.

After establishing protein adsorption onto AuNPs and concomitant partial unfolding, native protein, AuNPs, and protein-AuNPs were tested towards Langmuir lipid monolayers. BAM-pictures are shown in Figure 6.2. Using the Injected method it was not easy to

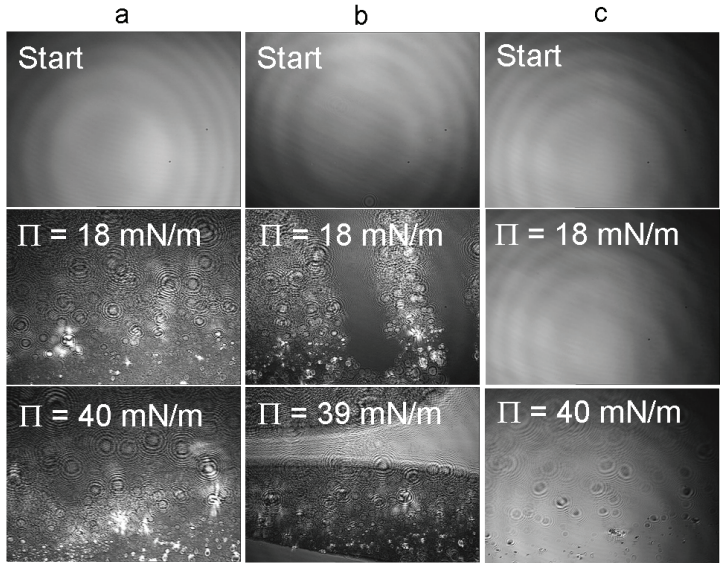

Figure 6.2: BAM images of BSA and BSA-AuNPs interacting with lipid Langmuir films. (a) Injected method with BSA, (b) Subphase method with BSA, and (c) Subphase method with BSA onto 30 nm AuNP

observe any differences between native protein (Figure 6.2 a) and protein-gold nanocon-

structs (not shown), but for the Subphase method there were large differences. BSA interacting with the phospholipid film (Figure 6.2 b, page 45) resulted in two distinct domains at high pressure: one corresponding to the lipid (dark regions with bright fields) and one corresponding to BSA (light, homogeneous regions). This means that introduction of BSA via the Subphase method resulted in mixed-film behavior, with immiscible lipid-like and protein-like domains.[148] Conversely, using the Subphase method BSA-AuNPs interacting with the lipid film (Figure 6.2 c) show no domain formation at any surface pressure. Rather, the morphology of the BSA-AuNPs-lipid film appear indistinguishable from that of a BSA film only (6.2 b, start), save for some small regular structures towards maximum compression (Figure 6.2 c, lower panel). Paper I demonstrates that BSA unfolds more on the 80 nm AuNP than on the 30 nm AuNP, and most importantly that BSA-AuNPs induce a film miscibility with L-α-phosphatidylethanolamine not seen for BSA or AuNP alone. The changes induced by partial unfolding clearly give better film penetration ability, as well as disruption of liquid crystalline domains in the film, thereby inducing film miscibility. The emergent membrane-affecting properties of BSA-AuNPs might enable the constructs to work as drug transporters across cell membranes, or the constructs might even be used as a medicines by themselves. In general the emergent properties are interesting from a medical point of view, especially since one of the theories behind the apoptosis-inducing properties of HAMLET is linked to the conformational changes in aLa and the high affinity to phospholipid membranes. This is also the reason why aLa was modified with AuNPs in paper II.

6.2 Immobilization onto gold nanoparticles alters α-lactalbumin interaction with pure and mixed phospholipid monolayers

Soft Matter, **2011**, 7, (24), p. 11501-11509

To get at closer link to HAMLET/BAMLET and medical use, similar protein-gold nanoparticles were made with aLa as for BSA (paper I). To be able to compare results for the two proteins, the protein concentration in the aLa experiments were the same as for the BSA experiments. At these concentrations aLa was not able to stabilize 80 nm AuNPs, thus only the 30 nm AuNPs were used for this study. The problems with stabilization can be due to that aLa is much smaller than BSA, and unfolded too much at the AuNPs so that too many hydrophobic groups were exposed.

HAMLET interacts differently with lipid membranes than aLa does, and this is probably due to conformational differences between the proteins. As seen for BSA in paper I, it is likely that adsorption of aLa onto AuNPs will alter the protein conformation. How the conformational changes in aLa affect interaction with lipid films can then be tested towards neutral, negatively charged and mixed neutral:negative phospholipid Langmuir monolayers at pH 7.4, where little or no interaction has been reported for native aLa.[166,167]

Characterization of aLa-AuNPs was performed using UV-vis and fluorescence (steady-state and time-resolved, using both intrinsic and extrinsic probes) spectroscopies. Paper II focuses on the interaction of bovine aLa-modified 30 nm AuNPs with the three different lipid monolayers mentioned above. The resulting equilibria and film properties were studied using surface pressure-area isotherms.

UV-vis measurements of aLa and aLa-AuNPs provided the same information as found for BSA in paper I, i.e. proteins were adsorbed onto gold, and the protein-gold nanoparticles did not aggregate. Steady-state data is presented in Figure 6.3, page 48 and TCSPC data is presented in Table 6.2 at the same page. Due to protein excess with respect to maximum surface coverage, the fluorescence shown in Figure 6.3 emanates from both free and bound protein. However, since aLa concentration was kept constant, alterations to the spectral signatures of both Trp and ANS can be attributed to adsorbed protein.

The loss of both Trp and ANS fluorescence intensities (Figure 6.3) were similar to what was observed for BSA-AuNPs in paper I. The changes in lifetimes and populations observed in Table 6.2 were also very similar to what was observed for BSA (Table 6.1,

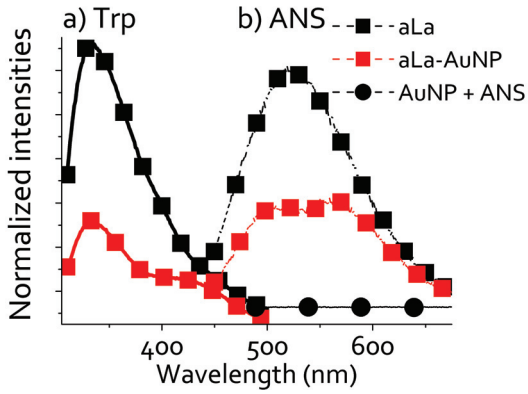

Figure 6.3: (a) Intrinsic Trp steady-state measurements of aLa and aLa-AuNP, λ_{ex} = 295 nm. (b) Extrinsic steady-state measurements of aLa and aLa-AuNP using ANS as extrinsic probe, λ_{ex} = 370 nm.

page 44) and it is very likely that the changes observed are due to conformational changes in aLa as it unfolds on AuNPs. Some of the loss in intensity will also be due to energy transfer from Trp to AuNPs, as AuNPs (acceptor) absorb the energy emitted by Trp (donor).[133–138]

Table 6.2: TCSPC of intrinsic emission (Trp, LED 280 nm), and extrinsic emission (ANS, LED 370 nm). T1 and T2 denote lifeteimes, and B1 and B2 are their respective populations.

	Intrinsic		**Extrinsic**	
	aLa	*aLa-AuNP*	*aLa*	*aLa-AuNP*
T1 (ns)	0.86 ± 0.01	0.85 ± 0.04	0.37 ± 0.01	0.35 ± 0.01
T2 (ns)	5.0 ± 0.2	4.6 ± 0.3	7.5 ± 0.2	8.8 ± 0.3
B1 (%)	91.5 ± 0.1	81.3 ± 0.1	86.1 ± 0.1	91.8 ± 0.1
B2 (%)	8.5 ± 0.1	18.7 ± 0.1	13.9 ± 0.1	8.2 ± 0.1

UV-vis-, DLS-, and fluorescence measurements confirmed that aLa had adsorbed onto the AuNPs and that the protein had partially unfolded at the surface. Then, Gibbs- and Langmuir monolayers were used to study how the conformational changes altered the constructs' surface activity and phospholipid affinity relative to the native protein. The Injected method was used (described in section 5.8, from page 37) for three different phospholipid monolayers: (1) neutral (EYPC = L-α-phosphatidylcholine), (2) negatively charged (PBPS = porcine brain phosphatidylserine), and (3) neutral:negative (1:1) molar ratio. The equilibria for aLa and aLa-AuNP injected under the different interfaces are shown in Figure 6.4.

Unmodified AuNPs precipitated under these conditions, and did not contribute to the

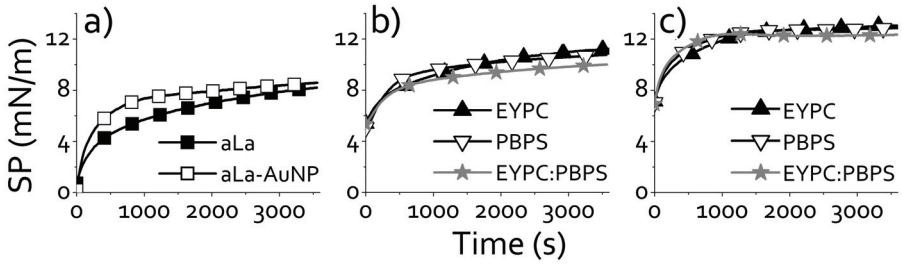

Figure 6.4: (a) Equilibria for native protein and protein on gold the first hour after injection under an air-water surface.(b) Equilibria for aLa injected under pure and mixed (1:1 molar ratio) phospholipid monolayers (compressed to 5 mN/m) (c) Same as b, but with aLa-AuNP injected under the lipid films.

increase in surface pressure observed in Figure 6.4. As seen from Figure 6.4 a, the initial surface pressure increased more rapidly for aLa-AuNP than for native aLa. However, the final surface pressures after one hour of equilibrium were approximately the same. For the aLa-AuNP experiments there were contributions from both free aLa and aLa-AuNP. It is likely that the initial rapid increase in surface pressure was due to more surface active aLa-AuNPs. The observation that the equilibrium pressures were more or less equal for both systems can be explained by the fact that both samples contained the same amount of aLa. Compression- and expansion isotherms (see paper II for graph) show no collapse pressure for the aLa and aLa-AuNP monolayers, meaning that both species were water soluble. The Gibbs monolayer studies also showed a higher surface pressure throughout the measurements for aLa-AuNP than for native aLa, indicating a higher surface activity.

When interacting with the three different phospholipid monolayers, aLa and aLa-AuNP displayed no phospholipid selectivity (Figure 6.4 b and c). However, there was an increase in surface pressure as aLa and aLa-AuNP were injected under the pre-compressed phospholipid films, indicating interaction between the phospholipid film and the injected species. This means that even though former studies have claimed little or no interaction between native aLa and lipid films at pH 7.4, interactions were observed in these experiments.[166,167] These differences in observations of interaction can be attributed to the introduction method of the protein. While proteins are subjected to a precompressed lipid film when using the Injected method, there is a mixed protein-lipid film present at the surface from the start when the Subphase method is used. (See also section 5.8 from page 37). Here, the Injected method was used, while former studies have used the Subphase method. The initial rates of surface pressure increase were higher for aLa-AuNP (Figure 6.4 c) than for native aLa (Figure 6.4 b), which is consistent with enhanced hydrophobic

interaction from partial exposure of hydrophobic residues in the adsorbed protein. Also, the equilibration of aLa-AuNP towards phospholipid monolayers (Figure 6.4 c) occurs faster than towards an air-water surface (Figure 6.4 a). Thus, the increased surface migration rates and the higher saturation plateaus in the presence of a phospholipid monolayer reveal an enhanced phospholipid affinity for the aLa-AuNPs as compared to native aLa. Compression and expansion isotherms also indicate that aLa-AuNP intercalates more with the phospholipid film than does native aLa, thereby making the films more compressible.

The fact that adsorption of aLa onto gold enhances film-penetration may be of value within studies of i.e. drug delivery systems, and also for a better understanding of protein based drug candidates where folding seems to matter, such as in the case of HAMLET. One possible hurdle to further clinical development of HAMLET or similar preparations may be their tendency to lose potency in many clinical situations, probably due to loss of oleic acid to scavenger proteins such as serum albumin.[168] This would have the effect of both reverting the protein to its native state and separating the components of HAMLET, both of which appear to be necessary for activity.[40]

Even though the increased interaction with phospholipid films seen for aLa-AuNP opens for a very interesting link to HAMLET/BAMLET, there are some problems associated with the adsorbance of proteins onto AuNPs. How much the conformation changes is protein dependent, and as several proteins adsorbes onto one AuNP there are more variables than if single proteins were manipulated. Moreover, an excess of protein was used in the adsorption process, making it difficult to distinguish between effects from protein-AuNP and native protein. Removal of excess protein through dialysis may cause uncertainties in protein concentration. Usually, this problem can be solved by UV-vis determination of protein concentration, but the prescence of gold influence the protein absorbance spectrum too much. Centrifugation/resuspension cannot be used either, as such experiments lead to aggregation of protein-AuNPs. Conformational changes induced by adsorption onto AuNPs are very large, and sometimes difficult to tune. One joint solution for both these problems could be protein-stabilized gold nanoclusters (protein-AuNCs). By varying the amount of reagents and reaction time, it should be possible to control the extent of conformational changes induced in the protein. All proteins present in the solution are also likely to take part in the reaction, leaving no unmodified excess protein. There are other benefits of using aLa-AuNCs as well. Due to intracellular leaching of oleic acid from HAMLET it is difficult to know whether the anticancer activity observed is due to the complex as a whole, or due to the single components. In the aLa-AuNC complex, the AuNCs are covalently bound to the protein and the uncertainties in data interpretation due to leaching can be circumvented.

6.3 Tunable photophysical properties, conformation and function of nano-sized protein-gold constructs

RSC Advances, **2013**, 3, (2), p. 482-495

One way of making protein-stabilized AuNCs is by mixing protein, gold precursor (Hydrogen tetrachloroaurate(III) x $3H_2O$, TCAA) and reducing agent.[57,58] Due to the addition of extrinsic reducing agent, this method is reffered to as the the extrinsic method. Figure 6.5 shows the different types of gold nanoconstructs formed.

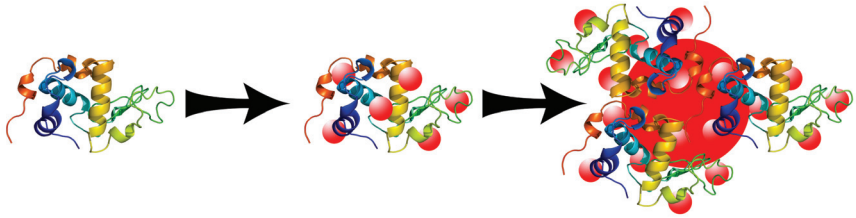

Figure 6.5: By controlling the reaction conditions, proteins can be modified with gold nanoconstructs varying from subnanometer clusters to plasmonic nanoparticles.

In the work presented in paper III, bovine serum albumin (BSA), bovine alpha-lactalbumin (aLa) and chicken egg white lysozyme (LYZ) were selected for manipulations with protein-stabilized AuNCs and AuNPs. The proteins were selected so as to allow for large variety with respect to variables such as size, isoelectric point (pI) and conformational stability. BSA is a readily available reference protein with the same pI as the much smaller aLa. This leads to comparable global charge density matching with the Au^{3+} and opens for protein size-dependent variations in gold nanocluster stabilization. LYZ is a classical rigid protein of the same size as aLa, but with a different pI, which allows for studying how protein charge and rigidity affects gold nanocluster formation and stabilization. In addition, LYZ also provide correlation between unfolding and concomitant protein function via a simple activity assay.

Sodium borohydride ($NaBH_4$) was used as reducing agent because it cannot stabilize AuNCs or AuNPs by itself, implying that all gold nanoconstructs formed must be protein-stabilized. The fast reduction rate of $NaBH_4$ also prevents competition from gold nanoclusters formed within the protein by amino acid residues such as tyrosine acting as reducing agents.[56] By adjusting the ratio between gold precursor and reducing agent, it is likely that AuNCs of variable sizes are formed, and that these constructs affect the protein conformation and function to different extents.

Native proteins, proteins with only reducing agent added, and proteins with both gold precursor and reducing agent added were studied using UV-vis (Figure 6.6 b) and fluorescence (Figure 6.6 c and d) to investigate the gold nanoconstructs formed as well as conformational changes in the protein-gold nanoconstructs. Circular dichroism (CD) was used for further evaluation of changes in conformation (Figure 6.7) while scanning transmission electron microscopy (STEM) was used for size and dispersity studies of the gold nanoconstructs. The LYZ activity was studied by measuring transmittance as LYZ digested the cell walls of *Micrococcus lysodeikticus* bacteria.[169] The rate of increase in transmittance reflects the activity of the LYZ-AuNCs compared to native LYZ (see Figure 6.8, page 53).

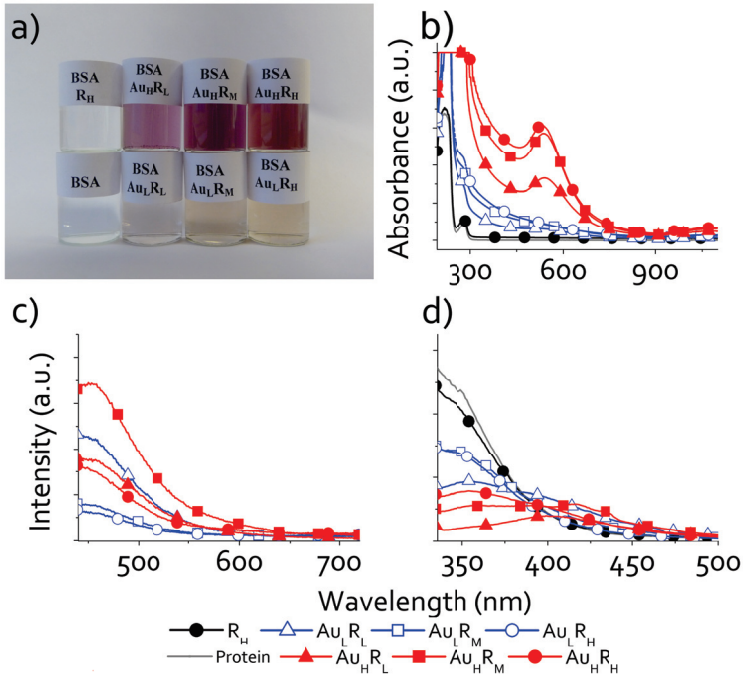

Figure 6.6: (a) Picture of the different BSA-gold nanoconstruct samples studied. (b) UV-vis spectra for BSA-gold nanoconstruct samples. (c) Steady-state fluorescence of aLa-gold nanoconstructs, λ_{ex} = 370 nm. (d) Steady-state fluorescence of aLa and aLa-gold nanoconstructs, λ_{ex} = 295 nm. Here the abbreviations denote the following; Au = gold, R = Reducing agent, L, M, H = Low, Medium and High concentrations, respectively.

Immediately after addition of reducing agent, gold nanoconstructs were formed and induced a color change in the reaction mixture (as depicted by BSA in Figure 6.6). The red color seen for samples with high content of TCAA is very typical of suspensions

containing AuNPs. The presence of AuNPs > 3 nm was confirmed by the LSPR band at ~530 nm observed in the UV-vis spectra in Figure 6.6 b. The distortion of the 280 nm absorbance band indicates the presence of multimeric gold species. Steady-state fluorescence with λ_{ex} = 370 nm (Figure 6.6 c) revealed that mostly small AuNCs (Au_8) were formed. However, low concentration of TCAA combined with medium and high concentration of $NaBH_4$ led to the formation of large AuNCs (Au_{25}) with BSA. As shown in Figure 6.6 d, steady-state fluorescence (λ_{ex} = 295 nm) imply a tunable conformational change in the protein as gold nanoconstructs are formed. This conformational tunability was further confirmed by CD measurements (Figure 6.7).

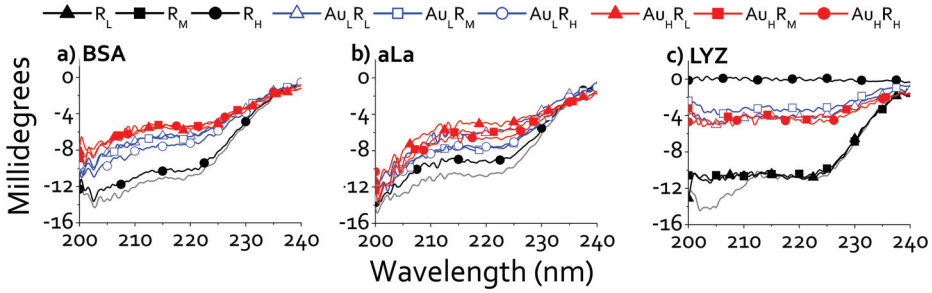

Figure 6.7: CD-spectra of (a) BSA and BSA-gold nanoconstructs, (b) aLa and aLa-gold nanoconstructs, and (c) LYZ and LYZ-gold nanoconstructs

Both CD and fluorescence studies showed that $NaBH_4$ disrupt the conformation of LYZ, while the formation of gold nanoconstructs partially stabilized it. The same trend was observed for the LYZ cell wall digesting activity data in Figure 6.8.

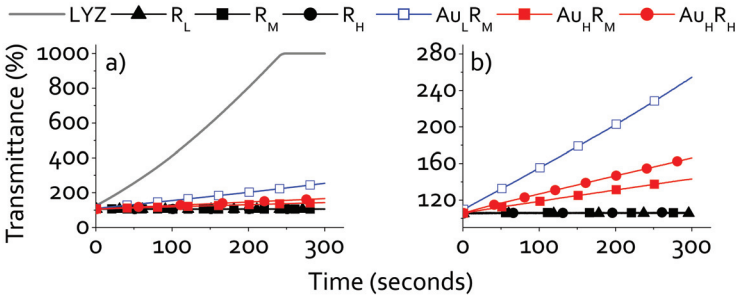

Figure 6.8: Cell wall digestion activity of lysozyme, Lysozyme with $NaBH_4$ and lysozyme-gold nanoconstructs at pH 6.2, and 30 °C. The change in transmittance starts at 100% and a transmittance increase means that *Micrococcus lysodeikticus* cell walls are digested. (a) All results, (b) the dataset for the native protein is removed.

UV-vis, fluorescence and CD results showed that by varying the gold precursor con-

centration it was possible to tune the constructs from protein-AuNCs to AuNPs stabilized by protein-AuNCs (Figure 6.5), and by simultaneously changing reducing agent concentration the sizes of both kinds of constructs could be tuned from small and monodisperse to larger and polydisperse. As an effect of the different construct sizes, the protein structure was also affected to different extents. For BSA, aLa and LYZ, aLa was the most tunable protein, while LYZ was most disrupted. Even though $NaBH_4$ severely disrupts LYZ conformation, the gold nanoconstructs formed seem to stabilize LYZ enough to maintain some cell-wall digesting activity. Although the functions of aLa and BSA were not assayed, it is reasonable to assume that these proteins may also be prepared with covalent cluster or particle modification in a manner that allows retaining at least part of their function. The spectroscopic data suggests an incremental perturbation of the protein fold, and it may be that this feature could be used to lock proteins in folding intermediates that would otherwise not be thermodynamically stable and amendable to investigation. Such a possibility would be of high relevance for the general study of folding intermediates and particle-associated states in particular, both problems being relatively inaccessible with traditional techniques.[24] The fact that aLa was the most tunable protein, both regarding protein conformation and in size of gold nanoconstructs, is very promising for comparison with HAMLET activity. It is also possible that aLa-gold nanoconstructs can aid in the understanding of the mechanism behind HAMLET. The fact that the AuNCs formed are fluorescent also provides for an optical label. The tunability in conformation and function combined with an inherent optical label make these protein-gold nanoclusters very interesting for medical use. It is likely that the constructs can be used for bio-imaging and biosensors.[5,74,90,91] However, $NaBH_4$ had destructive effects on LYZ and to some extent on aLa and BSA. This suggests that a milder reducing agent, which does not disrupt the protein by itself, is more preferable.

6.4 Generally applicable procedure for *in situ* formation of fluorescent protein-gold nanoconstructs

RSC Advances, **2012**, 2, (31), p. 11704 - 11711

One way to solve the problem observed in paper III with harsh $NaBH_4$ effects on some proteins in the synthesis of protein-AuNCs, is to utilize the reduction potential of amino acids already present in the protein through a biomineralization-like synthesis. Since the reducing agents are intrinsic in the protein, this method is referred to as the intrinsic method. The method was adapted from Xie *et al.*[56] wherein hydrogen tetrachloroaurate(III) x $3H_2O$ (TCAA, 10 mM) is added to an equal volume of BSA (50 mg/ml) at 37 °C under vigorous stirring. After 2 minutes NaOH (1M, 1/10 the volume of protein) is added. Xie *et al.* incubated their reaction mixture for 12 h at 37 °C. In the study presented here, the samples were incubated for 1 week. The amino acid composition of proteins, and hence their reductive ability, is very diverse. Thus, to make a generally applicable procedure for *in situ* formation of fluorescent protein-gold nanoconstructs it was necessary to study a small library of different proteins. The proteins included in this study were chosen based on differences in size, isoelectric point, flexibility and 3-dimensional structure. Some of their molecular properties are listed in Table 6.3.

Table 6.3: Molecular properties of the proteins used in this study

Protein	Abbreviation	Mw (kDa)	pI
Bovine serum albumin	BSA	67.0	4.7-4.9
Porcine plasma fibrinogen	Fib	340.0	N/A
Bovine milk holo alpha-lactalbumin (type I)	aLa	14.2	4.5
Chicken egg white lysozyme	LYZ	14.3	10.5
Bovine heart cytochrome C	CytC	12.4	10.1
Horse heart myoglobin	Mb	17.2	6.8-7.0
Bovine milk β-lactoglobulin	BLG	18.0	3.5-5.2
Bovine pancreas α-chymotrypsin	CTR	25.0	8.8

When the samples were illuminated with UV-light (Figure 6.9, page 56) it was possible to see from the varying colors that different types of gold nanoconstructs were formed. The different protein-gold nanoconstructs were further studied with UV-vis measurements and steady-state fluorescence (λ_{ex} = 370 nm, Figure 6.10, page 56). Only the a selection of proteins in the full study is represented in the further discussion. For more details please consult paper IV. From Figure 6.10 a and b it can be observed that the UV-vis spectra for the protein-gold nanoconstructs differ in both line shape and intensity as com-

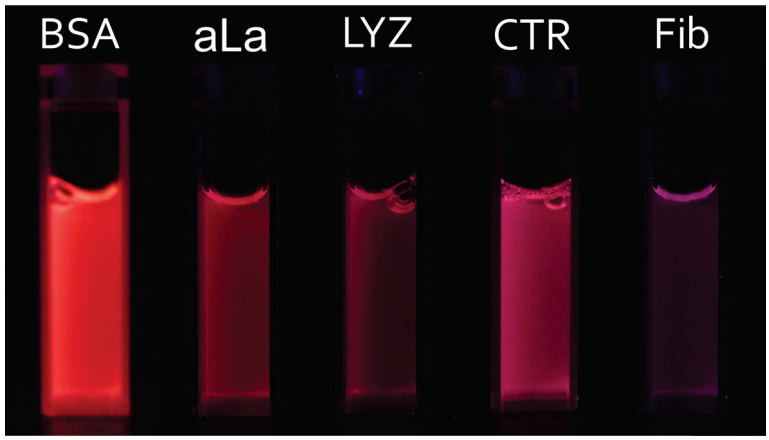

Figure 6.9: Photograph of aqueous solutions of five of the proteins used here (concentration 35.5 μM) upon illuminated with UV-light λ_{ex} = 365 nm.

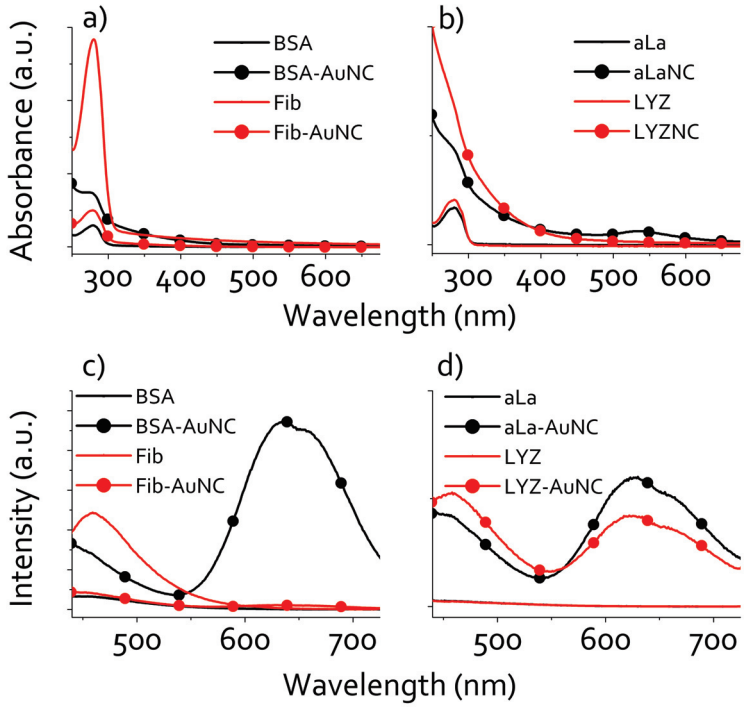

Figure 6.10: (a) and (b) represent UV-vis spectra of a selection of proteins and protein-gold nanoconstructs used in this study. (c) and (d) show fluorescence spectra of the same selection of proteins and protein-gold nanoconstructs (λ_{ex} = 370 nm).

pared to the native protein. The broad absorption below ~400 nm is likely due to the incorporation of gold nanoclusters. For some of the proteins (e.g. aLa) a LSPR band was also observed at ~550 nm, indicating formation of AuNPs as well. The emission spectra in Figure 6.10 c and d show that the ratio between small (Au_8, λ_{em} ~450 nm) and large (~Au_{25}, λ_{em} ~625-675 nm) nanoclusters was dependent on the protein wherein these were formed. The different types of gold nanoconstructs are likely to affect protein conformation to different extents, which is why protein conformation was studied with CD-measurements, steady-state Trp fluorescence (λ_{ex} = 295 nm) and TCSPC measurements. A selection of CD and steady-state Trp fluorescence data are given in Figure 6.11. The Trp emission profiles in Figure 6.11 a and b show a decrease in intensity for

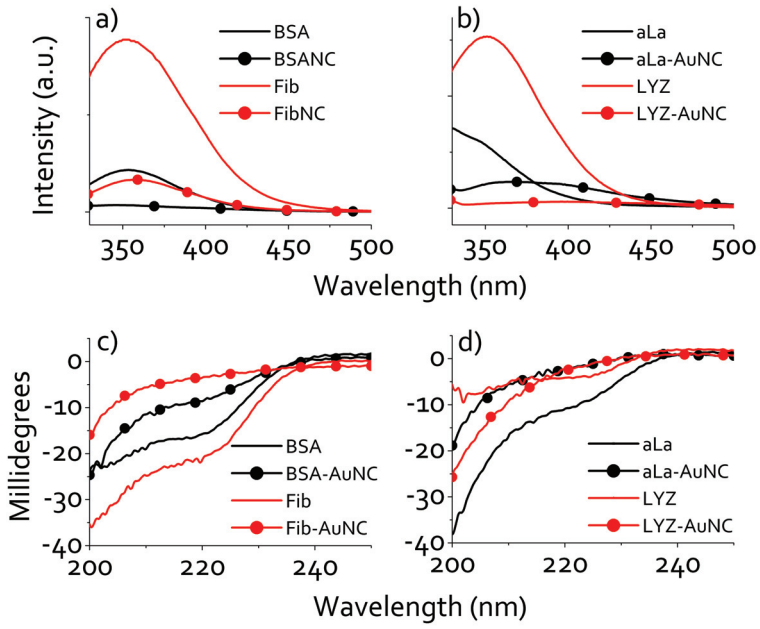

Figure 6.11: (a) and (b) show Trp fluorescence spectra of a selection of proteins and protein-gold nanoconstructs (λ_{ex} = 295 nm). (c) and (d) show CD spectra of this selection of proteins and protein-gold nanoconstructs

all the protein-gold nanoconstructs as compared to the native proteins, but to what extent the intensities change, varies for the different proteins. The emission profiles were also shifted to longer wavelengths (red shifted). The decrease in intensity can be due to energy transfer to AuNCs or AuNPs, which corresponds well with the UV-vis spectra in Figure 6.10, page 56. However, some of the reduction in Trp emission intensities and the red shifts were probably due to Trp being exposed to water as the proteins partially unfolded.

Also, the alterations in intensities and line shapes in the CD-spectra (Figure 6.11 c and d) indicated changes in protein conformation.

The type of gold nanostructure formed, the photophysical properties of the protein-gold nanoconstructs as well as the accompanying conformational changes were found to be highly protein-dependent. Using a combination of UV-vis spectroscopy and steady-state fluorescence measurements, three primary sets of gold nanoconstructs formed were identified as fluorescent clusters of ~8 and ~25 atoms (small and large AuNCs, respectively) and nanoparticles (AuNPs) of diameters > 3 nm displaying localized surface plasmon resonance (LSPR), with all three structures occurring within the same system for the two milk proteins studied here, aLa and BLG.

By combining the results above with Berti and Burley's postulated mechanism for nucleic acid and nucleotide-mediated synthesis of inorganic nanoparticles,[170] and Feldheim and Eaton's SELEX model for biomolecule-mediated crystal formation,[171] a mechanism for protein-gold nanoconstruct formation in four steps can be proposed:

1. **Nucleation.** Charge density matching between Au^{3+} and negatively charged amino acid residues yields high local metal ion concentrations, providing the necessary microenvironment for triggering the nucleation event. Nucleation occurs via reduction of the gold precursor by surrounding amino acid residues with a sufficiently high redox potential, including Tyr, Trp and His.

2. **Growth.** Small nuclei formed close to the protein surface are capped by anionic amino acid residues, and grow either (i) from influx of Au^{3+} ions as determined by charge density matching with negatively charged amino acid residues in the immediate vicinity, eventually leading to overlapping clusters, (ii) from partial unfolding of the polypeptide chain leading to close contact between adjacent nuclei and subsequent aggregation, (iii) collisions between proteins leading to contact between exposed nuclei, or (iv) a combination of (i)-(iii).

3. **Termination.** Termination can occur via depletion of metal precursor from the bulk phase, but more importantly via capping from anionic amino acid residues in the case of mechanisms (i) and (ii), or via a combination of electrostatic and steric (i.e.; electrosteric) capping in the case of mechanism (iii).

4. **Passivation and solubilization.** The capping ligands - either amino acid residues or proteins depending on the size and nature of the gold nanoconstructs - suppress defect surface states by forming covalent bonds (such as in the case of Cys), or simply by forming complexes with empty orbitals and dangling bonds.

The general mechanism suggested here accounts for the highly protein-dependent AuNC formation in that local negative charge, availability of electron-donors and the local stability of the secondary structure and overall flexibility of the fold determines where clusters form and when formation is terminated, as well as their concomitant effect on the protein. The mechanism is also in agreement with existing literature for comparable systems.[170,171]

From paper III and IV it is evident that aLa can easily be manipulated with different gold nanoconstructs both through the extrinsic method and the intrinsic method. The altered conformation of the new aLa-Au nanoconstructs are likely to result in emergent properties. Now two major questions arise. (1) How will the two different protocols affect aLa function, and (2) will the aLa-gold nanoconstructs formed have similar anticancer activity as BAMLET?

6.5 Anticancer activity from gold-alpha-lactalbumin nanoconstructs?

The Journal of Physical Chemistry C, **2013**, 117, (5), p. 2230-223

The main aim of paper V was to investigate the differences in properties between aLa-gold nanoconstructs made by using two different synthesis routes; (i) - the biomineralization-inspired protocol utilizing the intrinsic reduction potential of amino acid residues in the protein to reduce the gold precursor (forming aLa-Au_{int}), and (ii) - the protocol wherein an extrinsic reducing agent was added (forming aLa-Au_{ext}). Several aspects such as type of protein-gold nanoconstruct formed, changes in protein conformation, and altered interfacial activity were studied. Moreover, to test for emergent properties, aLa-Au_{int} was compared to BAMLET in HeLa cell-viability studies. In the study presented here, the mechanism behind HAMLET/BAMLET is not studied directly. Rather, aLa is modified with gold nanoconstructs. Maybe the gold nanoconstructs are able to alter protein conformation similar to how oleic acid alters and stabilizes aLa conformation (see section 2.4, page 7). The protein-gold nanoconstruct might then exhibit similar anticancer activity. While oleic acid may dissociate from aLa inside cells, the gold nanoconstructs are covalently bonded to aLa. Thus, it will be possible to study the effects on cancer cells of the entire construct, without the possibility of the construct to dissociate, and the concomitant confusion around which component is causing the observed effects is avoided.

The formation of different gold nanoconstructs was studied using UV-vis measurements, steady-state fluorescence and STEM, while alterations in protein conformation were studied using steady-state fluorescence, TCSPC and CD-measurements. Interfacial activity of protein and protein-gold nanoconstructs were studied using Langmuir monolayer studies and AFM. Cell-viability was studied using a trypan blue assay. Characterization of the different gold nanoconstructs formed and conformational changes in the protein were very similar to those in paper III and IV. Therefore, these results will not be discussed in detail here.

The prescence of LSPR in UV-vis and particles > 3 nm observed by STEM revealed that the intrinsic procedure led to AuNC-modified aLa linked together via AuNPs (aLa-Au_{int}). The lack of similar findings for aLa-Au_{ext}, means the aLa stayed as single proteins modified with AuNCs when the extrinsic protocol was used. This is illustrated in Figure 6.12 together with the CD spectra.

Fluorescence data and ζ-potentials implied that larger conformational changes were induced in aLa-Au_{int} when the gold nanoconstructs were formed, than for aLa-Au_{ext}.

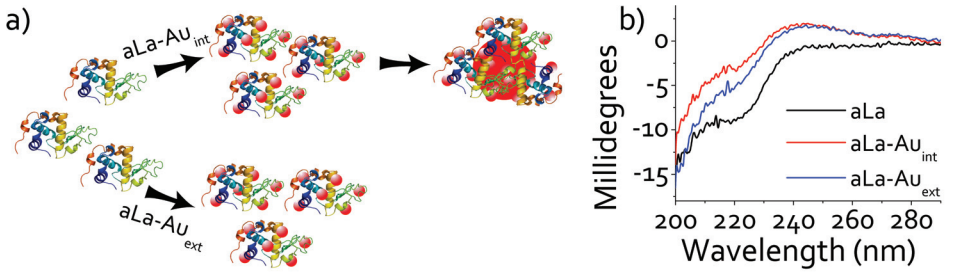

Figure 6.12: (a) The upper route show the formation of aLa-Au$_{int}$, where singular proteins with embedded gold nanoclusters are linked together by AuNPs. The lower route show synthesis of aLa-Au$_{ext}$, which stops at protein-embedded AuNCs. (b) CD-spectra of aLa and aLa-gold nanoconstructs.

This corresponds well with the changes in intensity observed in the CD-spectra (Figure 6.12 b). Since the relationship of the mean residual ellipticities at 200 nm and 222 nm changed between the samples, it is likely that the changes in the CD-spectra were due to changes in protein conformation, and not due to attenuation of the signal by gold species. All data have implied that the structural changes are larger for aLa-Au$_{int}$ than for aLa-Au$_{ext}$, and that the two different procedures for introducing gold nanoconstructs in aLa results in very different complexes (Figure 6.12). To study if the big difference in type of construct made also resulted in different interfacial activities (Figure 6.13), the constructs were tested using a standard Langmuir trough set-up and the intercalation of the different species into lipid films were studied with AFM.

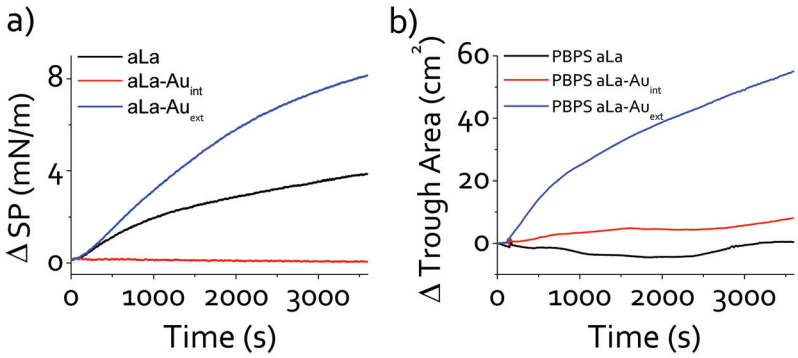

Figure 6.13: (a) Air-water surface activity studies of aLa and aLa-Au nanoconstructs at constant trough area. (b) aLa or aLa-Au nanoconstructs injected under a PBPS lipid film pre-compressed to 10 mN/m. The changes in trough area are recorded over time at constant surface pressure. The data displayed is corrected for contribution to area changes in the PBPS blank. The X-axis denotes time after injection of sample.

Of the three species studied, aLa-Au$_{ext}$ reached the highest surface pressure (8 mN/m after one hour) in the air-water surface studies (Figure 6.13 a, page 61). For native aLa, half the surface pressure observed for aLa-Au$_{ext}$ was obtained, while for aLa-Au$_{int}$ no significant change in surface pressure could be observed within the time frame of the experiment. As the protein/protein-gold nanoconstructs migrate to the surface, hydrophobic groups will be oriented towards the air and the hydrophilic ones towards the water, and the surface pressure increases.[148,167,172,173] Hydrophobic species travel more quickly to the surface than less hydrophobic species, and from Figure 6.13, page 61 it can be interpreted that aLa-Au$_{ext}$ is more hydrophobic than native aLa, while aLa-Au$_{int}$ showed no air-water surface activity, and is hydrophilic. This difference in surface activity supports the hypothesis about single aLa-Au in aLa-Au$_{ext}$ versus multimeric proteins in aLa-Au$_{int}$, as organization of nanocluster-modified aLa around a nanoparticle core allows for shielding of hydrophobic residues from the aqueous environment. When the three species were introduced underneath a lipid monolayer (Figure 6.13 b), aLa-Au$_{ext}$ still displayed the highest interfacial activity. However, aLa-Au$_{int}$ induced a larger increase in trough area in the presence of lipid as compared to native aLa. Combining the results from Figure 6.13 a and b, it seems that aLa-Au$_{int}$ displays lipid-specific interaction, in spite of the fact that both aLa-Au$_{int}$ and the lipid (PBPS) are negatively charged under these conditions. There are several reports on proteins and lipids of similar charge interacting.[174,175] AFM was used to study morphological changes as species from bulk interact with the lipid film. The AFM images showed that native aLa interacts weakly with the lipid film, but does not intercalate into it. Morover, collapse of the lipid regions was observed for both aLa-Au$_{ext}$ and aLa-Au$_{int}$ through AFM. However, the disruption of the lipid film was much more severe for aLa-Au$_{int}$. This is in good agreement with the Langmuir trough studies.

Some of the theories about the cancer killing effects seen for HAMLET and BAMLET are associated with stronger lipid interaction for HAMLET as compared to native aLa. Since aLa-Au$_{int}$ displayed the most severe effect on the lipid film, this was chosen as the candidate for comparison with BAMLET in cell-viability studies (Figure 6.14, page 63), where trypan blue was used to stain dead cells.

Triton was used as a standard for maximum cell death.[75,76] From Figure 6.14 it seems like neither native aLa or oleic acid had much influence on cell-viability, but aLa-Au$_{int}$ killed a similar amount of HeLa cancer cells as did BAMLET. This indicates that aLa-Au$_{int}$ might have anticancer activity.

HAMLET interacts with several parts of cells, and several of these interaction can contribute to cell death. However, not all these interaction contributes to apoptosis.[40] Cell death caused by aLa-AuNCs is not necessarily due to apoptosis, but can be due

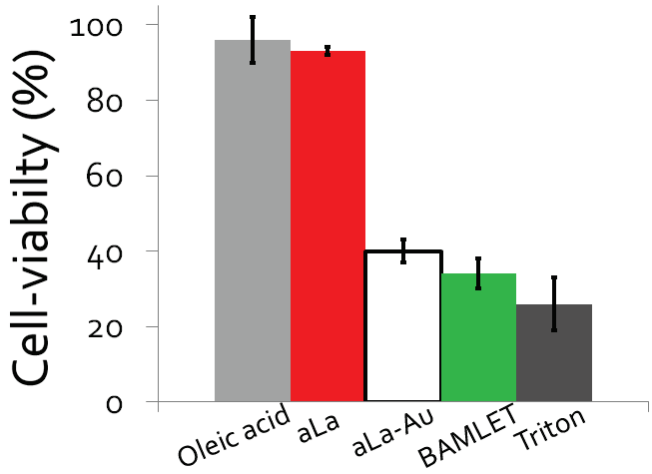

Figure 6.14: Cell-viability studies with oleic acid, aLa, aLa-Au$_{int}$, BAMLET and Triton. Protein concentration = 1.0 mg/ml, oleic acid concentration = 1.6 mM, and Triton concentration = 2.7 mM. Typical cell counts were 7x10^5 cells/ml

to disruption of the cell membrane as well. Such a disruption as a plausible cause of cell death is in accordance with the Langmuir and AFM studies that revealed aLa-Au$_{int}$ ability to disturb membranes at neutral conditions. Membrane disturbing features are also seen for HAMLET.[49]

Dependent on which one of the two different synthesis protocols presented here was used, either aLa-Au$_{int}$ or aLa-Au$_{ext}$ were formed. While aLa-Au$_{ext}$ are single aLa molecules modified with sub-nanometer gold clusters, exhibiting hydrophobic properties, aLa-Au$_{int}$ consists of multiple AuNC-modified aLa assembled around ~20 nm AuNP cores, and is hydrophilic. Both types of constructs are fluorescent due to the AuNCs, but aLa-Au$_{int}$ show LSPR as well due to the AuNPs. Moreover, aLa-Au$_{int}$ show lipid-specific interaction, and an ability to induce cell death in HeLa cancer cells at the same level as BAMLET. These results are very promising for further medical research since optical and interfacial properties of protein-gold nanoconstructs can be tuned, and thus provide constructs that make it possible to simultaneously image and kill cancer cells.

7. Concluding remarks and future work

By combining nanomaterials with proteins, bionanomaterials are formed. Such materials are very interesting within therapeutic and diagnostic research. In this thesis, bionanomaterials were made by modifying different proteins with AuNPs and AuNCs. The aim of this thesis can be divided into steps. The first step was to study if gold nanoconstructs could alter the structure of the proteins studied here. The next step was to study which properties, such as optical properties or interfacial activity, these new biomaterials exhibit. The goal of making the bionanomaterials was to utilize them in medical research, and some of the constructs were studied further for medical relevance.

Throughout this work, it was found that by adsorbing proteins onto gold nanoparticles, new membrane-affecting properties emerge, which are not seen for neither protein nor gold alone. Increased film-penetration ability and the ability to induce film miscibility are among the emergent properties that make protein-gold nanoparticles interesting as potential tools for drug delivery (papers I and II). However, the use of AuNPs has some drawbacks. When the AuNPs are larger than the protein it is at present problematic to tune the conformation of single proteins, as several proteins usually adsorb per gold nanoparticle. If the size of the protein-AuNP constructs exceeds ~100 nm, the size can also be a problem for cellular uptake via the vasculature.[7] The problems with using AuNPs can be circumvented by making small gold nanoclusters within the proteins instead, but then the benefits of LSPR are lost. Papers III and IV show that both intrinsic and extrinsic reducing agents are well suited for making protein-stabilized gold nanoclusters. Under some conditions gold nanoparticles stabilized by protein-AuNCs were made as well. It has been shown that, by varying the reaction conditions, it is possible to tune the gold nanoconstructs formed from small AuNCs, via large AuNCs, and all the way to AuNPs. This tunability in gold nanoconstruct formation provides for a good tunability of protein conformation, as well as protein activity. The latter was illustrated by LYZ digestion of cell-walls. Moreover, the formation of different gold nanoconstructs makes it possible to incorporate fluorescent markers, a property useful in both diagnostics and treatment. Of

the proteins studied here, aLa provided for the best tunability in protein conformation and type of gold nanoconstruct formed. aLa-gold nanoconstructs formed by the intrinsic procedure (aLa-Au_{int}) develop very different interfacial activities compared to those made by the extrinsic protocol (aLa-Au_{ext}). While aLa-Au_{ext} is hydrophobic and in general more surface active than native aLa, aLa-Au_{int} is hydrophilic and show little activity towards an air-water surface. However, aLa-Au_{int} displays phospholipid-specific interaction, and kills cancer cells at the level of BAMLET. This is very promising for further cancer research, as the contrast agent used to image the cancer cells also can kill them. In this way, treatment and imaging can be performed simultaneously.

The tunability in protein conformation, and the very different interfacial activities of the constructs created, might also be useful in the research on protein misfolding diseases as well. One possibility is to modify these constructs further by exchanging/adding different molecules, and use the new constructs to detect misfolded dimers, or early aggregates (see Figure 2.3, page 7) typical for neurodegenerative diseases such as Alzheimer's disease. Treatment could potentially start at a much earlier stage than today, and some of the severe consequences of neurodegeneration could be postponed or even eliminated.

As seen from section 4.3 and section 4.4 the toxicity of gold nanoconstructs remains to be ascertained. The constructs should be toxic towards e.g. cancer cells, but not for the patients. It is likely that a potential toxicity of gold nanoconstructs depends on construct size, surface ligands, route of administration and concentration, but still the information is scarce. Thus, toxicology studies must be implemented before aLa-gold nanoconstructs can be used in diagnostics or treatment in a way that exposes the patient directly to the constructs.

References

[1] Kane, R. S.; Stroock, A. D. *Biotechnology Progress*, **2007**, *23*, (2), p. 316–319.

[2] Selvan, S. T.; Tan, T. T. Y.; Yi, D. K.; Jana, N. R. *Langmuir*, **2010**, *26*, (14), p. 11631–11641.

[3] De, M.; Ghosh, P. S.; Rotello, V. M. *Advanced Materials*, **2008**, *20*, (22), p. 4225–4241.

[4] Wang, H.-H.; Su, C.-H.; Wu, Y.-J.; Lin, C.-A. J.; Lee, C.-H.; Shen, J.-L.; Chan, W.-H.; Chang, W. H.; Yeh, H.-I. *International Journal of Gerontology*, **2012**, *6*, (1), p. 1–4.

[5] Wang, Y.; Wang, Y.; Zhou, F.; Kim, P.; Xia, Y. *Small*, **2012**, *8*, (24), p. 3769–3773.

[6] Stewart, M. E.; Anderton, C. R.; Thompson, L. B.; Maria, J.; Gray, S. K.; Rogers, J. A.; Nuzzo, R. G. *Chemical Reviews*, **2008**, *108*, (2), p. 494–521.

[7] Glomm, W. R. *Journal of Dispersion Science and Technology*, **2005**, *26*, (3), p. 389 – 414.

[8] Sardar, R.; Funston, A. M.; Mulvaney, P.; Murray, R. W. *Langmuir*, **2009**, *25*, (24), p. 13840–13851.

[9] Huang, X.; Jain, P. K.; El-Sayed, I. H.; El-Sayed, M. A. *Nanomedicine*, **2007**, *2*, (5), p. 681–693.

[10] Hainfeld, J. F.; Slatkin, D. N.; Focella, T. M.; Smilowitz, H. M. *British Journal of Radiology*, **2006**, *79*, (939), p. 248–253.

[11] Kunzmann, A.; Andersson, B.; Thurnherr, T.; Krug, H.; Scheynius, A.; Fadeel, B. *Biochimica et Biophysica Acta (BBA) - General Subjects*, **2011**, *1810*, (3), p. 361–373.

[12] Kowlgi, K. N. K.; Koper, G. J. M.; Picken, S. J.; Lafont, U.; Zhang, L.; Norder, B. *Langmuir*, **2011**, *27*, (12), p. 7783–7787.

[13] Huang, H.-C.; Barua, S.; Sharma, G.; Dey, S. K.; Rege, K. *Journal of Controlled Release*, **2011**, *155*, (3), p. 344–357.

[14] NCBI, *Genes and Disease - The p53 tumor suppressor protein.*, http://www.ncbi.nlm.nih.gov/books/NBK22268/, Accessed: 30.10.2012.

[15] Hardy, J.; Allsop, D. *Trends in Pharmacological Sciences*, **1991**, *12*, (10), p. 383–388.

[16] Lyubchenko, Y. L.; Sherman, S.; Shlyakhtenko, L. S.; Uversky, V. N. *Journal of Cellular Biochemistry*, **2006**, *99*, (1), p. 53–70.

[17] Berg, J. M.; John L, T.; Stryer, L. *Biochemistry*, 5th ed.; W. H. Freeman and Company: New York, 2001.

[18] Tyka, M. *Beautiful Proteins*, http://beautifulproteins.blogspot.no/2010/06/insulin-hexamer.html, Accessed: 20.06.2012.

[19] Creighton, T. E. *Proteins - Structures and Molecular Properties*, 2nd ed.; W. H. Freeman and Copmany: New York, 1993.

[20] Branden, C.; Tooze, J. *Introduction to protein structure*, 2nd ed.; Garlan Publishing, Inc.: New York, 1998.

[21] Svensson, M.; Håkansson, A.; Mossberg, A.-K.; Linse, S.; Svanborg, C. *Proceedings of the National Academy of Sciences of the United States of America*, **2000**, *97*, (8), p. 4221–4226.

[22] Faber, K. *Biotransformations in Organic Chemistry*, 5th ed.; Springer-Verlag: Berlin, 2004.

[23] Ohgushi, M.; Wada, A. *FEBS Letters*, **1983**, *164*, (1), p. 21–24.

[24] Halskau, Ø.; Perez-Jimenez, R.; Ibarra-Molero, B.; Underhaug, J.; Muñoz, V.; Martínez, A.; Sanchez-Ruiz, J. M. *Proceedings of the National Academy of Sciences of the United States of America*, **2008**, *105*, (25), p. 8625–8630.

[25] Bañuelos, S.; Muga, A. *Journal of Biological Chemistry*, **1995**, *270*, (50), p. 29910–29915.

[26] Uversky, V. N.; Dunker, A. K. *Biochimica Et Biophysica Acta-Proteins and Proteomics*, **2010**, *1804*, (6), p. 1231–1264.

[27] Mercer, N.; Ramakrishnan, B.; Boeggeman, E.; Qasba, P. K. *PLoS one*, **2011**, *6*, (10), p. e26093.

[28] Chowdhury, F. A.; Raleigh, D. P. *Protein Science*, **2005**, *14*, (1), p. 89–96.

[29] Qasba, P. K.; Safaya, S. K. *Nature*, **1984**, *308*, (5957), p. 377–380.

[30] Wohlkönig, A.; Huet, J.; Looze, Y.; Wintjens, R. *PLoS one*, **2010**, *5*, (11), p. e15388.

[31] Raven, P. H.; Johnson, G. B.; Losos, J. B.; Singer, S. R. *Biology*, 7th ed.; McGraw Hill: New York, 2005.

[32] Giurleo, J. T.; He, X. L.; Talaga, D. S. *Journal of Molecular Biology*, **2008**, *381*, (5), p. 1332–1348.

[33] Reynaud, E. *Nature Education*, **2010**, *3*, (9), p. 28.

[34] Ehrnhoefer, D. E.; Bieschke, J.; Boeddrich, A.; Herbst, M.; Masino, L.; Lurz, R.; Engemann, S.; Pastore, A.; Wanker, E. E. *Nature structural & molecular biology*, **2008**, *15*, (6), p. 558–566.

[35] Aisenbrey, C.; Borowik, T.; Bystrom, R.; Bokvist, M.; Lindstrom, F.; Misiak, H.; Sani, M. A.; Grobner, G. *European Biophysics Journal with Biophysics Letters*, **2008**, *37*, (3), p. 247–255.

[36] Giacomelli, C. E.; Norde, W. *Macromolecular Bioscience*, **2005**, *5*, (5), p. 401–407.

[37] Selkoe, D. J. *Nature Cell Biology*, **2004**, *6*, (11), p. 1054–1061.

[38] Svensson, M.; Sabharwal, H.; Håkansson, A.; Mossberg, A.-K.; Lipniunas, P.; Leffler, H.; Svanborg, C.; Linse, S. *Journal of Biological Chemistry*, **1999**, *274*, (10), p. 6388–6396.

[39] Håkansson, A.; Andreasson, J.; Zhivotovsky, B.; Karpman, D.; Orrenius, S.; Svanborg, C. *Experimental Cell Research*, **1999**, *246*, (2), p. 451–460.

[40] Mossberg, A.-K.; Hun Mok, K.; Morozova-Roche, L. A.; Svanborg, C. *FEBS Journal*, **2010**, *277*, (22), p. 4614–4625.

[41] Permyakov, S. E.; Knyazeva, E. L.; Khasanova, L. M.; Fadeev, R. S.; Zhadan, A. P.; Roche-Hakansson, H.; Håkansson, A. P.; Akatov, V. S.; Permyakov, E. A. *Biological Chemistry*, **2012**, *393*, (1-2), p. 85–92.

[42] Kohler, C.; Håkansson, A.; Svanborg, C.; Orrenius, S.; Zhivotovsky, B. *Experimental Cell Research*, **1999**, *249*, (2), p. 260–268.

[43] Kohler, C.; Gogvadze, V.; Håkansson, A.; Svanborg, C.; Orrenius, S.; Zhivotovsky, B. *European Journal of Biochemistry*, **2001**, *268*, p. 186–191.

[44] Svensson, M.; Mossberg, A.-K.; Pettersson, J.; Linse, S.; Svanborg, C. *Protein Science*, **2003**, *12*, (12), p. 2805–2814.

[45] Svensson, M.; Fast, J.; Mossberg, A.-K.; Düringer, C.; Gustafsson, L.; Hallgren, O.; Brooks, C. L.; Berliner, L.; Linse, S.; Svanborg, C. *Protein Science*, **2003**, *12*, (12), p. 2794–2804.

[46] Wilhelm, K.; Darinskas, A.; Noppe, W.; Duchardt, E.; Mok, K. H.; Vukojevic, V.; Schleucher, J.; Morozova-Roche, L. A. *FEBS Journal*, **2009**, *276*, (15), p. 3975–3989.

[47] Tuei, V. C.; Ha, J. S.; Ha, C. E. *Life Sciences*, **2011**, *88*, (17-18), p. 810–818.

[48] Lišková, K.; Auty, M. A. E.; Chaurin, V.; Min, S.; Mok, K. H.; O'Brien, N.; Kelly, A. L.; Brodkorb, A. *European Journal of Lipid Science and Technology*, **2011**, *113*, (10), p. 1207–1218.

[49] Mossberg, A.-K.; Puchades, M.; Halskau, Ø.; Baumann, A.; Lanekoff, I.; Chao, Y.; Martínez, A.; Svanborg, C.; Karlsson, R. *PLoS ONE*, **2010**, *5*, (2), p. e9384.

[50] Baumann, A.; Gjerde, A. U.; Ying, M.; Svanborg, C.; Holmsen, H.; Glomm, W. R.; Martínez, A.; Halskau, Ø. *Journal of Molecular Biology*, **2012**, *418*, (1-2), p. 90–102.

[51] Fang, B.; Zhang, M.; Jiang, L.; Jing, H.; Ren, F. Z. *Protein Journal*, **2012**, *31*, (7), p. 564–572.

[52] Kataev, A. A.; Zherelova, O. M.; Grishchenko, V. M. *Biologicheskie Membrany*, **2012**, *29*, (4), p. 276–283.

[53] Mossberg, A.-K.; Wullt, B.; Gustafsson, L.; Månsson, W.; Ljunggren, E.; Svanborg, C. *International Journal of Cancer*, **2007**, *121*, (6), p. 1352–1359.

[54] Gustafsson, L.; Leijonhufvud, I.; Aronsson, A.; Mossberg, A.-K.; Svanborg, C. *New England Journal of Medicine*, **2004**, *350*, (26), p. 2663–2672.

[55] Aili, D.; Gryko, P.; Sepulveda, B.; Dick, J. A. G.; Kirby, N.; Heenan, R.; Baltzer, L.; Liedberg, B.; Ryan, M. P.; Stevens, M. M. *Nano Letters*, **2011**, *11*, (12), p. 5564–5573.

[56] Xie, J.; Zheng, Y.; Ying, J. Y. *Journal of the American Chemical Society*, **2009**, *131*, (3), p. 888–889.

[57] Guével, X. L.; Hötzer, B.; Jung, G.; Hollemeyer, K.; Trouillet, V.; Schneider, M. *The Journal of Physical Chemistry C*, **2011**, *115*, (22), p. 10955–10963.

[58] Guével, X. L.; Daum, N.; Schneider, M. *Nanotechnology*, **2011**, *22*, (27), p. 275103/1–275103/7.

[59] Link, S.; Beeby, A.; FitzGerald, S.; El-Sayed, M. A.; Schaaff, T. G.; Whetten, R. L. *The Journal of Physical Chemistry B*, **2002**, *106*, (13), p. 3410–3415.

[60] Link, S.; El-Sayed, M. A. *International Reviews in Physical Chemistry*, **2000**, *19*, (3), p. 409–453.

[61] de Heer, W. A. *Reviews of Modern Physics*, **1993**, *65*, (3), p. 611–676.

[62] Hayat, M. A. *Colloidal Gold: Principles Methods and Applications*; Academic Press, INC: New York, 1989; Vol. 1.

[63] Lakowicz, J. R. *Principles of Fluorescence Spectroscopy*, 3rd ed.; Springer: New York, 2006.

[64] Creighton, J. A.; Eadon, D. G. *Journal of the Chemical Society-Faraday Transactions*, **1991**, *87*, (24), p. 3881–3891.

[65] Hiemenz, P. C.; Rajagopalan, R. *Principles of Colloid and Surface Chemistry*, 3rd ed.; CRC Press Taylor & Francis Group: Boca Raton, 1997.

[66] Berne, B. J.; Pecora, R. *Dynamic Light Scattering: With Applications to Chemistry, Biology and Physics*; Dover Publications: New York, 2000.

[67] van de Hulst, H. C. *Journal of Colloid Science*, **1949**, *4*, (1), p. 79–87.

[68] Volden, S.; Kjøniksen, A.-L.; Zhu, K.; Genzer, J.; Nyström, B.; Glomm, W. R. *ACS Nano*, **2010**, *4*, (2), p. 1187–1201.

[69] Mulvaney, P. *Langmuir*, **1996**, *12*, (3), p. 788–800.

[70] Templeton, A. C.; Pietron, J. J.; Murray, R. W.; Mulvaney, P. *The Journal of Physical Chemistry B*, **2000**, *104*, (3), p. 564–570.

[71] Aili, D.; Enander, K.; Rydberg, J.; Lundström, I.; Baltzer, L.; Liedberg, B. *Journal of the American Chemical Society*, **2006**, *128*, (7), p. 2194–2195.

[72] Kerker, M. *Journal of Colloid and Interface Science*, **1985**, *105*, (2), p. 297–314.

[73] Shan, J.; Chen, H.; Nuopponen, M.; Viitala, T.; Jiang, H.; Peltonen, J.; Kauppinen, E.; Tenhu, H. *Langmuir*, **2006**, *22*, (2), p. 794–801.

[74] Shiang, Y. C.; Huang, C. C.; Chen, W. Y.; Chen, P. C.; Chang, H. T. *Journal of Materials Chemistry*, **2012**, *22*, (26), p. 12972–12982.

[75] Retnakumari, A.; Jayasimhan, J.; Chandran, P.; Menon, D.; Nair, S.; Mony, U.; Koyakutty, M. *Nanotechnology*, **2011**, *22*, (28), p. 285102/1–285102/11.

[76] Retnakumari, A.; Setua, S.; Menon, D.; Ravindran, P.; Muhammed, H.; Pradeep, T.; Nair, S.; Koyakutty, M. *Nanotechnology*, **2010**, *21*, (5), p. 055103/1–055103/12.

[77] Forestier, J. *Annals of the Rheumatic Diseases*, **1949**, *8*, (2), p. 132–134.

[78] Liu, Y.; Mounkes, L. C.; Liggitt, H. D.; Brown, C. S.; Solodin, I.; Heath, T. D.; Debs, R. J. *Nature Biotechnology*, **1997**, *15*, (2), p. 167–173.

[79] Feldherr, C. M.; Akin, D. *Journal of Cell Science*, **1999**, *112*, (12), p. 2043–2048.

[80] Tkachenko, A. G.; Xie, H.; Coleman, D.; Glomm, W.; Ryan, J.; Anderson, M. F.; Franzen, S.; Feldheim, D. L. *Journal of the American Chemical Society*, **2003**, *125*, (16), p. 4700–4701.

[81] Tkachenko, A. G.; Xie, H.; Liu, Y.; Coleman, D.; Ryan, J.; Glomm, W. R.; Shipton, M. K.; Franzen, S.; Feldheim, D. L. *Bioconjugate Chemistry*, **2004**, *15*, (3), p. 482–490.

[82] Ryan, J. A.; Overton, K. W.; Speight, M. E.; Oldenburg, C. N.; Loo, L.; Robarge, W.; Franzen, S.; Feldheim, D. L. *Analytical Chemistry*, **2007**, *79*, (23), p. 9150–9159.

[83] Iosin, M.; Toderas, F.; Baldeck, P.; Astilean, A. *Journal of Molecular Structure*, **2009**, *924-926*, p. 196–200.

[84] Lee, J.-S.; Green, J. J.; Love, K. T.; Sunshine, J.; Langer, R.; Anderson, D. G. *Nano Letters*, **2009**, *9*, (6), p. 2402–2406.

[85] Guo, S.; Huang, Y.; Jiang, Q.; Sun, Y.; Deng, L.; Lian, Z.; Du, Q.; Xing, J.; Zhao, Y.; Wang, P. C.; Dong, A.; Liang, X.-J. *ACS Nano*, **2010**, *4*, (9), p. 5505–5511.

[86] Dorsett, Y.; Tuschl, T. *Nature Reviews Drug Discovery*, **2004**, *3*, (4), p. 318–329.

[87] Elbakry, A.; Zaky, A.; Liebl, R.; Rachel, R.; Goepferich, A.; Breunig, M. *Nano Letters*, **2009**, *9*, (5), p. 2059–2064.

[88] Aili, D.; Stevens, M. M. *Chemical Society Reviews*, **2010**, *39*, (9), p. 3358–3370.

[89] Izquierdo-Lorenzo, I.; Sanchez-Cortes, S.; Garcia-Ramos, J. V. *Langmuir*, **2010**, *26*, (18), p. 14663–14670.

[90] Chen, T. H.; Tseng, W. L. *Small*, **2012**, *8*, (12), p. 1912–1919.

[91] Chen, H.; Li, B.; Ren, X.; Li, S.; Ma, Y.; Cui, S.; Gu, Y. *Biomaterials*, **2012**, *33*, (33), p. 8461–76.

[92] Hu, L. Z.; Han, S.; Parveen, S.; Yuan, Y. L.; Zhang, L.; Xu, G. B. *Biosensors & Bioelectronics*, **2012**, *32*, (1), p. 297–299.

[93] Zhang, J.; Sajid, M.; Na, N.; Huang, L. Y.; He, D. C.; Ouyang, J. *Biosensors & Bioelectronics*, **2012**, *35*, (1), p. 313–318.

[94] Guével, X. L.; Hotzer, B.; Jung, G.; Schneider, M. *Journal of Materials Chemistry*, **2011**, *21*, (9), p. 2974–2981.

[95] Brewer, S. H.; Glomm, W. R.; Johnson, M. C.; Knag, M. K.; Franzen, S. *Langmuir*, **2005**, *21*, (20), p. 9303–9307.

[96] Glomm, W. R.; Halskau, Ø.; Hanneseth, A.-M. D.; Volden, S. *The Journal of Physical Chemistry B*, **2007**, *111*, (51), p. 14329–14345.

[97] De, M.; You, C.-C.; Srivastava, S.; Rotello, V. M. *Journal of the American Chemical Society*, **2007**, *129*, (35), p. 10747–10753.

[98] Malmsten, M. *Biopolymers at interfaces*, 2nd ed.; Marcel Dekker, Inc.: New York, 2003; Vol. 110.

[99] Haynes, C. A.; Norde, W. *Colloids and Surfaces B-Biointerfaces*, **1994**, *2*, p. 517–566.

[100] Vertegel, A. A.; Siegel, R. W.; Dordick, J. S. *Langmuir*, **2004**, *20*, (16), p. 6800–6807.

[101] Lundqvist, M.; Sethson, I.; Jonsson, B. H. *Langmuir*, **2004**, *20*, (24), p. 10639–10647.

[102] Roach, P.; Farrar, D.; Perry, C. C. *Journal of the American Chemical Society*, **2006**, *128*, (12), p. 3939–3945.

[103] Cedervall, T.; Lynch, I.; Lindman, S.; Berggård, T.; Thulin, E.; Nilsson, H.; Dawson, K. A.; Linse, S. *Proceedings of the National Academy of Sciences of the United States of America*, **2007**, *104*, (7), p. 2050–2055.

[104] Wang, Y. S.; Aili, D.; Selegard, R.; Tay, Y.; Baltzer, L.; Zhang, H.; Liedberg, B. *Journal of Materials Chemistry*, **2012**, *22*, (38), p. 20368–20373.

[105] Turkevich, J. *Gold Bulletin*, **1985**, *18*, (3), p. 86–91.

[106] Bredig, G. *Angewandte Chemie*, **1898**, *11*, (41), p. 952.

[107] Baignet, C.; Muller, G. *Experimentia*, **1980**, *36*, p. 472.

[108] Kurihara, K.; Kizling, J.; Stenius, P.; Fendler, J. H. *Journal of the American Chemical Society*, **1983**, *105*, (9), p. 2574–2579.

[109] Connor, E. E.; Mwamuka, J.; Gole, A.; Murphy, C. J.; Wyatt, M. D. *Small*, **2005**, *1*, (3), p. 325–327.

[110] Lynch, I.; Salvati, A.; Dawson, K. A. *Nature Nanotechnology*, **2009**, *4*, (9), p. 546–547.

[111] Haynes, C. L. *Analytical and Bioanalytical Chemistry*, **2010**, *398*, (2), p. 587–588.

[112] Uboldi, C.; Bonacchi, D.; Lorenzi, G.; Hermanns, M. I.; Pohl, C.; Baldi, G.; Unger, R. E.; Kirkpatrick, C. J. *Particle and Fibre Toxicology*, **2009**, *6*, (18), p. 1–12.

[113] Choi, S. Y.; Jeong, S.; Jang, S. H.; Park, J.; Park, J. H.; Ock, K. S.; Lee, S. Y.; Joo, S.-W. *Toxicology in vitro*, **2012**, *26*, (2), p. 229–37.

[114] Geffroy, B.; Ladhar, C.; Cambier, S.; Treguer-Delapierre, M.; Brethes, D.; Bourdineaud, J. P. *Nanotoxicology*, **2012**, *6*, (2), p. 144–160.

[115] Sonavane, G.; Tomoda, K.; Makino, K. *Colloids and Surfaces B: Biointerfaces*, **2008**, *66*, (2), p. 274–280.

[116] Harwood, L.; Moody, C.; Percy, J. *Experimental Organic Chemistry - Standard and Microscale*, 2nd ed.; Blackwell Science, 2005.

[117] Schmid, F.-X. *Encyclopedia of Life Sciences*, **2001**, http://www.els.net [doi: 10.1038/npg.els.0003142].

[118] Herberhold, H.; Marchal, S.; Lange, R.; Scheyhing, C. H.; Vogel, R. F.; Winter, R. *Journal of Molecular Biology*, **2003**, *330*, (5), p. 1153–1164.

[119] Glomm, W. R.; Volden, S.; Sjöblom, J.; Lindgren, M. *Chemistry of Materials*, **2005**, *17*, (22), p. 5512–5520.

[120] Moskovits, M.; J. S, S. *Journal of Physical Chemistry*, **1984**, *88*, (27), p. 5526–5530.

[121] Baalousha, M.; Lead, J. R. *Environmental Science & Technology*, **2012**, *46*, (11), p. 6134–6142.

[122] Xia, H.; Xiao, Y. Y.; Huang, H.; Tao, S. H.; Lin, X. *Journal of Colloid and Interface Science*, **2012**, *367*, p. 527–530.

[123] Jans, H.; Liu, X.; Austin, L.; Maes, G.; Huo, Q. *Analytical Chemistry*, **2009**, *81*, (22), p. 9425–9432.

[124] Khlebtsov, B.; Khlebtsov, N. *Colloid Journal*, **2011**, *73*, (1), p. 118–127.

[125] Hermanson, G. T. *Bioconjugate Techniques*, 2nd ed.; Pierce Biotechnology, Thermo Fisher Scientific: Rockford, 2008.

[126] Kalluri, J. R.; Arbneshi, T.; Khan, S. A.; Neely, A.; Candice, P.; Varisli, B.; Washington, M.; McAfee, S.; Robinson, B.; Banerjee, S.; Singh, A. K.; Senapati, D.; Ray, P. C. *Angewandte Chemie - International edition*, **2009**, *48*, (51), p. 1–5.

[127] Liu, X.; Dai, Q.; Austin, L.; Coutts, J.; Knowles, G.; Zou, J.; Chen, H.; Huo, Q. *Journal of the American Chemical Society*, **2008**, *130*, (9), p. 2780–2782.

[128] Stenius, P. *Forest Products Chemistry*; Fapet Oy: Helsinki, 2000; Vol. 3.

[129] Kim, T.; Lee, K.; Gong, M.-s.; Joo, S.-W. *Langmuir*, **2005**, *21*, (21), p. 9524–9528.

[130] Nellist, P. D. *Scanning Transmission Electron Microscopy*, 1st ed.; Springer: New York, 2011.

[131] Wall, J.; Langmore, J.; Isaacson, M.; Crewe, A. V. *Proceedings of the National Academy of Sciences of the United States of America*, **1974**, *71*, (1), p. 1–5.

[132] Browning, N.; Buban, J.; Chi, M.; Gipson, B.; Herrera, M.; Masiel, D.; Mehraeen, S.; Morgan, D.; Okamoto, N.; Ramasse, Q.; Reed, B.; Stahlberg, H. *Modeling Nanoscale Imaging in Electron Microscopy*, 1st ed.; Nanostructure Science and Technology; Springer: New York, 2012.

[133] Togashi, D.; Ryder, A.; O'Shaughnessy, D. *Journal of Fluorescence*, **2010**, *20*, (2), p. 441–452.

[134] Tiera, M. J.; dos Santos, G. R.; Tiera, V. A. d. O.; Vieira, N. A. B.; Frolini, E.; da Silva, R. C.; Loh, W. *Colloid & Polymer Science*, **2005**, *283*, (6), p. 662–670.

[135] Gabellieri, E.; Strambini, G. B. *Biophysical Journal*, **2006**, *90*, (9), p. 3239–3245.

[136] Semisotnov, G. V.; Rodionova, N. A.; Razgulyaev, O. I.; Uversky, V. N.; Gripas', A. F.; Gilmanshin, R. I. *Biopolymers*, **1991**, *31*, (1), p. 119–128.

[137] Togashi, D. M.; Ryder, A. G. *Experimental and Molecular Pathology*, **2007**, *82*, (2), p. 135–141.

[138] Togashi, D.; Ryder, A. *Journal of Fluorescence*, **2008**, *18*, (2), p. 519–526.

[139] Xie, H.; Tkachenko, A. G.; Glomm, W. R.; Ryan, J. A.; Brennaman, M. K.; Papanikolas, J. M.; Franzen, S.; Feldheim, D. L. *Analytical Chemistry*, **2003**, *75*, (21), p. 5797–5805.

[140] Lakowicz, J. R. *Topics in Fluorescence Spectroscopy - Protein Fluorescence*; Kluwer Academic/Plenum Publishers: New York, 2000; Vol. 6.

[141] APL, *Alliance Protein Laboratories Home Page*, http://www.ap-lab.com/circular_dichroism.htm, Accessed: 10.09.2012.

[142] Warnke, I.; Furche, F. *Wiley Interdisciplinary Reviews: Computational Molecular Science*, **2011**, *2*, (1), p. 150–166.

[143] Whitmore, L.; Wallace, B. A. *Biopolymers*, **2008**, *89*, (5), p. 392–400.

[144] Sethuraman, A.; Vedantham, G.; Imoto, T.; Przybycien, T.; Belfort, G. *Proteins*, **2004**, *56*, (4), p. 669–678.

[145] Sreerama, N.; Venyaminov, S. Y.; Woody, R. W. *Protein Science*, **1999**, *8*, p. 370–380.

[146] Holmberg, K.; Jönsson, B.; Kronberg, B.; Lindeman, B. *Surfactants and Polymers in Aqueous Solution*, 2nd ed.; John Wiely & Sons: West Sussex, 2007.

[147] Rogalska, E.; Bilewicz, R.; Brigaud, T.; Moujahid, C. E.; Foulard, G.; Portella, C.; Steébé, M.-J. *Chemistry and Physics of Lipids*, **2000**, *105*, (1), p. 71–91.

[148] Glomm, W. R.; Volden, S.; Halskau, Ø.; Ese, M. H. G. *Analytical Chemistry*, **2009**, *81*, (8), p. 3042–3050.

[149] Glomm, W. R.; Volden, S.; Ese, M.-H. G.; Halskau, Ø. *Journal of Dispersion Science and Technology*, **2011**, *32*, (2), p. 150 – 158.

[150] Junghans, A.; Champagne, C.; Cayot, P.; Loupiac, C.; Köper, I. *Langmuir*, **2010**, *26*, (14), p. 12049–12053.

[151] Kaganer, V. M. *Reviews of Modern Physics*, **1999**, *71*, (3), p. 779–819.

[152] Ekelund, K.; Sparr, E.; Engblom, J.; Wennerström, H.; Engström, S. *Langmuir*, **1999**, *15*, (20), p. 6946–6949.

[153] Sparr, E.; Ekelund, K.; Engblom, J.; Engström, S.; Wennerström, H. *Langmuir*, **1999**, *15*, (20), p. 6950–6955.

[154] Sparr, E.; Eriksson, L.; Bouwstra, J. A.; Ekelund, K. *Langmuir*, **2001**, *17*, (1), p. 164–172.

[155] Gillgren, H.; Stenstam, A.; Ardhammar, M.; Norden, B.; Sparr, E.; Ulvenlund, S. *Langmuir*, **2002**, *18*, (2), p. 462–469.

[156] KSV, *Brewster Angle Microscopy*, http://www.ksvnima.com/brewster-angle-microscopy, Accessed: 01.08.2012.

[157] Jalili, N.; Laxminarayana, K. *Mechatronics*, **2004**, *14*, (8), p. 907–945.

[158] Kada, G.; Kienberger, F.; Hinterdorfer, P. *Nano today*, **2008**, *3*, (1-2), p. 12–19.

[159] Butt, H.-J.; Cappella, B.; Kappl, M. *Surface Science Reports*, **2005**, *59*, (1-6), p. 1–152.

[160] Gan, Y. *Surface Science Reports*, **2009**, *64*, (3), p. 99–121.

[161] Gadegaard, N. *Biotechnic and Histochemistry*, **2006**, *81*, (2-3), p. 87–97.

[162] Tennant, J. R. *Transplantation*, **1964**, *2*, (6), p. 685–694.

[163] Strober, W. *Current Protocols in Immunology (Trypan Blue Exclusion Test of Cell Viability)*; Current Protocols in Immunology; John Wiley & Sons, Inc., 2001.

[164] Lokhov, P. G.; Balashova, E. E. *Journal of Cancer*, **2010**, *1*, p. 230–41.

[165] Halskau, Ø.; Frøystein, N. Å.; Muga, A.; Martínez, A. *Journal of Molecular Biology*, **2002**, *321*, (1), p. 99–110.

[166] Chenal, A.; Vernier, G.; Savarin, P.; Bushmarina, N. A.; Gèze, A.; Guillain, F.; Gillet, D.; Forge, V. *Journal of Molecular Biology*, **2005**, *349*, (4), p. 890–905.

[167] Cornell, D. G.; Patterson, D. L.; Hoban, N. *Journal of Colloid and Interface Science*, **1990**, *140*, (2), p. 428–435.

[168] Nielsen, S. B.; Wilhelm, K.; Vad, B.; Schleucher, J.; Morozova-Roche, L. A.; Otzen, D. *Journal of Molecular Biology*, **2010**, *398*, (2), p. 351–361.

[169] Shugar, D. *Biochimica et Biophysica Acta*, **1952**, *8*, (0), p. 302–309.

[170] Berti, L.; Burley, G. A. *Nature Nanotechnology*, **2008**, *3*, (2), p. 81–87.

[171] Feldheim, D. L.; Eaton, B. E. *ACS Nano*, **2007**, *1*, (3), p. 154–159.

[172] Yano, Y. F.; Uruga, T.; Tanida, H.; Terada, Y.; Yamada, H. *Journal of Physical Chemistry Letters*, **2011**, *2*, (9), p. 995–999.

[173] Yano, Y. F.; Uruga, T.; Tanida, H.; Toyokawa, H.; Terada, Y.; Takagaki, M.; Yamada, H. *Langmuir*, **2009**, *25*, (1), p. 32–35.

[174] Rytömaa, M.; Kinnunen, P. K. J. *The Journal of Biological Chemistry*, **1995**, *270*, (7), p. 3197–3202.

[175] Mattila, J.-P.; Sabatini, K.; Kinnunen, P. K. J. *Langmuir*, **2008**, *24*, (8), p. 4157–4160.

Appended papers

Paper I

Paper II

Paper III

Paper IV

Paper V

Contributions

Paper I was planned in cooperation with Ph.D. Volden and Associate Professor Glomm. Volden did several preliminary experiments. Except for the Bradford experiments, which were conducted by Associate Professor Yasuda, Lystvet did most of the experimental work presented in paper I. Glomm, Volden, and Lystvet wrote most of the article, but all authors contributed to the interpretation of data and writing.

All experiments in Paper II are performed by Lystvet, and planned by Lystvet, Volden and Glomm. They also wrote most of the article, but all authors contributed to the interpretation of data and writing.

Some of the preliminary studies to Paper III were done by Volden, who also did all the preliminary studies for Paper IV. Paper III was mainly planned by Lystvet and Volden. The STEM imaging in paper III was performed by Ph.D. Singh. Yasuda helped with the lysozyme activity studies. The remaining data was collected by Lystvet. Associated Professor Halskau contributed much to the completion of the CD experiments and interpretation of these results (this is also true for paper IV and V). Lystvet, Glomm and Volden wrote most of paper III, but all authors contributed to the writing. Volden and Lystvet did the experiments for Paper IV. Glomm and Volden did most of the writing. Most of Paper V was planned by Lystvet, Volden and Glomm. AFM studies were conducted by Singh, and the cell-viability experiments were planned and conducted by Ida Maria Rundgren and Hanzhen Wen. The remaining experiments were conducted by Lystvet. Lystvet, Glomm and Volden did most of the writing, but all authors contributed in this process.

Paper I

Emergent membrane-affecting properties of BSA-gold nanoparticle constructs

Nanoscale

Dynamic Article Links

Cite this: *Nanoscale*, 2011, **3**, 1788

www.rsc.org/nanoscale

PAPER

Emergent membrane-affecting properties of BSA–gold nanoparticle constructs

Sina M. Lystvet,*[a] Sondre Volden,[a] Masahiro Yasuda,[b] Øyvind Halskau Jr[c] and Wilhelm R. Glomm*[a]

Received 6th December 2010, Accepted 19th January 2011
DOI: 10.1039/c0nr00948b

By adsorbing bovine serum albumin (BSA) on gold nanoparticles (Aunps) with diameters 30 nm and 80 nm, different degrees of protein unfolding were obtained. Adsorption and adlayer conformation were characterized by UV-vis spectroscopy, ζ-potential measurements, steady-state and time-resolved fluorescence. The unfolding was also studied using 1-anilino-8-naphthalene sulfonate (ANS) as an extrinsic probe, showing that BSA unfolds more on 80 nm Aunp than on 30 nm Aunp. Langmuir monolayer studies using two distinct methods of introducing the BSA and BSA–Aunp constructs accompanied with Brewster Angle Microscopy (BAM) and Digital Video Microscope (DVM) imaging demonstrated that BSA–Aunp constructs induce film miscibility with L-α-phosphatidylethanolamine not seen for BSA or Aunp alone. The changes induced by partial unfolding clearly give better film-penetration ability, as well as disruption of liquid crystalline domains in the film, thereby inducing film miscibility. Gold or protein only does not possess the nanoscale film-affecting properties of the protein–gold constructs, and as such the surface-active and miscibility-affecting characteristics of the BSA–Aunp represent emergent qualities.

Introduction

As a large number of biological reactions take place at interfaces where lipids and proteins are the main constituents, understanding how to influence lipid film miscibility, domain formation and constituent packing is important for a number of applications ranging from pharmacology (*e.g.* countering interfacial formation of amyloidal plaque and oligomers in Alzheimer's) and enzymatic catalysis to emulsion formation in food.[1,2] Langmuir phospholipid monolayers are often used as model systems for half of a cell membrane,[3,4] as they mimic the interface between the membrane phospholipid and the surrounding aqueous medium.[4] In addition to control of the molecular arrangement, orientation and composition at the surface, this versatile technique also allows different ways to introduce protein into the film. Glomm *et al.*[4] have reported that how the protein is introduced into a lipid film greatly affects the result. The most common approach for studying protein–lipid interactions using the Langmuir monolayer technique is dissolving the protein in the subphase followed by spreading of the lipid on the air–water surface—hereafter referred to as the *subphase method* (see *e.g.* Glomm[4] *et al.* and references therein). While this approach is suitable for the study of interaction between small-molecule solutes and a lipid film, the amphiphilic nature of proteins makes it difficult to avoid inducing mixed protein–lipid behavior if the protein is present in the subphase prior to spreading. Another approach more in line with the use of Langmuir monolayers as a model for half of a cell membrane is to inject a protein solution under an already-formed, compressed lipid film (hereafter referred to as the *injected method*). Here, the lipid film can be tuned to the desired state prior to introduction of other film-forming species, enabling the study of the interaction between proteins from the subphase with the lipid film without any artefacts emanating from lateral interactions between monolayer domains. Also, this approach will preclude formation of mixed protein–lipid films, a concern when the solute is itself highly surface active.[4]

In recent years, there has been a lot of research focused on protein–gold nanoparticle constructs for applications in intracellular delivery.[5–9] By using gold nanoparticles (Aunps) as scaffolds for proteins and other biomolecules, the unique optical properties of nanosized gold can be used as a diagnostic tool to track the nanoparticle construct and the surrounding physicochemical environment. Gold nanoparticles can carry proteins, DNA, peptides as well as small compounds and penetrate into individual cells,[5–7,10] and the mechanisms reported to mediate these imports must reasonably involve encounters between protein–Aunp constructs and biological membranes. Bovine serum albumin (BSA) is often used in the preparation of protein–Aunp constructs.[10–12] Since it is the most abundant plasma

[a]*Ugelstad Laboratory, Department of Chemical Engineering, Norwegian University of Science and Technology (NTNU), N-7491 Trondheim, Norway. E-mail: lystvet@chemeng.ntnu.no; glomm@nt.ntnu.no; Tel: +47 73550325*
[b]*Department of Chemical Engineering, Osaka Prefecture University, 1-1 Gakuen-cho, Sakai, 5998531, Osaka, Japan*
[c]*Department of Molecular Biology, University of Bergen, Thormøhlensgt 55 90, 5008 Bergen, Norway*

This journal is © The Royal Society of Chemistry 2011

protein, BSA can act as an immunoprotective layer on the inorganic particle, and further modification of the protein *i.e.* with targeting peptides or oligonucleotides is straightforward.[5,13]

The interaction between BSA and aqueous Aunp suspensions has been shown to be predominantly electrostatic in nature.[11,14] It is also known that upon binding, BSA might undergo some conformational changes[10,11,15,16] with the degree of conformational changes/unfolding being inversely proportional to particle curvature,[15] *i.e.* smaller particles promote a native-like structure of the surface-bound protein. To the best of our knowledge, however, there have been no studies of the interaction between protein–Aunp constructs and Langmuir monolayers of phospholipids compared to that of the native protein. Depending on how the protein is oriented on the nanoparticle surface, its interaction with a lipid film might be significantly altered compared to the native protein. Conformational changes in the surface-bound protein should also result in an increased interfacial activity of the protein, owing to partial exposure of hydrophobic residues and a loosening of the tertiary structure which permits a more efficient adaption to a non-bulk environment relative to the compact, folded native protein. Thus, we undertake this study to examine to which extent protein–nanoparticle constructs have enhanced interfacial activity and how they affect the monolayer membrane model. Such properties would be "emergent" if they could not be found to a significant extent in the individual components making up the system under scrutiny. Differences in physical and optical properties of BSA only compared to those of BSA–Aunp constructs were monitored using ζ-potential measurements, UV-vis and fluorescence spectroscopies. Aunps of two different sizes were used (30 nm and 80 nm) to study how the curvature can influence unfolding and interfacial activity of the protein. Steady-state fluorescence and time-correlated single photon counting (TCSPC) using intrinsic (Trp) and extrinsic (ANS) probes indicate that BSA unfolds more on 80 nm Aunp than on 30 nm Aunp. Thereafter, the interfacial activity and interaction of the BSA–Aunp constructs with Langmuir monolayers of phospholipids were compared to those of the native protein. In order to assess effects imparted by the protein introduction method on interfacial activity, film-penetrating properties and film miscibility, both the *injected* and the *subphase methods*[4] as defined above were used. We found that the BSA–Aunp constructs display different interfacial and lipid interaction properties from what is found in either the Aunps only or the native protein. Significant differences were also found with respect to the protein introduction method. Using the *subphase method*, BSA and lipid formed separate domains. However, when BSA was adsorbed on gold, the constructs appeared to enhance lipid film miscibility, yielding mixed films where no domains were observable *via* optical microscopy. For the *injected method* neither the protein nor the protein–gold constructs penetrated the lipid film, but rather interacted mostly with the charged polar headgroups of the lipid.

Materials and methods

Materials and solutions

Bovine serum albumin (BSA), 1-anilino-8-naphthalene sulfonate (ANS) and L-α-phosphatidylethanolamine were purchased from Sigma. The Aunps (30 nm and 80 nm) were purchased from Ted Pella. The 80 nm Aunp suspension contains 1.1×10^{10} Aunps per ml and the 30 nm Aunp suspension contains 2×10^{11} Aunps per ml.

The solutions and suspensions used for fluorescence, UV-vis, and ζ-potential measurements were all made in the same manner. For pure BSA samples a stock solution (1 mg ml^{-1} in ultrapure Milli-Q water, ~13.7 μM) was adjusted to pH 7 with NaOH (0.25 M). This solution was then diluted to 3.6 μM with Milli-Q water, pH was checked and UV-vis was used to control the concentration. The molar absorptivity for BSA at 278 nm is 44 000 mol^{-11} cm^{-1}.[17]

The BSA–Aunp suspensions were made by mixing gold (1 ml) with BSA (0.525 ml, 13.7 μM, pH 7). The suspensions were then allowed to equilibrate for 1 hour before Milli-Q water (0.475 ml) was added, and the pH adjusted to 7 again. Suspensions were allowed to equilibrate overnight prior to analysis. The concentration of BSA in BSA–Aunp suspensions is chosen in line with Kaufman *et al.* who used a protein : gold ratio equal to 2000 : 1, on 12.8 nm Aunps,[14] giving a BSA/gold nm^2 ratio = 3.9. This corresponds to a BSA : gold ratio equal to 10 986 : 1 for the 30 nm Aunp and 78 125 : 1 for the 80 nm Aunp. The BSA concentration was kept constant at 3.6 μM in all solutions and suspensions, so that any change observed would be due to the amount of adsorbed BSA. For fluorescence measurements with ANS, ANS (10 μl, 5 mM) was added to a BSA solution (3 ml, 3.6 μM) and to BSA–Aunp suspensions (3 ml) made as described above. The final concentration of ANS was 17 μM. ANS is commonly used as an extrinsic fluorescence probe for studying proteins.[18–20]

UV-vis spectroscopy

UV-vis spectra were collected using a Shimadzu UV-2401PC spectrophotometer over the wavelength range of 200–800 nm.

ζ-Potential measurements

The ζ-potential and size (dynamic light scattering, DLS) measurements of BSA and the protein–gold constructs were measured on a Zetasizer Nano-ZS instrument from Malvern instruments using DTS software.

Fluorescence

The fluorescence measurements were performed on a Fluorolog-3 HORIBA Jobin Yvon apparatus. For the *steady-state measurements* of BSA solutions and BSA–Aunp conjugates, the excitation wavelength was $\lambda_{ex} = 295$ nm. If BSA is excited with $\lambda_{ex} = 280$ nm, tyrosine and phenylalanine contribute to the emission signal. By using $\lambda_{ex} = 295$ nm only signals from tryptophan (Trp) are measured.[21] For intrinsic fluorescence measurements the slits were 10 nm, and polarizator was used. For all samples containing ANS the excitation wavelengths were $\lambda_{ex} = 370$ nm and $\lambda_{ex} = 388$ nm. The excitation wavelength $\lambda_{ex} = 388$ nm was chosen as specified by the supplier. The secondary excitation wavelength $\lambda_{ex} = 370$ nm was chosen based on earlier studies of ANS as a fluorescence probe for proteins.[19] For all the figures shown here, the excitation wavelength was $\lambda_{ex} = 388$ nm and slits = 1 nm.

Time correlated single photon counting (TCSPC) of samples without ANS a 280 nm LED lamp was used. The prompt was recorded with the emission monochromator (Em. mono) = 280 nm, and the samples using Em. mono = 350 nm. The bandpass was 5 nm. For samples with ANS the LED lamp for the TCSPC measurements had $\lambda_{ex} = 370$ nm. The prompt was recorded with the Em. mono = 370 nm, and the samples using Em. mono = 470 nm. The bandpass was 14 nm. Detailed descriptions of this technique can be found elsewhere.[13,22] Briefly, relaxation from the radiative excited states was modeled using a weighted sum of exponential decays:

$$Y(t) = \sum_{i=1}^{N} B_i e^{-(\frac{t}{T_i})} \quad (1)$$

where N is the total number of fluorescent components and B_i represents the amplitude (population) associated with lifetime T_i. The final fit was approached using an iterative process where exponentials were added until no significant improvements in the χ^2 value of the fit could be seen.

Bradford assays

The amount of adsorbed protein on Aunps was determined using a Bradford assay. First, size determination of BSA was performed using a Zetasizer 3000HSA from Malvern instruments. The size was determined in three different buffers. Acetate buffer (pH 3.8) gave a size of 7.9 nm, phosphate buffer (pH 7) gave a size of 5.6 and finally borate buffer (pH 9) gave a size of 8.9. The size of BSA in citrate was assumed to be 8, 6 or 4 nm. A stock solution of BSA (7.2 μM; 600 μl, 300 μl or 150 μl) was mixed with gold colloid suspension (600 μl) to give final concentrations of BSA of 3.6 μM, 1.8 μM or 0.9 μM. Following equilibration, the samples were centrifuged to precipitate the BSA–Aunp constructs, and the remaining protein concentration in the supernatant was measured using the Bradford method.[23] The size measurements and Bradford assays were then combined to give a layer calculation.

Langmuir isotherms

Surface pressure–area measurements were recorded using a KSV Langmuir Minitrough double barrier system (KSV LTD, Finland) controlled through the manufacturer's own software. The trough was made of Teflon, with barriers of Delrin. Two different methods for investigating protein–lipid interactions were applied, both adopted from Glomm *et al.*[4] For the *injected method* the subphase used was Milli-Q water adjusted to pH 7 with NaOH. The surface was swept with a vacuum pump-connected Pasteur pipette and then compressed and decompressed to check for impurities at the surface prior to introduction of the lipid film (L-α-phosphatidylethanolamine, 1 mg ml^{-1} in chloroform, 30 μl). The film was spread with a 50 μl Hamilton syringe. Initial compression to 5 mN m^{-1} was started 15 minutes after film introduction. Film compression was carried out with a constant barrier speed of 5 mm min^{-1} while an electrobalance recorded the surface tension through means of a paper probe. The sample was then introduced under the lipid film from outside and under the barriers (Scheme 1). The system was allowed to equilibrate for one hour at a constant trough area before the compression continued to 40 mN m^{-1}. When lipid was not present the barriers were moved to position 10 mm, and the sample introduced under the air–water surface. The rest of the procedure was executed as if lipid was present. In all cases the final BSA concentration was 50 nM, and the trough volume was 250 ml.

The different samples injected were:

1. BSA (1 ml, 12.5 μM, pH 7).
2. BSA–Aunp construct (0.5 ml, 50% (v/v) gold suspension, 25 μM BSA, pH 7). This was done with both 30 nm Aunps and 80 nm nanoparticles.

For the *subphase method* the BSA–Aunp suspensions (1.2 ml, 50% (v/v) gold suspension, 12.5 μM BSA, pH 7) were diluted to 300 ml for both the 80 nm Aunp and the 30 nm Aunp. The protein only subphase was made by diluting a BSA solution (0.3 ml, 50 μM) to 300 ml.

Directly after the subphase was poured into the trough, the surface was vacuumed. For experiments without lipid the subphase was then compressed and decompressed. After the decompressing, the lipid film was spread on top. After 15 minutes a new cycle of compressing/decompressing was started. For illustration of these two methods, see Scheme 1. All the Langmuir experiments were simultaneously monitored by Brewster Angle Microscopy.

Brewster Angle Microscopy (BAM)

BAM was used to visualize monolayers using a KSV BAM 300. The instrument consists of a standard 10 mW He–Ne laser, emitting p-polarized light at a wavelength of $\lambda = 632.8$ nm by the use of a high-quality Glan–Thomson polarizer. The reflected light is imaged onto a computer controlled CCD camera with 768 × 44 pixels through a 10× magnification objective, yielding a spatial resolution of ~2 μm. A black wedge-shaped glass plate is placed at the bottom of the trough to reflect any light that is transmitted through the subphase out of the optical axis and to minimize convection in the trough. The method is adopted from Glomm *et al.*[4]

To obtain DVM pictures, first a Langmuir–Blodgett film was deposited with the equipment described above for the Langmuir experiments. A microscope slide was washed with ethanol and blown dry with air before being submerged vertically into the

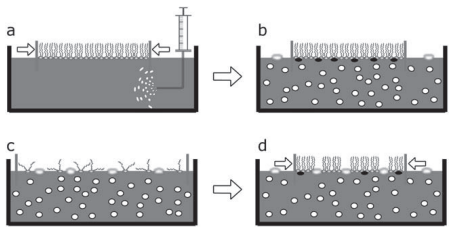

Scheme 1 Situation before (left column) and after (right column) introduction of protein or protein–gold constructs to the lipid film. The upper pictures (a and b) show the injected method, and the lower pictures (c and d) show the *subphase method*. Solutes in bulk indicated by white spheres, while solutes interacting with lipid monolayer headgroups indicated by black ellipsoids. Solutes spreading along the air–water interface indicated by blurred ellipsoids (Adapted from Glomm *et al.*[4]).

 This journal is © The Royal Society of Chemistry 2011

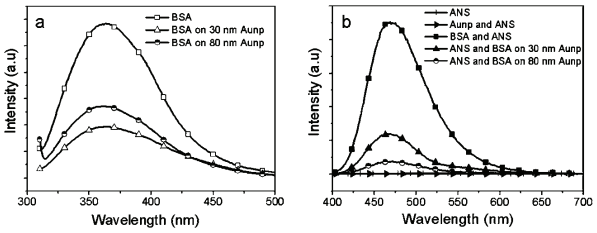

Fig. 1 (a) Steady-state fluorescence measurements of BSA and BSA–Aunp constructs ($\lambda_{ex} = 295$ nm). (b) Steady-state measurements of ANS with BSA and with BSA–Aunp constructs ($\lambda_{ex} = 388$ nm).

subphase, which was vacuumed first. Compression to 25 mN m^{-1} was started 15 minutes after film introduction. While the pressure was kept constant at 25 mN m^{-1}, the microscope slide was lifted up with a speed of 1 mm min^{-1}. The deposited film was then studied using cross-polarized light and a Digital Video Microscope (DVM). The microscope used was Nikon eclipse ME 600, and the camera was a CoolSnap Proof Monochrome, an integrated solution from Media Cypernetics, "the imaging experts"™. The software used was Image-Pro Plus5.0.

Lipid only was studied at both 25 mN m^{-1} and 30 mN m^{-1}. DVM pictures were also taken using the *injected method*, where the lipid film was compressed to 5 mN m^{-1} before the BSA or BSA–Aunp conjugate was introduced and allowed to equilibrate as for the Langmuir isotherm recordings. After one hour the system was compressed to 25 mN m^{-1} and the dipping procedure continued as for the *subphase* experiments.

Results and Discussion

In the following sections, the results are presented in terms of protein binding to Aunp surfaces, the interaction between BSA–Aunp constructs and Langmuir lipid films, and the ability of the BSA–Aunp constructs to enhance film miscibility and disrupt lipid monolayers.

Immobilization onto Aunps modulates BSA conformation

Sample preparation and characterization. UV-vis showed a ~3 nm bathochromic (red) shift in the localized surface plasmon resonance (LSPR) band for both 30 nm and 80 nm Aunps upon introduction of BSA. The red shifts displayed by the BSA–Aunp constructs as compared to unmodified particles are consistent with a change in the dielectric function on the nanoparticle surface upon protein adsorption.[24–26] Introduction of BSA to the particle suspension did not significantly alter the lineshape of the absorption spectra, indicating that the BSA–Aunp constructs remained as single colloids rather than flocs under these conditions.

To quantify the amount of BSA adsorbed on the Aunps, Bradford assays were performed.[23] At pH 7 and at a protein concentration of 3.6 μM, BSA adsorption resulted in a monolayer coverage on the Aunps, with BSA : Aunp ratios of ~60 and ~400 for 30 nm and 80 nm Aunps, respectively. The BSA diameter was estimated to be 6 nm as determined by dynamic light scattering (DLS). This is in agreement with other DLS results showing that for both Aunp sizes studied here the particle diameter increased with 10 nm upon BSA adsorption. It should be noted that in ultrapure (Milli-Q) water without any pH adjustment (pH ~5.5), the layer calculation showed an equivalent of 11.5 and 24.7 layers for 80 and 30 nm Aunps, respectively. This corresponds well with findings of Kaufman *et al.*[14] where the authors observed multilayer formation for binding of BSA to negatively charged Aunps, with an irreversibly bound inner layer surrounded by loosely associated protein molecules.

The ζ-potential measurements of BSA–Aunp constructs showed for both sizes of Aunp a reduction of the absolute value compared to Aunps only ($\zeta \approx -45$ mV for Aunp only and $\zeta \approx -37$ mV for BSA–Aunp constructs. For BSA only, the ζ-potential was −26 mV under these conditions). The negative surface charge of Aunps emanates from a layer of stabilizing citrate molecules remaining from the particle synthesis. These changes in ζ-potential value together with the red shift of the LSPR confirm that BSA is associated with the Aunp. Binding of BSA to Aunps is thought to occur primarily through electrostatic interactions between the citrate-covered particles and oppositely charged patches on the protein surface.[11,27]

Steady-state fluorescence. UV-vis and ζ-measurements show that binding occurs but reveal little about any conformational changes in the adsorbed layer. To get a better understanding of what happens with BSA upon binding to gold, both intrinsic (Trp) and extrinsic (1-anilino-8-naphthalene sulfonate; ANS) fluorescence were measured (Fig. 1). Fig. 1a shows Trp emission spectra of BSA, both free in solution and immobilized on Aunps. It is well known that the Trp fluorescence is highly influenced by changes in the local environment.[21] As the intensity and position of the peak maximum are sensitive to solvent exposure, the Trp fluorescence is often used to indicate changes in protein conformation. BSA contains two Trp residues: one buried in the hydrophobic interior and one residing closer to the surface.[12] From Fig. 1a, it can be seen that upon introduction of Aunps, the Trp emission is reduced, with the magnitude of signal reduction being proportional to Aunp diameter. This again confirms adsorption, as interaction between protein and Aunps will cause a reduction of fluorescence due to static quenching when the protein is physi- or chemisorbed to gold.[16] As BSA is present in large excess compared to surface coverage, the emission spectra contain contributions from free and immobilized BSA. Any

Table 1 Fluorescence lifetimes and corresponding populations of BSA, BSA–Aunp constructs and samples with added ANS. T = lifetimes in nanoseconds (ns), B = populations in %[a]

	$T1$ (ns)	$B1$ (%)	$T2$ (ns)	$B2$ (%)	χ^2
Protein–gold constructs (λ_{ex} = 280 nm)					
BSA	4.0	23 ± 4	7.1	77 ± 4	0.86
BSA + 30 nm Aunp	3.8	32 ± 3	7.1	68 ± 3	1.21
BSA + 80 nm Aunp	3.7	30 ± 4	6.9	70 ± 4	1.11
ANS and protein–gold constructs (λ_{ex} = 370 nm)					
BSA	4.7	6 ± 1	18.5	94 ± 1	0.99
BSA + 30 nm Aunp	5.7	8.4 ± 0.1	19.0	91.6 ± 0.1	1.00
BSA + 80 nm Aunp	6.6	11.4 ± 0.6	19.1	88.7 ± 0.6	0.98

[a] For aqueous ANS the lifetime in nanoseconds was $T1 = 5.4 \pm 0.8$, $T2 = 18 \pm 2$, and $T3 = 0.27$ with the corresponding populations $B1 = 8 \pm 1$, $B2 = 12 \pm 2$, and $B3 = 80 \pm 2$, respectively.

changes in lineshape or position of the emission maximum emanating from the surface-bound protein will likely be drowned by spectral contributions from the free protein. Thus, the Trp fluorescence only provides confirmation of protein binding in this study.

ANS is a frequently used extrinsic fluorescence probe for studying changes in protein conformation.[1,18–20,28,29] To the best of our knowledge there are presently no studies using ANS to follow BSA adsorption on Aunps. ANS is highly fluorescent when associated with the hydrophobic interior of the protein, but is almost completely quenched in water due to solvent effects.[21] Consequently, ANS fluorescence is expected to decrease if the protein unfolds on the surface, reducing access to hydrophobic domains. From Fig. 1b, it can be seen that there is an intensity loss upon introduction of Aunps which is larger for 80 nm than for 30 nm Aunp. Suspensions containing only ANS or gold with ANS in water gave negligible signal intensity compared to the protein-containing samples. The BSA concentration was kept constant, so the reduction in emission intensity from the BSA–Aunp constructs compared to the free protein is likely due to reduced access to hydrophobic domains. These results could be due to unfolding of the adsorbed protein, leading both to solvent exposure and compression of the protein adlayer. The emission intensity decrease is significantly more pronounced for the larger Aunp core. Assuming that the observed reduction in emission intensity is due to unfolding of the adsorbed BSA, the results obtained here fit well with the well-established observation that the propensity for surface-induced unfolding is inversely proportional to the curvature.[15]

Time-correlated single photon counting (TCSPC). Calculated lifetimes and corresponding populations for intrinsic and ANS fluorescence are shown in Table 1. In the case of intrinsic fluorescence, the acquired data were best modeled using a biphasic decay, revealing one short and one long lifetime, $T1$ and $T2$, with relative populations $B1$ and $B2$, respectively. Since a 280 nm LED was used for lifetime measurements other intrinsic fluorophores such as tyrosine were excited as well as tryptophan. However, the response is expected to be dominated by the tryptophan emission. No significant changes in lifetimes were observed for the BSA–Aunp constructs relative to the free protein. Immobilization of BSA onto Aunps results in an increase in the relative population $B1$ corresponding to the short lifetime ($T1$ in Table 1). No significant changes in relative populations can be observed between the two particle sizes applied here. An increase in the fraction of fluorophores corresponding to the short lifetime compared to free BSA indicates an increased exposure to solvent for the BSA–Aunp constructs. The increase in $B1$ upon adsorption on gold is likely due to conformational changes of the surface-bound protein compared to the free BSA. The total available surface area in the 30 nm Aunp suspension is 5.65 cm^2 ml^{-1}, while for 80 nm Aunp it is only 2.21 cm^2 ml^{-1}. As both particle concentration and available surface area are lower for the 80 nm Aunp, changes in protein conformation are likely larger for the 80 nm BSA–Aunp construct in order to elicit the same population changes as the 30 nm BSA–Aunp constructs. This is in accordance with the steady-state fluorescence results, in that a lower curvature appears to promote a higher degree of unfolding of the protein.

Time resolved fluorescence data of ANS associated with BSA and BSA–Aunp constructs are shown in Table 1 (lower panel). Decay times in aqueous ANS solutions were best modeled with a tri-exponential fit, in accordance with literature.[21] The lifetimes of ANS only were found to be significantly different from the lifetimes obtained in the presence of BSA and BSA–Aunp constructs (Table 1). This is expected as the quantum yield of aqueous ANS is negligible compared to when ANS resides in the hydrophobic interior of BSA, which is in accordance with the steady-state results (Fig. 1). Hence, only contributions from ANS associated with BSA were found to be statistically significant in this study. A two-state model comprised of one short and one long lifetime was found to yield the best fit of ANS in the presence of BSA or BSA–Aunps (Table 1). Similar to the results obtained for intrinsic fluorophores, the lifetimes and corresponding populations are interpreted as emanating from states close to and shielded from the solvent, respectively. The short lifetime ($T1$) increases progressively upon introduction of Aunps and with increasing particle size, whereas the long lifetime ($T2$) remained unchanged for all three systems. This slight increase in $T1$ can probably be attributed to close packing of BSA on the

 This journal is © The Royal Society of Chemistry 2011

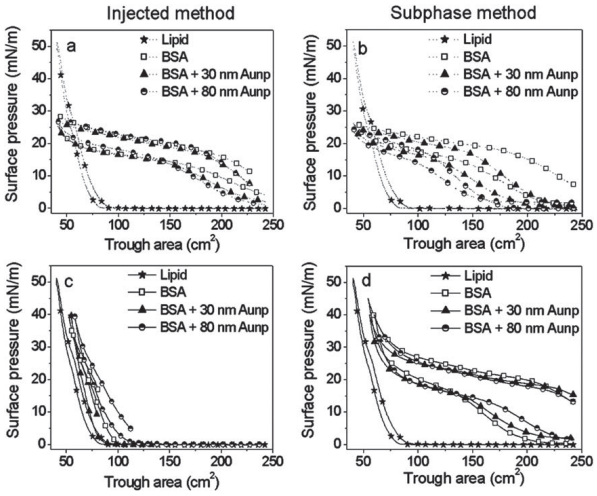

Fig. 2 Langmuir isotherms where (a) and (b) are without the lipid present when protein or protein–Aunp construct is introduced. In (c) the lipid is introduced first and the protein/construct injected underneath. (d) The panel depicts a subphase containing protein/construct added first and the lipid introduced on top. Isotherm for a pure lipid film has been included in all figures for an easier comparison. For each dataset the upper line corresponds to compression and the lower line represents expansion.

Aunp surfaces, which is expected to increase with increasing core diameter. Analogous with results obtained from intrinsic fluorophores, there is an increase in population when BSA is immobilized on Aunps. Moreover, the population of *T*1 increases with Aunp diameter, indicating that ANS is more exposed to water upon immobilization, and with increasing particle diameter.

The steady-state and TCSPC measurements for both intrinsic and extrinsic probes indicate that BSA exposes more of its hydrophobic residues to the solvent when adsorbed. On 80 nm Aunps this is more pronounced than on 30 nm particles, indicating that a lower curvature promotes larger changes in the protein adlayer. We interpret these changes as unfolding of BSA when immobilized on gold, with the extent of conformational change being proportional to Aunp core diameter. Larger unfolding of the protein on the bigger Aunp is in agreement with literature.[15] Hence, for a given set of Aunp surface characteristics, the conformation and polarity of the protein adlayer and concomitant interfacial activity of protein–Aunp constructs might be tunable by varying the Aunp diameter.

Immobilization onto Aunps modulates BSA interfacial activity

Film-forming properties of BSA–Aunp constructs relative to reference systems. Two different protein introduction procedures were employed: the *injected* and *subphase methods*, respectively.[4] In the *injected method*, the lipid layer was first compressed to a surface pressure of 5 mN m^{-1} before either the protein or BSA–Aunp constructs were injected under the lipid layer from outside the barriers. Conversely, in the *subphase method* BSA was already mixed into the subphase before lipid was introduced. For more details on the different methodologies employed see the Materials and methods section and also illustrated in Scheme 1.

Surface pressure–area (Π–A) isotherms of the reference systems—lipid, BSA and BSA–Aunp constructs—are given in Fig. 2a and b for the *injected* and *subphase methods*, respectively. Suspensions of unmodified (citrate coated) Aunps did not result in measurable film formation at these concentrations, irrespective of the introduction method (*injected* or *subphase*). From the compression part of the Π–A isotherm of the lipid, the mean molecular area (MMA), determined from the inflection point marking the transition from a 2D gaseous to a liquid state, was found to be 52 Å^2 per molecule. The collapse pressure of the pure lipid film (*i.e.* the highest surface pressure to which a monolayer can be compressed without collapsing and/or forming multilayers) was found to be ~51 mN m^{-1}. The compression–expansion isotherm of the lipid (Fig. 2) shows a narrow hysteresis loop, with a steep slope indicating a low compressibility of the monolayer.

In all the systems where BSA or BSA–Aunp constructs are used, the resulting Π–A isotherms contain contributions from film-forming species which do not fulfill the criteria for a Langmuir monolayer. Specifically both BSA and BSA–Aunp constructs are soluble in the subphase. Thus, all Π–A isotherms are shown as surface pressure *versus* trough area. As seen from Fig. 2a and b, introduction of BSA or BSA–Aunp constructs *via* the *injected* or *subphase method* resulted in strong film formation with surface pressures exceeding 25 mN m^{-1} at full compression. Due to both BSA and BSA–Aunp being soluble in the subphase, the maximum surface pressures never exceeded 30 mN m^{-1}. Thus, as shown by Glomm *et al.*,[4] spreading of lipid after introduction of another film-forming agent, such as in the

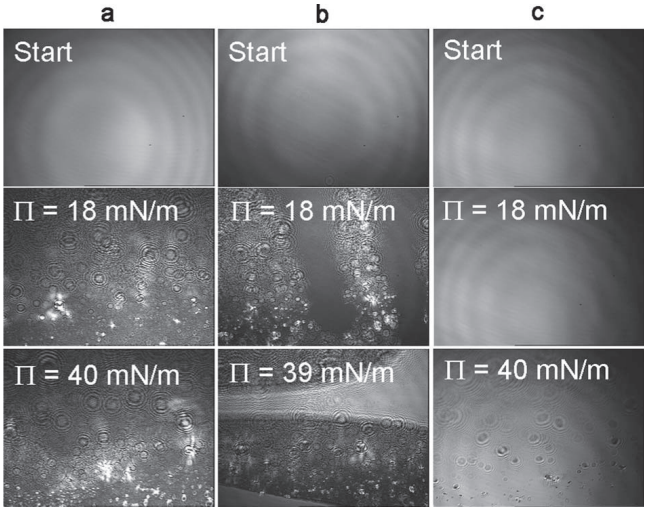

Fig. 3 BAM images of BSA/BSA–Aunp constructs interacting with lipid Langmuir films. (a) *Injected method* with BSA, (b) *subphase method* with BSA, and (c) *subphase method* with BSA on 30 nm Aunp.

subphase method, will lead to a mixed monolayer behavior. Compared to the lipid, BSA and BSA–Aunp constructs result in a more compressible film with a broader hysteresis loop (Fig. 2a and b). For the *injected method*, no significant differences could be observed between the isotherms for BSA and BSA–Aunp constructs.

At lower trough areas (<100 cm^2) the isotherms for the *subphase method* (Fig. 2b) closely resemble those of the *injected method*. Unlike what was found for the *injected method*, clear differences in the compression–expansion isotherms for BSA and BSA–Aunp constructs are observable when using the *subphase method* (Fig. 2b). Compared to the parent protein, the initial surface pressure of the BSA–Aunp constructs is lower and the hysteresis loop is significantly narrower. Moreover, the compression–expansion isotherms for the two sizes of BSA–Aunp constructs are clearly discernible with the initial surface pressure increase starting at lower trough areas and yielding a narrower hysteresis loop for the larger Aunp core. This indicates that the less film-forming material is present at the surface for the BSA–Aunp systems compared to the native protein, and that the surface concentration of the BSA–Aunp constructs is lowest for the larger Aunp core. When using a BSA solution or a BSA–Aunp suspension as a subphase, a bulk–surface equilibrium is assumed to be in place.[4] In the *subphase method* the surface is vacuumed and Π set to zero immediately following introduction of the (film-forming) subphase. Thus, the baseline prior to compression does not represent a film-free surface. Depending on the interfacial activity of film-forming species in the subphase, different concentrations will be present at the surface when this is vacuumed. From Fig. 2b, it is evident that less material is available for compression of the BSA–Aunp constructs than of the native protein, indicating a higher surface activity for the former. Additionally the surface activity increases with the larger Aunp core size. Immobilization of BSA on Aunps alters the proteins' hydrophobicity, and by applying larger particles a larger change in interfacial activity can be induced. This corresponds well with steady-state fluorescence and TCSPC measurements.

Fig. 2c and d illustrate compression–expansion isotherms for mixed systems using the *injected* and *subphase method*, respectively. For none of these systems the isotherms distinguish between the protein and the protein–Aunp constructs. When using the *injected method* (Fig. 2c) the mixed films display mostly lipid characteristics. This indicates that when interacting with a precompressed film, the BSA and BSA–Aunp constructs reside mostly under the lipid, near the polar headgroups. The differences between the isotherms are representative of the inherent uncertainties for the *injected method*.[4] Using the *subphase method* (Fig. 2d) the resulting isotherms for mixed systems all display protein-like behavior, with lipid characteristics only being prevalent at high compression. Since protein is much more compressible than the lipid, the protein (or BSA–Aunp constructs) will dominate the film behavior as long as the protein is on the surface. But when the pressure is high enough most of the protein will be solubilized into the subphase and the isotherms will adopt more of a lipid character. Depending on the introduction method used, the resulting mixed isotherm displays either a lipid-like (*injected*) or a protein-like (*subphase*) behavior.

Miscibility and domain properties of mixed films. Brewster Angle Microscopy (BAM) can be used to visualize the morphology and heterogeneity of a film at air–water surfaces.[4,30–33]

 This journal is © The Royal Society of Chemistry 2011

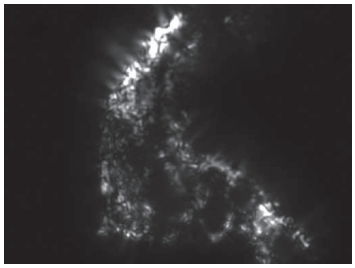

Fig. 4 DVM image of the lipid film using cross-polarized light. Magnification 50×.

In this study the BAM pictures in Fig. 3 provide complementary information about the film morphology. For clarity, dark regions represent film-free surfaces, whereas bright regions show film-forming material. BAM images of mixed films using the *injected* (3a) and *subphase method* for BSA (3b) and BSA–Aunp constructs (3c) are shown in Fig. 3. The upper panels represent the film conditions immediately prior to compression, *i.e.* a mixed lipid–BSA or lipid–BSA–Aunp film. In the *injected method*, the lipid film was precompressed to 5 mN m^{-1}, whereas no precompression was done in the *subphase method*. Prior to compression of the pure lipid film, no film formation was evident, as represented by a homogeneous dark surface (not shown). Upon compression, a monolayer is formed, with a morphology similar to the two lower panels of Fig. 3a. The bright structures observed for the lipid film might be indicative of liquid crystal structures. For BSA or BSA–Aunp constructs only there is already a complete monolayer present prior to compression, similar to the upper panels of Fig. 3. Upon compression, the images grew increasingly brighter, indicating formation of an increasingly thicker film. BAM images of mixed films obtained using the *injected method* (Fig. 3a) appear indistinguishable from those of lipid only at surface pressures exceeding 5 mN m^{-1}. No distinctive differences could be observed between BSA and BSA–Aunp constructs. This corroborates the assumption drawn from the compression–expansion isotherms, in that the proteins (or protein–Aunp constructs) interact mainly with the lipid headgroups.

BAM images of mixed films using the *subphase method* are shown in Fig. 3b and c for BSA and BSA–Aunp constructs, respectively. For BSA interacting with the lipid film (Fig. 3b, top panel), the film morphology at low surface pressures is indistinguishable from that of protein-only. At higher lateral pressures (Fig. 3b, middle panel), the BAM images show two distinct domains: one corresponding to the lipid (structured regions) and one corresponding to BSA (light, homogeneous regions). At ~40 mN m^{-1}, the lipid-like domains appear unchanged, whereas the protein-like domains are significantly brighter, indicating a denser/thicker protein film. Thus, introduction of BSA *via* the *subphase method* results in mixed-film behavior, with immiscible lipid-like and protein-like domains.[4] Conversely, BSA–Aunp constructs interacting with the lipid film (Fig. 3c) show no domain formation at any surface pressure. Rather, the morphology of the BSA–Aunp construct-lipid film appears indistinguishable from that of a BSA film only, save for some small regular structures towards maximum compression (Fig. 3c, lower panel). This absence of distinguishable domains was observed for both sizes of Aunps used here.

As the protein concentration was kept constant, the pictures in Fig. 3b and c indicate that the BSA–Aunp constructs promote film miscibility. We believe that this feature of the BSA–Aunp constructs can be attributed to a difference in conformation of the immobilized BSA compared to the native protein, as indicated by the steady-state and time-resolved fluorescence discussed above. Hence, modulating the protein fold by attachment to colloidal structures might result in an altered interfacial activity and concomitant lipid film interaction.

BSA–Aunp constructs disrupt liquid crystal lipid domains

Digital video microscopy (DVM) birefringence. The BAM images of the lipid used here displayed features which might be attributed to liquid crystalline domains. A liquid crystalline phase is classified as having short-range disorder but some distinct ordering over larger distances, with a liquid-like state of the alkyl chains.[34] To ascertain whether the lipid formed liquid crystalline domains under the conditions studied here, cross-polarized light microscopy images of Langmuir–Blodgett films deposited on microscope slides were acquired. The sample image shown in Fig. 4 clearly indicates that the lipid film contains liquid crystalline domains, as represented by the bright regions.

When only lipid film was studied, there were many larger structures of liquid crystals. Introduction of BSA only by either method, or BSA–Aunp constructs by using the *injected method*, yielded no observable effect on these structures. However, when applying BSA–Aunp constructs of either size to the lipid film using the *subphase method*, the liquid crystalline domains were significantly reduced both with respect to size, brightness and number. This indicates that BSA–Aunp constructs disrupt the ordered lipid structures, as no such effect was observed for the native protein, coinciding well with the BAM images showing that BSA–Aunp constructs induce film miscibility.

Conclusion

UV-vis, ζ-potential, and fluorescence measurements all show that BSA adsorbs on Aunps, forming monolayers at neutral pH. From the steady-state and time-resolved fluorescence measurements using intrinsic and extrinsic probes, surface-bound BSA is partially unfolded compared to the native protein. The ANS fluorescence approach, often used to probe the extent of protein unfolding and the identification of intermediately folded states such as the molten globule state,[35,36] can also be used in assessing the degree of unfolding on protein–Aunp systems although some care must be taken when assessing potential steric effects the Aunps has on quencher access. When studying the interactions of BSA and BSA–Aunp constructs with a lipid monolayer using the Langmuir technique, the resulting isotherms were found to depend greatly on whether the protein (or protein–Aunp constructs) was injected under a pre-compressed lipid monolayer (*injected method*) or introduced into the subphase prior to spreading of the lipid (*subphase method*). Specifically, the behavior of the mixed film is largely dependent on the amount of

protein embedded in the monolayer. BAM images reveal that when applying the *subphase method*, BSA and lipid form an immiscible monolayer with distinct lipid and protein domains. However, when BSA was adsorbed onto Aunps, the resulting BSA–Aunp constructs resulted in film miscibility, indicating that the BSA–Aunp constructs are more effective at lipid film penetration than the native protein. Moreover, cross-polarized microscopy images show that unlike the native protein, the BSA–Aunp constructs disrupt liquid crystalline domains seen in the lipid film at a high lateral compression. The results show that modification of a protein by immobilization onto nanoparticles may affect its ability to penetrate lipid films and affect film miscibility, which holds great potential for biomedical applications of protein–nanoparticle constructs.

That protein conformational changes take place at interfaces is established for many systems.[27,37–41] In this study, two effects of these conformational changes are documented and explored: (i) the modulation of the surface activity of BSA–Aunps and (ii) the enhanced film miscibility of the BSA–Aunp mixed monolayers. Both these characteristics of the BSA–Aunps appear to be emergent qualities of the construct, as the protein component and the nanoparticle component alone do not have these characteristics at the conditions tested here. There exist conflicting reports as to whether BSA unfolding is consistent with a simple two-state model.[42–44] It is thus possible to envision conditions (*i.e.* denaturating conditions) where BSA has similar characteristics. However, protein–Aunp constructs have the advantages of multifunctionality and optical traceability of the construct,[8] as well as heat-induced apoptosis *via* excitation of the localized surface plasmon resonance (LSPR) band.[25,45] Moreover, the Aunp-induced characteristics are gained independently of any non-physiological condition or reagent. The degree of unfolding appears to increase with increasing Aunp diameter, which agrees with earlier studies.[15] This, together with modification of the adlayer characteristics, offers the opportunity of controlling the construct properties further. The surface activity of such constructs may play an important role in drug delivery and targeting, as a high affinity for membranes relative to native proteins has been strongly implicated in the activity of drugs based on intermediately folded protein states.[46,47] The emergent qualities of BSA–Aunps must stem from how the protein exposes its hydrophobic motifs to the solvent. The exact details of the conformational changes are beyond both the scope of this study and the resolution of the applied techniques. Indeed, only a few such studies exist for nanoparticle–protein constructs, one notable example being Engel *et al.*[37] BSA is a zinc- and small organic molecule-binding protein constructed from three homologous helical domains,[48] each containing two sub-domains, which in principle provides many possibilities for partial unfolding and specific orientation upon adsorption to Aunps. It would be interesting to apply the approach of Engel *et al.*, which provides information on which parts of the protein retain a native fold and/or are shielded by the nanoparticle, provided that efficient displacement procedures and protein size limitations could be managed properly.

Acknowledgements

The authors acknowledge the Department of Chemical Engineering, NTNU, for financial support. Wilhelm R. Glomm and Sondre Volden acknowledge financial support from the Research Council of Norway (NFR).

References

1 D. Togashi, A. Ryder and D. O'Shaughnessy, *J. Fluoresc.*, 2010, **20**(2), 441–452.
2 A. Junghans, C. Champagne, P. Cayot, C. Loupiac and I. Köper, *Langmuir*, 2010, **26**(14), 12049–12053.
3 T. Nylander, Protein–Lipid Interactions, in *Studies in Interface Science 7*, ed. D. Möbius and R. Miller, Elsevier Science, B.V., 1998, pp. 385–429.
4 W. R. Glomm, S. Volden, Ø. Halskau and M. H. G. Ese, *Anal. Chem.*, 2009, **81**(8), 3042–3050.
5 C. M. Feldherr and D. Akin, *J. Cell Sci.*, 1999, **112**, 2043–2048.
6 A. G. Tkachenko, H. Xie, D. Coleman, W. Glomm, J. Ryan, M. F. Anderson, S. Franzen and D. L. Feldheim, *J. Am. Chem. Soc.*, 2003, **125**(16), 4700–4701.
7 A. G. Tkachenko, H. Xie, Y. Liu, D. Coleman, J. Ryan, W. R. Glomm, M. K. Shipton, S. Franzen and D. L. Feldheim, *Bioconjugate Chem.*, 2004, **15**(3), 482–490.
8 W. R. Glomm, *J. Dispersion Sci. Technol.*, 2005, **26**(3), 389–414.
9 J. A. Ryan, K. W. Overton, M. E. Speight, C. N. Oldenburg, L. Loo, W. Robarge, S. Franzen and D. L. Feldheim, *Anal. Chem.*, 2007, **79**, 9150–9159.
10 M. Iosin, F. Toderas, P. L. Baldeck and A. Astilean, *J. Mol. Struct.*, 2009, **924–926**, 196–200.
11 S. H. Brewer, W. R. Glomm, M. C. Johnson, M. K. Knag and S. Franzen, *Langmuir*, 2005, **21**, 9303–9307.
12 A. Housni, M. Ahmed, S. Liu and R. Narain, *J. Phys. Chem. C*, 2008, **112**, 12282–12290.
13 H. Xie, A. G. Tkachenko, W. R. Glomm, J. A. Ryan, M. K. Brennaman, J. M. Papanikolas, S. Franzen and D. L. Feldheim, *Anal. Chem.*, 2003, **75**(21), 5797–5805.
14 E. D. Kaufman, J. Belyea, M. C. Johnson, Z. M. Nicholson, J. L. Ricks, P. K. Shah, M. Bayless, T. Petterson, Z. Feldtö, E. Blomberg, P. Claesson and S. Franzen, *Langmuir*, 2007, **23**, 6053–6062.
15 R. S. Kane and A. D. Stroock, *Biotechnol. Prog.*, 2007, **23**(2), 316–319.
16 T. Sen, K. K. Haldar and A. Patra, *J. Phys. Chem. C*, 2008, **112**, 17945–17951.
17 C. N. Pace, F. Vaidos, L. Fee, G. Grimsley and T. Grey, *Protein Sci.*, 1995, **4**, 2411–2423.
18 M. J. Tiera, G. R. d. Santos, V. A. d. O. Tiera, N. A. B. Vieira, E. Frolini, R. C. d. Silva and W. Loh, *Colloid Polym. Sci.*, 2005, **283**, 662–670.
19 E. Gabellieri and G. B. Strambini, *Biophys. J.*, 2006, **90**, 3239–3245.
20 G. V. Semisotnov, N. A. Rodionova, O. I. Razgulyaev, V. N. Uversky, A. F. Gripas' and R. I. Gilmanshin, *Biopolymers*, 1991, **31**(1), 119–128.
21 J. R. Lakowicz, *Principles of Fluorescence Spectroscopy*, Springer, New York, 2006.
22 W. R. Glomm, S. J. Moses, M. K. Brennaman, J. M. Papanikolas and S. Franzen, *J. Phys. Chem. B*, 2005, **109**(2), 804–810.
23 M. M. Bradford, *Anal. Biochem.*, 1976, **72**(1–2), 248–254.
24 S. Volden, A.-L. Kjøniksen, K. Zhu, J. Genzer, B. Nyström and W. R. Glomm, *ACS Nano*, 2010, **4**(2), 1187–1201.
25 P. Mulvaney, *Langmuir*, 1996, **12**, 788–800.
26 A. C. Templeton, J. J. Pietron, R. W. Murray and P. Mulvaney, *J. Phys. Chem. B*, 2000, **104**, 564–570.
27 W. R. Glomm, Ø. Halskau, A. M. D. Hanneseth and S. Volden, *J. Phys. Chem. B*, 2007, **111**(51), 14329–14345.
28 D. M. Togashi and A. G. Ryder, *Exp. Molec. Pathol.*, 2007, **82**(2), 135–141.
29 D. Togashi and A. Ryder, *J. Fluoresc.*, 2008, **18**(2), 519–526.
30 W. R. Glomm, M.-H. G. Ese, S. Volden, C. Pitois, A. Hult and J. Sjöblom, *Colloids Surf., A*, 2007, **299**(1–3), 186–197.
31 Q. He and J. Li, *Adv. Colloid Interface Sci.*, 2007, **131**(1–2), 91–98.
32 G. Sui, M. Micic, Q. Huo and R. M. Leblanc, *Colloids Surf., A*, 2000, **171**(1–3), 185–197.
33 Ø. Brandal, T. Viitala and J. Sjöblom, *J. Dispersion Sci. Technol.*, 2007, **28**(1), 95–106.

 This journal is © The Royal Society of Chemistry 2011

34 K. Holmberg, B. Jönsson, B. Kronberg, and B. Lindman, *Surfactants and Polymers in Aqueous Solution*, John Wiley & Sons, West Sussex, 2nd edn, 2007.
35 A. P. D. A. Bom, M. S. Freitas, F. S. Moreira, D. Ferraz, D. Sanches, A. M. O. Gomes, A. P. Valente, Y. Cordeiro and J. L. Silva, *J. Biol. Chem.*, 2010, **285**, 2857–2866.
36 T. Koshiba, M. Yao, Y. Kobashigawa, M. Demura, A. Nakagawa, I. Tanaka, K. Kuwajima and K. Nitta, *Biochemistry*, 2000, **39**(12), 3248–3257.
37 M. F. M. Engel, A. Visser and C. P. M. van Mierlo, *Proc. Natl. Acad. Sci. U. S. A.*, 2004, **101**(31), 11316–11321.
38 C. E. Giacomelli and W. Norde, *Macromol. Biosci.*, 2005, **5**(5), 401–407.
39 A. Kondo, S. Oku and K. Higashitani, *J. Colloid Interface Sci.*, 1991, **143**(1), 214–221.
40 A. M. Moulin, S. J. O'Shea, R. A. Badley, P. Doyle and M. E. Welland, *Langmuir*, 1999, **15**(26), 8776–8779.
41 P. Roach, D. Farrar and C. C. Perry, *J. Am. Chem. Soc.*, 2005, **127**(22), 8168–8173.
42 S. K. Singh and N. Kishore, *J. Phys. Chem. B*, 2006, **110**(19), 9728–9737.
43 C. Giancola, C. De Sena, D. Fessas, G. Graziano and G. Barone, *Int. J. Biol. Macromol.*, 1997, **20**(3), 193–204.
44 A. A. Moosavi-Movahedi, A. K. Bordbar, A. A. Taleshi, H. M. Naderimanesh and P. Ghadam, *Int. J. Biochem. Cell Biol.*, 1996, **28**(9), 991–998.
45 D. Pissuwan, S. M. Valenzuela and M. B. Cortie, *Trends Biotechnol.*, 2006, **24**(2), 62–67.
46 A.-K. Mossberg; M. Puchades; Ø. Halskau; A. Baumann; I. Lanekoff; Y. Chao; A. Martinez; C. Svanborg; R. Karlsson, *PLoS One*5((2)), 2010, e9384.
47 A. V. Agasøster, Ø. Halskau, E. Fuglebakk, N. A. Frøystein, A. Muga, H. Holmsen and A. Martínez, *J. Biol. Chem.*, 2003, **278**, 21790–21797.
48 C. A. Blindauer, I. Harvey, K. E. Bunyan, A. J. Stewart, D. Sleep, D. J. Harrison, S. Berezenko and P. J. Sadler, *J. Biol. Chem.*, 2009, **284**, 23116–23124.

This journal is © The Royal Society of Chemistry 2011

Paper II

Immobilization onto gold nanoparticles alters α-lactalbumin interaction with pure and mixed phospholipid monolayers

Soft Matter

Dynamic Article Links

Cite this: *Soft Matter*, 2011, **7**, 11501

www.rsc.org/softmatter

PAPER

Immobilization onto gold nanoparticles alters α-lactalbumin interaction with pure and mixed phospholipid monolayers

Sina M. Lystvet,*[a] Sondre Volden,[a] Øyvind Halskau, Jr.[b] and Wilhelm R. Glomm*[a]

Received 15th July 2011, Accepted 27th September 2011
DOI: 10.1039/c1sm06337e

Binding to colloidal structures such as gold nanoparticles (Aunps) is known to affect protein conformation, potentially altering the function and bioinvasiveness of the biopolymer. As the use of protein–Aunp constructs is widespread and increasing, an improved understanding of the invasiveness of nanomaterials is of fundamental interest and crucial for the burgeoning fields of nanotherapy and nanotoxicology. Here, we report on the interaction of bovine α-lactalbumin (BLA) modified 30 nm Aunps with neutral, negatively charged and mixed neutral : negative phospholipid Langmuir monolayers at pH 7.4, where little or no interaction has been reported for native BLA. The resulting equilibria and film properties were studied using surface pressure–area isotherms. Interaction of BLA with Aunps was investigated using UV-vis and fluorescence (steady-state and time-resolved, using intrinsic and extrinsic probes) spectroscopies. We find that upon binding to the Aunps, BLA partially unfolds, which in turn imparts higher interfacial activity and a stronger affinity towards phospholipid monolayers compared to the native protein.

Introduction

Understanding protein adsorption in general and protein phospholipid interactions in particular, is important to biomedical[1,2] and biochemical[1] research to *e.g.* better understand protein misfolding diseases,[2] drug design based on proteins,[3] and better incorporation of medical implants.[4] Although even cytosolic proteins with a well-defined fold will have some affinity to surfaces,[5] the so-called amphitropic proteins are expected to have a greater potential for surface binding as their function involves both being soluble and associated with membranes.[6] The function of amphitropic proteins is regulated by their reversible binding to the phospholipid bilayer.[7] Since their classification in 1988,[8] there has been an increase in publications on amphitropic proteins such as cytochrome C[9,10] and α-lactalbumin (BLA)[1,11–15] and their interaction with phospholipid membranes.[16] BLA is a 14.2 kDa globular calcium-binding protein with isoelectric point (pI) 4.5, and is a part of the lactose synthase complex that binds to galactosyltransferase and promotes synthesis of lactose.[17] An oleic acid stabilized conformer of human α-lactalbumin (human α-lactalbumin made lethal to tumours, HAMLET) has been shown to induce apoptosis in immature cells and cancer cells, while having lesser or no effects on healthy cells.[18] An analogous conformer of bovine α-lactalbumin (BAMLET) shows a similar effect.[13,19] The pharmacological potential of this phenomenon has been tested with positive results for bladder cancer, human xenograft glioblastomas in rats, and for skin papillomas.[20–22] While the exact mechanism behind HAMLET and BAMLET function remains unknown, and many processes beyond the initial contact with the outer cellular membrane are seen, one working hypothesis is that the initial step involves a direct interaction between HAMLET and the phospholipid membrane.[14] HAMLET has been shown to have a broad and high affinity to phospholipid membranes in vesicle systems, cell remnants and whole cells, while the native protein shows much lower tendencies to interact with these systems at physiological conditions.[22] In HAMLET and similar preparations, oleic acid may be an example of a folding manipulator which alters protein function.[23] It is thus possible that stabilizing alternative folds of BLA can lead to greatly altered protein characteristics.

In this study, we're interested in exploring whether a protein–nanoparticle construct can be prepared so as to enhance the ability of native BLA to interact with and perturb phospholipid monolayers. We have recently documented that nanoparticles change the interfacial properties of bovine serum albumin (BSA) and induce film miscibility.[24]

BLA binding to a phospholipid membrane is known to depend on protein–phospholipid charge density matching, calcium concentration, membrane curvature, pH,[25] and phospholipid composition and degree of acyl chain saturation.[6,13] Earlier Langmuir monolayer and vesicle leakage studies have shown that BLA interacts significantly with negatively and mixed neutral : negative phospholipid membranes close to the pI,[13,16,26] but

[a]*Ugelstad Laboratory, Department of Chemical Engineering, Norwegian University of Science and Technology (NTNU), N-7491 Trondheim, Norway. E-mail: lystvet@chemeng.ntnu.no; glomm@nt.ntnu.no; Tel: +47 73550325*
[b]*Department of Molecular Biology, University of Bergen, Thormøhlensgt 55 90, 5008 Bergen, Norway*

This journal is © The Royal Society of Chemistry 2011

at pH 7, only negligible interactions have been reported.[25] The curvature of the phospholipid film is important: while negatively charged Langmuir monolayers and large unilamellar vesicles (LUV) show no interaction with BLA above pH 6, small unilamellar vesicles (SUV) display BLA-interaction at a wider range including pH 7.[25] At pH 7, BLA has a global negative charge, and the lack of interaction between BLA and negative or neutral : negative phospholipid films has been predominantly attributed to electrostatic repulsion.[25,26] However, it is well known[5,24,27–29] that proteins—including BLA—interact strongly with negatively charged surfaces well above their pI.[5] Thus, electrostatic repulsion between the phospholipid headgroups and the global protein charge cannot solely account for the interaction patterns observed for BLA and phospholipid films. In addition to the phospholipid composition and charge, pH and curvature, the introduction method, *i.e.*, whether the protein is present in the system upon spreading of the phospholipid film, is of great importance.[6,30]

In order to investigate how binding to a "folding manipulator" such as Aunps changes BLA interfacial activity, phospholipid interaction, selectivity and penetration ability compared to the native protein, we have investigated the interaction of BLA and BLA–Aunp constructs with Langmuir phospholipid monolayers at pH 7.4, where the native protein has been reported to display little or no interaction. We also investigate how adsorption onto Aunps changes BLA conformation and subsequently influences the surface activity of the resulting Aunp constructs, which despite the high interest in BLA has not been reported before. The study presented here includes both BLA and BLA–Aunp interactions with neutral, negative and mixed 1 : 1 neutral : negative phospholipid Langmuir monolayers. In this study, we demonstrate using the Langmuir monolayer method that BLA–Aunp constructs have higher surface activities and display a stronger affinity towards phospholipid monolayers compared to the native protein when injected under pre-compressed phospholipid films. This activity correlates well with extrinsic fluorescence data and TCSPC measurements of fluorescence lifetimes that indicate an altered protein fold for adsorbed protein.

Materials and methods

Materials and solutions

Bovine α-lactalbumin (BLA) type I, L-α-phosphatidylcholine, type XVI-E approximately 99% purity TLC, lyophilized powder (EYPC), and 1-anilino-8-naphthalene sulfonate (ANS) were purchased from Sigma. Porcine brain phosphatidylserine (PBPS) was purchased from Avanti Polar Lipids. The citrate-coated 30 nm gold nanoparticles (Aunps) were purchased from Ted Pella and the suspension contains 2×10^{11} Aunp ml^{-1}. Potassium dihydrogen phosphate (KH_2PO_4), potassium chloride (KCl), and di-potassium hydrogen phosphate (K_2HPO_4) were purchased from Merck. The buffer solution (PBS) was made by adding the potassium di-hydrogen phosphate and potassium chloride solution (KH_2PO_4 50 mM, KCl 150 mM) into a di-potassium hydrogen phosphate and potassium chloride solution (K_2HPO_4 50 mM, KCl 150 mM) until pH = 7.4. The BLA-stock solution (25 μM) was made of α-lactalbumin (0.0133 g, ~0.9 μmol) in PBS (37.5 ml), then the solutions and suspensions used for fluorescence, and UV measurements were made by diluting the BLA-stock solution to 3.6 μM in PBS pH 7.4. The isoelectric point (pI) for BLA is 4.5. The concentration of BLA in BLA–Aunp suspensions is chosen in line with Kaufman *et al.* who used a protein : gold number ratio equal to 2000 : 1, for 12.8 nm Aunps,[31] corresponding to a protein : gold molar ratio equal to ~11 000 : 1 for the 30 nm Aunp. It should be noted that the molar ratio does not correspond to the number of proteins adsorbed per gold nanoparticle, but the sum of adsorbed and free protein in the system. Taking the total surface area into consideration, the BLA-concentration should be 3.6 μM for a suspension containing 50% citrate-coated gold stock-solution. This is in correspondence with a previous article concerning bovine serum albumin (BSA).[24] The BLA–Aunp suspension was made by adding BLA (25 μM, 432 μl) to 30 nm Aunp suspension (1.5 ml). After one hour the solution was diluted with PBS pH 7.4 (1.068 ml). This gave a final BLA concentration of 3.6 μM.

For extrinsic fluorescence ANS (10 μl, 5 mM) was added to a BLA-solution (3 ml, 3.6 μM) and to BLA–Aunp suspensions (3 ml), so that the final ANS concentration was 17 μM. ANS is a commonly used extrinsic-fluorescence probe for studying proteins.[32–34]

For the Langmuir experiments the BLA-stock solution was diluted to 12.5 μM in PBS before injection. The BLA–Aunp suspension for the Langmuir experiments was made by mixing 30 nm Aunp (7.5 ml) with BLA solution (25 μM, 7.5 ml). Three phospholipid in chloroform solutions were used: EYPC (0.25 mg ml^{-1}), PBPS (0.25 mg ml^{-1}) and a 1 : 1 EYPC : PBPS solution made by mixing the EYPC solution (0.25 mg ml^{-1}, 1.5 ml), with PBPS solution (0.25 mg ml^{-1}, 1.5 ml). Molecular weight for EYPC is 760.9 g mol^{-1}, and for PBPS it is 812.05 g mol^{-1}.

UV-visible spectroscopy

A Shimadzu UV-2401PC spectrophotometer was used to collect the UV-vis spectra. The wavelength range was 200–800 nm.

Dynamic light scattering (DLS)

The DLS was measured using a Malvern Zetasizer Nano-ZS instrument, and the manufacturers own software.

Fluorescence

The fluorescence measurements were executed on a Fluorolog-3 HORIBA Jobin Yvon apparatus. For intrinsic fluorescence *steady-state measurements* the slits were 10 nm, and a polarizator was used. The excitation wavelength was $\lambda = 295$ nm. The choice of wavelength was such that mainly tryptophan was excited and contribution from tyrosine and phenylalanine avoided.[35] It was observed that if fluorescence was measured on the same sample more than once, the intensity increased. This is probably due to protein denaturation, and then aggregation induced by the strong light.[36] The aggregation will lead to Trp being buried in a more hydrophobic environment, hence increasing the intensity. For extrinsic fluorescence on ANS the excitation wavelength was $\lambda_{ex} = 370$ nm, slits 5 nm, and the measurements were done without the polarizator. The excitation wavelength $\lambda_{ex} = 370$ nm

 This journal is © The Royal Society of Chemistry 2011

was chosen based on earlier studies of ANS as the fluorescence probe for proteins.[24,33]

For intrinsic lifetime studies *time correlated single photon counting (TCSPC)* was performed using a 280 nm LED lamp, the bandpass was 5 nm, the prompt was recorded with the emission monochromator (Em. mono) = 280 nm, and the samples using Em. mono = 350 nm. For extrinsic fluorescence a LED-lamp with $\lambda_{ex} = 370$ nm was used, and the bandpass was 14 nm. As the prompt was recorded the Em. mono was 370 nm, and for the samples the Em. mono was 470 nm. More details about the TCSPC technique can be found elsewhere.[28,37]

Langmuir isotherms

For the surface pressure–area measurements a KSV Langmuir Minitrough double barrier system (KSV LTD, Finland) controlled through the manufacturer's own software was used. While the barriers were made of Delrin, the trough (250 ml) was made of Teflon. The Injected protocol for investigating protein–phospholipid interactions was adopted from Glomm *et al.*[24,30] The subphase used was a PBS buffer pH 7.4. Prior to the introduction of the phospholipid film the surface was swept with a vacuum pump-connected Pasteur pipette. Three different phospholipid solutions (60 µl, 0.25 mg ml^{-1}) were used (see above). Initial compression to 5 mN m^{-1} with a constant barrier speed of 5 mm min^{-1} started 15 minutes after the film was spread with a 100 µl Hamilton syringe. BLA or BLA–Aunp suspensions (12.5 µM protein, 1 ml) were injected directly under the pre-compressed phospholipid film from outside the barriers using an angled syringe needle. At constant trough area the system was then allowed to equilibriate for one hour before compression started. During the measurements an electrobalance recorded the surface tension using a paper probe. For both BLA and BLA–Aunp, the experiments without phospholipid being present were also performed. The barriers were then moved to a position 10 mm from complete expansion, and the sample was introduced as described above under the air/water surface. Equilibration and compression were done as if phospholipid was present. Stability for the films was measured by spreading the phospholipid (60 µl, 0.25 mg ml^{-1}) on the surface, waiting 15 minutes before compressing the phospholipid film to 25 mN m^{-1} and then recording what changes in trough area occurred for the next two hours.

Results and discussion

This section includes the characterization of BLA on citrate-coated gold nanoparticles using UV-vis and fluorescence spectroscopies, and the subsequent unfolding additionally studied with ANS as an extrinsic fluorescence probe. Film-forming properties of pure systems, *i.e.*, phospholipid Langmuir monolayers and Gibbs monolayers of protein and protein–Aunp constructs are then described using the Langmuir monolayer method. Finally, the interaction between native BLA and pure and mixed phospholipid monolayers is then compared with BLA–Aunp–phospholipid interactions using the Injected method,[30] wherein the protein or protein–Aunp constructs are injected into the subphase under a phospholipid film pre-compressed to a target surface pressure.

Characterization of BLA–Aunp constructs

In assembling protein–nanoparticle constructs, the final properties of the system depend on (i) whether the protein binds to the nanoparticle scaffolds, (ii) the extent of surface-induced conformational changes, (iii) average protein orientation, and (iv) the flocculation state of the protein–nanoparticle constructs (*i.e.*, single particles *versus* flocs).[38,39]

UV-vis spectra showed that introduction of BLA to the gold nanoparticle (Aunp) solution did not significantly alter the lineshape of the gold nanoparticle localized surface plasmon resonance (LSPR) band with respect to absorption intensity and full-width at half maximum (FWHM), but resulted in a slight red-shift of the LSPR band (~1 nm), which is in agreement with earlier studies.[24] From dynamic light scattering measurements of the Aunps before and after introduction of BLA, the estimated particle diameter increased by ~2 nm. This reveals that BLA is adsorbed onto the Aunps, and that the BLA–Aunps reside as single particles.[24,27,28] In an earlier study, we have investigated the binding of bovine serum albumin (BSA) to citrate-coated Aunps and surfaces.[27] Here, the data were found to support that BSA binding was predominantly electrostatic in nature, but with contributions from hydrophobic interactions. Thus our hypothesis is that BLA binding to Aunps is primarily electrostatic. Since UV-vis and dynamic light scattering indicate binding, but do not reveal much about adsorption induced conformational changes, the BLA–Aunp constructs were further investigated by steady-state fluorescence (Fig. 1) using both the intrinsic (Trp) and extrinsic (ANS) fluorescence.

As the protein is present in excess with respect to maximum surface coverage, the fluorescence shown in Fig. 1 emanates both from free and bound protein. However, as the BLA concentration was kept constant, alterations to the spectral signatures of both Trp and ANS can be attributed to adsorbed protein.[24] Intensity and position of the Trp emission peak depend on the local environment[35] and changes in fluorescence spectra indicate a combination of conformational changes and steric blockage as some of the Trp groups can be turned towards the gold surface. Fig. 1a reveals a loss in intrinsic fluorescence for BLA–Aunp constructs compared to native BLA. This trend is the same as seen for BSA–Aunp constructs studied previously.[24] Two factors gives rise to this loss. One reason is that as BLA adsorbs onto Aunps, the gold nanoparticles will quench some of the

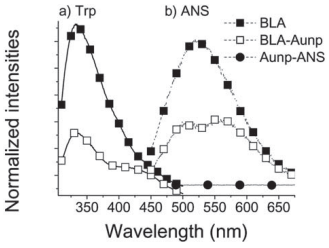

Fig. 1 (a) Intrinsic steady state measurements of BLA and BLA–Aunp, $\lambda_{ex} = 295$ nm. (b) Extrinsic steady state measurements of BLA and BLA–Aunp using ANS as probe, $\lambda_{ex} = 370$ nm.

fluorescence from Trp.[40] Moreover, as BLA–Aunp constructs are formed BLA can partially unfold, as was observed for the adsorption of BSA onto Aunps of similar size.[24] This unfolding might expose Trp to a more hydrophilic environment and decrease the intensity.[35] Unfolding is traditionally accompanied by a red-shift of the Trp signature when the protein is in free-space conditions.[35] No spectral shifts were observed for the BLA–Aunp constructs. However, for the systems studied here, two factors counteract this effect: (i) The collected signal contains contributions from free and bound protein, and thus a spectral shift from (quenched) adsorbed species will likely be drowned by signals from bulk species. (ii) Adsorbed proteins will most likely reside in a more or less close-packed state. Hence, the protein is enclosed by surrounding proteins as well as in contact with the nanoparticle scaffold, leaving only one protein face exposed to the solvent. Thus, intrinsic fluorescence confirms adsorption (as reported previously for BSA), but does not elucidate changes in the adsorbed layer.[24]

To gain more information about conformational changes, extrinsic (ANS) fluorescence was measured (Fig. 1b). ANS is highly fluorescent in a hydrophobic environment, but has a very low quantum yield in water and is often used as an extrinsic probe in protein studies.[32–34,41–43] ANS is also quite soluble in water and will stay close to a polar environment. Exposure to a less polar environment such as hydrophobic patches on a protein results in an increased quantum yield of the probe, as well as a shift of the emission profile. Upon protein unfolding, the intensity will decrease as ANS will be released from the hydrophobic interior of the protein into the surrounding buffer which quenches the signal.[35] As seen in Fig. 1b the emission intensity of ANS is lower for the BLA–Aunp constructs than with native BLA. Solutions of ANS in buffer, or ANS in aqueous Aunp suspensions showed negligible fluorescence (data not shown), which is in accordance with an earlier report.[24] In Fig. 1b there is also a change in lineshape of the emission spectra. The loss of intensity can be explained by quenching of ANS as it becomes exposed to water when BLA partially unfolds at the gold surface. The change in lineshape is best explained by partial energy transfer between the ANS donor and the Aunp acceptor, as the LSPR of 30 nm Aunp falls within the spectral range of ANS emission.[35,37]

TCSPC (time correlated single photon counting) was used as a fluorescence lifetime measuring technique to further investigate the properties of the protein adlayer. The data were best modeled using biphasic decay, and the calculated lifetimes are shown in Table 1. In this context, biphasic decay can be interpreted as the relaxation from the excited states corresponding to two sets of populations with distinctive relaxation dynamics, representing two different chemical environments.[24,28,37]

Table 1 TCSPC of intrinsic emission was measured with LED 280 nm, and extrinsic emission was measured with LED 370 nm. T1 and T2 denote lifetimes, and B1 and B2 are the corresponding populations

	Intrinsic		Extrinsic	
	BLA	BLA–Aunp	BLA	BLA–Aunp
T1 (ns)	0.86 ± 0.01	0.85 ± 0.04	0.37 ± 0.01	0.35 ± 0.01
T2 (ns)	5.0 ± 0.2	4.6 ± 0.3	7.5 ± 0.2	8.8 ± 0.3
B1 (%)	91.5 ± 0.1	81.3 ± 0.1	86.1 ± 0.1	91.8 ± 0.1
B2 (%)	8.5 ± 0.1	18.7 ± 0.1	13.9 ± 0.1	8.2 ± 0.1

Since a 280 nm LED was used for the intrinsic measurements, not only tryptophan but also other fluorescent amino acid residues such as tyrosine, contributed to the observed lifetimes. TCSPC for both intrinsic and extrinsic fluorescence shows one short (T1) and one long (T2) lifetime, and for both methods the short lifetime has the highest associated population (B1). Here, the calculated lifetimes are inversely proportional to the degree of quenching. For the intrinsic fluorescence the lifetimes remain unchanged within their respective confidence intervals, but there are significant changes in the associated populations upon introduction of Aunps. For the short lifetime (T1) there is a decrease in the associated population (B1), whereas adsorption onto Aunps results in a corresponding population increase for the long lifetime (B2) from 8.5% to 18.7%. This indicates that upon binding to Aunps, Trp and Tyr residues on BLA are protected from the solvent compared to free-space conditions, which is consistent with close-packing of the proteins on the Aunp surface. Also for the extrinsic fluorescence there is no significant change in T1, but in contrast to intrinsic fluorescence B1 increases upon BLA–Aunp formation. The long lifetime and its population also differ from those of the intrinsic fluorescence. For the extrinsic fluorescence T2 increases when BLA-Aunps are formed, and B2 decreases.

The short lifetime population (B1) is highest for intrinsic and ANS fluorescence. As BLA is a small protein (14.2 kDa) with two of four Trps exposed to the solvent, its intrinsic fluorescence is efficiently quenched. For the BLA–Aunp constructs, the long lifetime population (B2) for intrinsic fluorescence increased due to displacement of water as the protein adsorbs to the Aunp, shielding the fluorophores from the solvent. The extrinsic fluorescence population associated with the short lifetime, B1, is higher for BLA–Aunp constructs since ANS is partitioned out from the hydrophobic interior of the protein and into more hydrophilic surroundings. For the ANS still trapped in the protein in the BLA–Aunp constructs, the T2 increases from 7.5 ns to 8.8 ns because the water expulsion ensures a more hydrophobic environment for the remaining ANS. These techniques let us describe a rough picture of the protein conformation, packing and environment close to the Aunp surface. Relative to the native protein at bulk conditions, there exists a larger volume fraction which is protected from solvent quenchers. The results obtained here are consistent with surface-induced conformational changes, as has been reported earlier.[5,24] Based on the intrinsic fluorescence quenching behaviour, *i.e.*, from the increase in the long lifetime population upon binding to Aunps, the adsorbed proteins appear to be densely packed, leaving the overall properties of the BLA–Aunp constructs dependent on the exposed side of the protein and the degree of unfolding relative to the native state.

Gibbs- and Langmuir monolayer studies of protein and phospholipids

As the fluorescence results indicate partial unfolding of the surface bound BLA, as well as a high degree of Aunp coverage, this is expected to result in altered surface activity and phospholipid affinity relative to the native protein. To explore this

 This journal is © The Royal Society of Chemistry 2011

aspect of the BLA–Aunp construct, we studied its film-forming properties relative to the native protein, as well as the Langmuir monolayer properties of the zwitterionic and anionic phospholipids employed in the subsequent phospholipid protein interaction studies. For all experiments the Injected protocol described by Glomm *et al.*[30] was used, thus ensuring that the solute interacted with an already formed monolayer, rather than from partitioning at the air–water interface due to the inherent surface activity of the protein or protein–Aunp constructs. Interactions were studied towards three sets of phospholipid films: EYPC (L-α-phosphatidylcholine), PBPS (porcine brain phosphatidylserine) and EYPC : PBPS 1 : 1 molar ratio. As a reference, Langmuir monolayers of phospholipids only were studied. The isotherms for these systems, as well as the Gibbs monolayers of the BLA and BLA–Aunp constructs, are found in Fig. 2a.

The compression–expansion profiles of EYPC, PBPS and EYPC : PBPS (Fig. 2a) are all similar, with rapid increase in surface pressure and a narrow hysteresis. The shape of the phospholipid isotherms and the steep incline after onset of film formation, show that the films are rigid. Stability studies, where the phospholipid was precompressed to 25 mN m^{-1}, showed that all three water insoluble phospholipid films were stable during the timescale of the experiments. The film miscibility of the EYPC : PBPS phospholipid film was studied using the excess function ΔA_{XS}.

$$\Delta A_{XS} = A_{12} - (\chi_1 A_1 + \chi_2 A_2) \quad (1)$$

where ΔA_{XS} is the excess function, A_{12} is the mean molecular area (MMA) occupied by the mixed film at a given surface pressure, χ_1 and χ_2 are the mole fractions of phospholipid one and two respectively, and A_1 and A_2 are the MMA occupied by pure phospholipid one and two at the same surface pressure as A_{12}. If $\Delta A_{XS} < 0$, then there is attraction between the phospholipids, and if $\Delta A_{XS} > 0$, then there is repulsion between the phospholipids.[44] The ΔA_{XS} are shown in Fig. 3.

ΔA_{XS} is positive all through the compression confirming repulsion between the phospholipids in the mixture. As the trough area decreases EYPC and PBPS are forced closer together, resulting in an increased repulsion as illustrated by the increasing ΔA_{XS}.

In addition to pure phospholipid systems unmodified Aunps, native BLA and BLA–Aunp interactions towards a water–air surface were studied as well. Unmodified Aunps precipitated out of solution under these conditions and so did not contribute to the recorded surface pressure. However the pure native BLA and BLA–Aunp systems are found in Fig. 2a together with phospholipid systems, and the equilibration curves, *i.e.*, the time-dependent surface pressure following the injection under an air–water surface for BLA and BLA–Aunp, are represented in Fig. 2b. From Fig. 2b it is evident that the equilibrium curve for BLA–Aunp increases more rapidly initially than for native BLA, but they both end up at approximately the same surface pressure (~8 mN m^{-1}). For the BLA–Aunp experiment there will be contributions from free BLA as well as from the BLA–Aunp constructs. It is likely that the rapid increase in the beginning is due to bound BLA, and that the end surface pressure is similar in both experiments because the total amount of BLA is the same in both. For the pure system with protein, the small slope in surface pressure as the trough area decreases, indicates that BLA was dissolved in the subphase. In Fig. 2a, no collapse pressure can be observed for the Gibbs films of protein or protein–gold constructs due to their inherent solubility in the subphase.[30] For native BLA the lower surface pressure (Π) upon expansion can be attributed to loss of film-forming material from solubilization of BLA into the subphase at low trough areas.[24,30] All the Gibbs- and Langmuir monolayer studies show a higher surface pressure for BLA–Aunp constructs than for native BLA, indicating a higher surface activity. This effect can be attributed to exposure of more hydrophobic groups, and to the constructs being less water soluble. The result is also in agreement with the fluorescence data that implied a partial protein unfolding. While

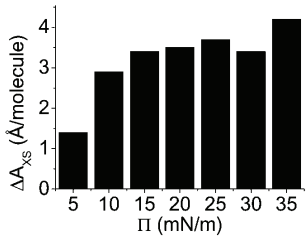

Fig. 3 Calculated excess area (ΔA_{XS}) as a function of the surface pressure (Π) for phospholipid monolayers.

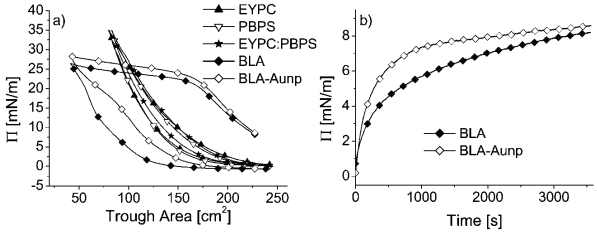

Fig. 2 (a) Compression and expansion isotherms in the absence of phospholipid–protein interactions(Π = surface pressure). (b) Equilibrium for native protein, and for protein on gold the first hour after injection under an air/water surface.

unmodified Aunp precipitated under these conditions, we have previously shown that citrate-coated Aunps do not possess any measurable surface activity in the absence of a passivating protein layer.[24] The protein–gold constructs possess qualities not seen for either of the components alone.

Langmuir monolayer interaction studies—BLA–Aunp constructs interact more with phospholipid monolayers than native protein does

Earlier studies have shown that BLA interaction with a phospholipid film is optimal at a neutral:charged phospholipid ratio of 1 : 1, as compared to phospholipid films consisting of only one type of phospholipid or in other ratios.[13] This theory can also be enhanced by the excess area studies (Fig. 3), which showed that there is repulsion between the individual phospholipid molecules in the monolayers. Some differences (but far from all) in the results presented here compared to earlier studies can be attributed to different protein introduction methods being used. The most common protein introduction method for Langmuir monolayer studies of protein–phospholipid interactions is the so-called Subphase method, in which the phospholipid is spread on top of a protein-containing subphase.[13,30] Due to the intrinsic surface activity of any protein, which is high for the only marginally stable amphitropic BLA,[6] the Subphase introduction method results in mixed protein–phospholipid films. Thus, by using this introduction protocol, the surface pressure–area isotherms inherently display contributions from lateral protein–phospholipid interactions as well as from bulk proteins interacting with the phospholipid film. Moreover, as the protein is introduced prior to 2D organization (*via* lateral compression) of the phospholipid film, the obtained results are not easily comparable to those obtained *via* vesicle leakage studies, wherein the protein is introduced to organized phospholipid structures at lateral pressures comparable to those of living cells. An alternative introduction method more in line with vesicle studies is the so-called Injected method, wherein the protein is injected under a pre-compressed (to a target surface pressure) phospholipid film, and the resulting protein–phospholipid interaction is recorded as a function of time prior to further film compression and expansion.[30] Here, interactions between the phospholipid monolayer and subphase protein can be elucidated with respect to kinetics, affinity and packing density, and from the concomitant compression–expansion isotherms the interaction mode of the protein (*i.e.*, *via* insertion or interaction with headgroups) can be rationalized.

We have used the Injected protocol, while the previous study by Rødland *et al.* was done with the Subphase protocol.[13,30] In our study both BLA and BLA–Aunp constructs interact with all three monolayer films, without revealing any clear phospholipid selectivity. However, there are significant differences when comparing native BLA interactions with phospholipid films, and those for BLA–Aunp constructs (Fig. 4).

Fig. 4 shows the equilibration of BLA (Fig. 4a) and BLA–Aunp (Fig. 4b) injected under phospholipid films precompressed to 5 mN m^{-1}. Upon injection of BLA and BLA–Aunp, there is a marked increase in surface pressure for all the phospholipid monolayers studied here, indicating interaction between the phospholipid film and the injected species. All systems studied here display a single saturation plateau, indicating that the protein–phospholipid interaction occurs in a single step, with the BLA–Aunp constructs reaching higher surface pressure at equilibrium (2–3 mN m^{-1} higher). From Fig. 4, the initial rates of surface pressure increase are higher for the BLA–Aunp constructs (Fig. 4b) than for BLA only (Fig. 4a), which is consistent with enhanced hydrophobic interaction from partial exposure of hydrophobic residues in the adsorbed protein. No discernible differences in interaction with the injected species could be observed for the pure and mixed phospholipid monolayers used here. Moreover, the first data points for the rate of migration of BLA–Aunp constructs towards the phospholipid monolayers occur faster than the instrument response, as evidenced by the ~2 mN m^{-1} discontinuity in time dependent surface pressure with respect to the injection pressure of 5 mN m^{-1}. This discontinuity in surface pressure is not seen for BLA only. This reveals that surface partitioning of BLA is slower than for the BLA–Aunp constructs. This corresponds well with the equilibration curves of BLA and BLA–Aunp towards an air–water surface (Fig. 2) which revealed a higher rate of interfacial partitioning for the BLA–Aunp constructs. Interestingly, while there was no significant difference in surface pressure at saturation between BLA and BLA–Aunp constructs when injected under an air–water surface, the BLA–Aunp constructs display a higher affinity for the phospholipid monolayers than BLA only. Also, the equilibration of BLA–Aunp towards phospholipid monolayers occurs faster than towards an air–water surface. Thus, the increased surface migration rates and the higher saturation plateaus in the presence of a phospholipid monolayer reveal an enhanced phospholipid affinity for the BLA–Aunp constructs. Recently, Lystvet *et al.* have shown that protein–Aunp constructs display enhanced film-penetration ability compared to the native protein due to partial unfolding on the Aunp surface.[24] From our observations and previous studies on the interaction between protein–Aunp constructs and phospholipid monolayers, we hypothesize that the BLA–Aunp constructs most likely reside partially embedded in the phospholipid monolayer.

Compression–expansion isotherms for native BLA and BLA–Aunp constructs injected under the three different phospholipid monolayer systems studied here are shown in Fig. 5. As discussed for the equilibrium curves above (Fig. 4), no discernible differences could be observed for interaction with different phospholipid monolayers, whereas marked differences were found between BLA and BLA–Aunp. In Table 2 the difference in slope is investigated further.

Within each set of experiments (Fig. 5) there seems to be little difference in interaction when comparing the different phospholipid monolayers even though earlier studies have shown that a 1 : 1 mixture gives the highest interaction.[13] This difference between previous studies and our study is most likely due to the introduction protocols. The overall Π–A isotherms for BLA–Aunp (Fig. 5b) closely resemble those of the parent protein (Fig. 5a), but at low trough areas there seems to be a smaller slope for the Π–A isotherms of BLA–Aunp (Fig. 5d) than for BLA (Fig. 5c). This is also seen from Table 2, where the slope found with linear regression is smaller for experiments with BLA–Aunp than with native BLA. A steep slope indicates a rigid film of water-insoluble species, while a small slope is achieved for

 This journal is © The Royal Society of Chemistry 2011

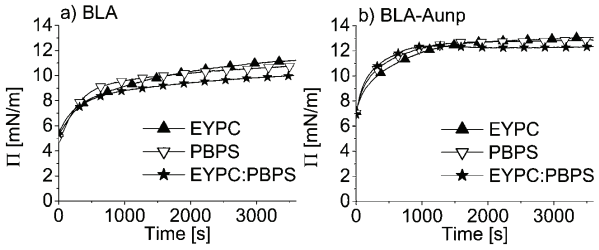

Fig. 4 (a) Equilibration of BLA injected under pure and mixed (1 : 1 molar ratio) phospholipid monolayers (compressed to 5 mN m^{-1}). (b) Equilibration of BLA–Aunp injected under phospholipid monolayers used here.

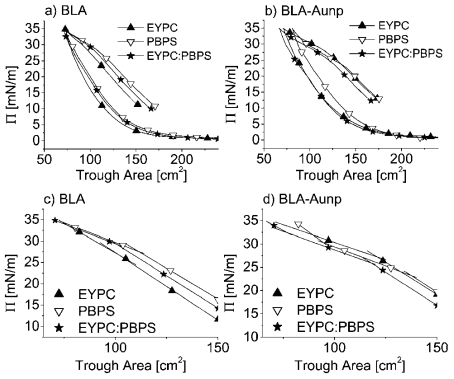

Fig. 5 (a) Isotherms of native BLA injected under various phospholipid films. (b) Isotherms of BLA–Aunp injected under various phospholipid films. (c) Magnification of the compression for native BLA injected under various phospholipid films. (d) Magnification of the compression for BLA–Aunp injected under various phospholipid films. (c) and (d) are shown with trend lines.

a more compressible film or with water soluble species. It seems like BLA–Aunp has a greater affinity for, and penetrates more into, the phospholipid film than does BLA only, thereby making the films more compressible. This fits well with the equilibrium experiments (Fig. 4) which showed that BLA–Aunp has a greater affinity towards the phospholipid films, and also with the previous findings for BSA.[24] Some of the effect may be increased by the fact that BLA–Aunp also shows a greater air–water surface affinity (Fig. 2) and that there is some free spacing between the phospholipids. The BSA study also showed that the air–water surface population of the immobilized protein increased when gold was present, and that larger gold nanoparticles gave a larger surface population of protein. The fact that adsorption enhances film-penetration may be of value within studies of *i.e.* drug delivery systems, and also for a better understanding of protein based drug candidates where folding seems to matter, like human α-lactalbumin made lethal to tumor cells (HAMLET). One possible hurdle to further clinical development of HAMLET or similar preparations may be their tendency to lose potency in many clinical situations, probably due to loss of oleic acid to scavenger proteins such as serum albumin.[45] This would have the effect of both reverting the protein to its native state and separating the components of HAMLET, both of which appear to be necessary for activity.[23] Adsorption onto nanoparticles may serve a double purpose in that it stabilizes the non-native fold and provides a protected environment for the construct as a whole. A more general consequence of the enhanced membrane-affecting qualities reported here and in Lystvet *et al.*,[24] is that although a nanoparticle can be inert and the protein-component non-toxic, the resulting construct may behave as neither component. In particular, their tendency to be taken up into living systems depend to a large extent on the surface activity of the constructs.[46] The mechanism of uptake depends on both the cellular system and the polypeptide coating of the particle.[29,47,48] It is possible to tune[49] the overall fold and packing of proteins on a nanoparticle surface, thus ensuring low surface activity for non-drug applications and high surface activity for medical applications which require this. Such a tuning can be done by choice of solution conditions, nanoparticle surface chemistry, particle curvature[50] and by altering the rate of deposition.[5]

Table 2 Calculated slopes for compression of phospholipid films with either native BLA or BLA–Aunp constructs injected underneath. 1, 2 and 3 stand for the different sections in Fig. 5c and d, numbering from right to left

	EYPC			PBPS			EYPC : PBPS		
	1	2	3	1	2	3	1	2	3
Native BLA	−0.317	−0.278	N/A	−0.289	−0.185	N/A	−0.303	−0.185	N/A
BLA–Aunp	−0.275	−0.151	N/A	−0.281	−0.165	−0.319	−0.283	−0.158	−0.239

Conceivably, the protein conformation can be continuously tuned from native-like to fully denatured, although this depends on the particular folding properties of the protein.[51] Proteins adsorbed to the nanoparticle surface would, on average, have some parts exposed more than others due to their preferential orientation.[5]

Conclusion

The adsorption of BLA onto Aunps, and subsequently the interaction of BLA and BLA–Aunp constructs with Langmuir monolayers of neutral, negatively charged and mixed neutral : negative phospholipids have been studied. Adsorption of BLA onto Aunps was confirmed by UV-vis and steady-state fluorescence measurements. Steady-state and TCSPC measurements, using both intrinsic and extrinsic fluorescence probes, strongly indicated that adsorption induced partial unfolding of BLA, in line with earlier studies.[24]

Both BLA–Aunp constructs and native BLA were shown to be strongly film-forming, with the BLA–Aunp constructs being the most surface active species. We attribute this to partial unfolding of BLA adsorbed onto Aunps, exposing hydrophobic residues thus enhancing hydrophobic interactions. When injected under precompressed Langmuir monolayers of the phospholipids studied here, both BLA and BLA–Aunp constructs revealed protein–phospholipid interaction, with the BLA–Aunp constructs displaying the highest affinity for the phospholipid films. This increased bioinvasiveness of protein–gold nanoconstructs is potentially applicable within protein based drugs and drug delivery, as well as of fundamental interest within nanotoxicology.

Acknowledgements

The authors acknowledge the Department of Chemical Engineering, NTNU, for financial support. Wilhelm R. Glomm and Sondre Volden acknowledge financial support from the Research Council of Norway (NFR).

References

1 Ø. Halskau, N. A. Frøystein, A. Muga and A. Martínez, *J. Mol. Biol.*, 2002, **321**(1), 99–110.
2 J. Fantini and N. Yahi, *Expert Rev. Mol. Med.*, 2010, **12**, e27.
3 C. Pan, L. Cai, H. Lu, L. Lu and S. Jiang, *J. Biol. Chem.*, 2011, **286**, 28425.
4 B. Kasemo, *Surf. Sci.*, 2002, **500**(1–3), 656–677.
5 W. R. Glomm, Ø. Halskau, A. M. D. Hanneseth and S. Volden, *J. Phys. Chem. B*, 2007, **111**(51), 14329–14345.
6 Ø. Halskau, A. Muga and A. Martínez, *Curr. Protein Pept. Sci.*, 2009, **10**, 339–359.
7 J. E. Johnson and R. B. Cornell, *Mol. Membr. Biol.*, 1999, **16**, 217–235.
8 P. Burn, *Trends Biochem. Sci.*, 1988, **13**(3), 79–83.
9 T. Heimburg, P. Hildebrandt and D. Marsh, *Biochemistry*, 1991, **30**, 9084–9089.
10 I. Bertini, P. Turano, P. R. Vasos, A. Bondon, S. Chevance and G. Simonneaux, *J. Mol. Biol.*, 2004, **336**(2), 489–496.
11 S. Bañuelos and A. Muga, *J. Biol. Chem.*, 1995, **270**(50), 29910–29915.
12 S. Bañuelos and A. Muga, *Biochemistry*, 1996, **35**(13), 3892–3898.
13 I. Rødland, Ø. Halskau, A. Martínez and H. Holmsen, *Biochim. Biophys. Acta, Biomembr.*, 2005, **1717**(1), 11–20.
14 A. V. Agasøster, Ø. Halskau, E. Fuglebakk, N. A. Frøystein, A. Muga, H. Holmsen and A. Martínez, *J. Biol. Chem.*, 2003, **278**, 21790–21797.
15 Ø. Halskau, J. Underhaug, N. A. Frøystein and A. Martínez, *J. Mol. Biol.*, 2005, **349**(5), 1072–1086.
16 W. R. Glomm, S. Volden, M.-H. G. Ese and Ø. Halskau, *J. Dispersion Sci. Technol.*, 2011, **32**(2), 150–158.
17 E. A. Permyakov and L. J. Berliner, *FEBS Lett.*, 2000, **473**(3), 269–274.
18 M. Svensson, H. Sabharwal, A. Håkansson, A.-K. Mossberg, P. Lipniunas, H. Leffler, C. Svanborg and S. Linse, *J. Biol. Chem.*, 1999, **274**(10), 6388–6396.
19 M. Svensson, J. Fast, A.-K. Mossberg, C. Düringer, L. Gustafsson, O. Hallgren, C. L. Brooks, L. Berliner, S. Linse and C. Svanborg, *Protein Sci.*, 2003, **12**(12), 2794–2804.
20 W. Fischer, L. Gustafsson, A.-K. Mossberg, J. Gronli, S. Mork, R. Bjerkvig and C. Svanborg, *Cancer Res.*, 2004, **64**(6), 2105–2112.
21 L. Gustafsson, I. Leijonhufvud, A. Aronsson, A.-K. Mossberg and C. Svanborg, *N. Engl. J. Med.*, 2004, **350**(26), 2663–2672.
22 A.-K. Mossberg, M. Puchades, Ø. Halskau, A. Baumann, I. Lanekoff, Y. Chao, A. Martinez, C. Svanborg and R. Karlsson, *PLoS One*, 2010, **5**(2), e9384.
23 A.-K. Mossberg, K. Hun Mok, L. A. Morozova-Roche and C. Svanborg, *FEBS J.*, 2010, **277**(22), 4614–4625.
24 S. M. Lystvet, S. Volden, M. Yasuda, Ø. Halskau, Jr and W. R. Glomm, *Nanoscale*, 2011, **3**(4), 1788–1797.
25 A. Chenal, G. Vernier, P. Savarin, N. A. Bushmarina, A. Gèze, F. Guillain, D. Gillet and V. Forge, *J. Mol. Biol.*, 2005, **349**(4), 890–905.
26 D. G. Cornell, D. L. Patterson and N. Hoban, *J. Colloid Interface Sci.*, 1990, **140**(2), 428–435.
27 S. H. Brewer, W. R. Glomm, M. C. Johnson, M. K. Knag and S. Franzen, *Langmuir*, 2005, **21**, 9303–9307.
28 H. Xie, A. G. Tkachenko, W. R. Glomm, J. A. Ryan, M. K. Brennaman, J. M. Papanikolas, S. Franzen and D. L. Feldheim, *Anal. Chem.*, 2003, **75**(21), 5797–5805.
29 A. G. Tkachenko, H. Xie, D. Coleman, W. Glomm, J. Ryan, M. F. Anderson, S. Franzen and D. L. Feldheim, *J. Am. Chem. Soc.*, 2003, **125**(16), 4700–4701.
30 W. R. Glomm, S. Volden, Ø. Halskau, Jr and M. H. G. Ese, *Anal. Chem.*, 2009, **81**(8), 3042–3050.
31 E. D. Kaufman, J. Belyea, M. C. Johnson, Z. M. Nicholson, J. L. Ricks, P. K. Shah, M. Bayless, T. Petterson, Z. Feldtö, E. Blomberg, P. Claesson and S. Franzen, *Langmuir*, 2007, **23**, 6053–6062.
32 M. J. Tiera, G. R. d. Santos, V. A. d. O. Tiera, N. A. B. Vieira, E. Frolini, R. C. d. Silva and W. Loh, *Colloid Polym. Sci.*, 2005, **283**, 662–670.
33 E. Gabellieri and G. B. Strambini, *Biophys. J.*, 2006, **90**, 3239–3245.
34 G. V. Semisotnov, N. A. Rodionova, O. I. Razgulyaev, V. N. Uversky, A. F. Gripas' and R. I. Gilmanshin, *Biopolymers*, 1991, **31**(1), 119–128.
35 J. R. Lakowicz, *Principles of Fluorescence Spectroscopy*, Springer, New York, 2006.
36 M. Correia, M. T. Neves-Petersen, A. Parracino, A. K. di Gennaro and S. B. Petersen, *J. Fluoresc.*, 2011, DOI: 10.1007/s10895-011-0963-7.
37 W. R. Glomm, S. J. Moses, M. K. Brennaman, J. M. Papanikolas and S. Franzen, *J. Phys. Chem. B*, 2005, **109**(2), 804–810.
38 T. Cedervall, I. Lynch, S. Lindman, T. Berggård, E. Thulin, H. Nilsson, K. A. Dawson and S. Linse, *Proc. Natl. Acad. Sci. U. S. A.*, 2007, **104**(7), 2050–2055.
39 S. Lindman, I. Lynch, E. Thulin, H. Nilsson, K. A. Dawson and S. Linse, *Nano Lett.*, 2007, **7**(4), 914–920.
40 T. Sen, K. K. Haldar and A. Patra, *J. Phys. Chem. C*, 2008, **112**, 17945–17951.
41 D. Togashi, A. Ryder and D. O'Shaughnessy, *J. Fluoresc.*, 2010, **20**(2), 441–452.
42 D. Togashi and A. Ryder, *J. Fluoresc.*, 2008, **18**(2), 519–526.
43 D. M. Togashi and A. G. Ryder, *Exp. Mol. Pathol.*, 2007, **82**(2), 135–141.
44 K. S. Birdi, *Lipid and Biopolymer Monolayers at Liquid Interfaces*, Plenum Press, New York, 1989.
45 S. B. Nielsen, K. Wilhelm, B. Vad, J. Schleucher, L. A. Morozova-Roche and D. Otzen, *J. Mol. Biol.*, 2010, **398**(2), 351–361.
46 A. Kunzmann, B. Andersson, T. Thurnherr, H. Krug, A. Scheynius and B. Fadeel, *Biochim. Biophys. Acta, Gen. Subj.*, 2011, **1810**(3), 361–373.

 This journal is © The Royal Society of Chemistry 2011

47 A. G. Tkachenko, H. Xie, Y. Liu, D. Coleman, J. Ryan, W. R. Glomm, M. K. Shipton, S. Franzen and D. L. Feldheim, *Bioconjugate Chem.*, 2004, **15**(3), 482–490.
48 J. A. Ryan, K. W. Overton, M. E. Speight, C. N. Oldenburg, L. Loo, W. Robarge, S. Franzen and D. L. Feldheim, *Anal. Chem.*, 2007, **79**, 9150–9159.
49 S. Dhar, N. Kolishetti, S. J. Lippard and O. C. Farokhzad, *Proc. Natl. Acad. Sci. U. S. A.*, 2011, **108**(5), 1850–1855.
50 R. S. Kane and A. D. Stroock, *Biotechnol. Prog.*, 2007, **23**(2), 316–319.
51 Ø. Halskau, R. Perez-Jimenez, B. Ibarra-Molero, J. Underhaug, V. Muñoz, A. Martinez and J. M. Sanchez-Ruiz, *Proc. Natl. Acad. Sci. U. S. A.*, 2008, **105**(25), 8625–8630.

Paper III

Tunable photophysical properties, conformation and function of nanosized protein-gold constructs

RSC Advances RSC Publishing

PAPER

Tunable photophysical properties, conformation and function of nanosized protein–gold constructs

Cite this: *RSC Advances*, 2013, **3**, 482

Sina M. Lystvet,*[a] Sondre Volden,[a] Gurvinder Singh,[a] Masahiro Yasuda,[b] Øyvind Halskau[c] and Wilhelm R. Glomm*[a]

Protein-stabilized gold nanoconstructs are widely studied due to their potential applications in biosensing, drug and gene delivery, and bioimaging. While a number of studies have focused on the novel properties of such materials emanating from the gold, there has been little focus on how the protein shell is affected by nanocluster formation with respect to conformation, stability and function. Herein, we show the synthesis of protein-stabilized gold nanoconstructs varying in size from small clusters (~8 Au atoms) dispersed within proteins to nanoparticles stabilized by multiple proteins by varying the concentration of gold precursor and reducing agent. Proteins used were bovine serum albumin (BSA), bovine α-lactalbumin (BLA) and lysozyme (LYZ). Photophysical properties of the gold nanostructures were monitored using UV-vis and fluorescence measurements, revealing that the gold constructs can be tuned from luminescent clusters to nanoparticles displaying localized surface plasmon resonance (LSPR). Conformational changes of the protein following conjugation to gold nanostructures were studied using steady-state and time-resolved Trp fluorescence measurements and circular dichroism. The degree of conformational perturbation varied greatly between the proteins used, with BLA being the most tunable in terms of gradual unfolding, whereas the conformational stability of LYZ was very sensitive to the reducing agent used. To assess the impact of the gold nanostructures as well as the reducing agent on protein function, the LYZ–gold nanoconstructs were subjected to an activity test by degradation of *Micrococcus lysodeikticus* cell walls, revealing that the activity of the LYZ–Au constructs was retained and tunable, albeit at attenuated levels.

Received 30th August 2012,
Accepted 5th November 2012

DOI: 10.1039/c2ra22479h

www.rsc.org/advances

Introduction

Hybrid nanomaterials consisting of a gold nanoparticle core and a protein corona, *i.e.* protein–gold nanoparticle constructs, have attracted much attention over the last decade, owing to a wide range of potential applications in biological sensing, drug and gene delivery, and bioimaging. See *e.g.* reviews by Rotello and references therein.[1–11] The colloidal gold core provides a versatile scaffold for integrating biological function onto a colloidal carrier, and dictates the optical properties. Specifically, gold nanoparticles of diameters larger than ~3 nm display a collective excitation of conduction electrons known as a localized surface plasmon resonance (LSPR) band when irradiated by incident light.[6,12] In addition to the linear combination of the colloidal metal core and the multivalent protein corona, protein–gold nanoparticle constructs (hereafter referred to as protein–AuNP constructs) have also been reported to display emergent properties, *i.e.* properties not present for the protein or the nanoparticle only, such as an increased propensity for accumulation at interfaces and lipid miscibility-affecting characteristics.[10,11] Recently, a number of studies have focused on the integration of proteins and sub-nanometer gold clusters, resulting in protein-stabilized nanoclusters (hereafter referred to as protein–AuNCs).[13–17] While the exact formation mechanism remains to be elucidated and also depends on whether a reducing agent is added to the reaction mixture, it is generally agreed that formation involved initial electrostatic attraction between Au^{3+} and negatively charged residues, followed by reduction, growth and passivation within the polypeptide chain by covalent binding.[18–20] Gold nanoclusters (AuNCs) vary in size from a few atoms to tens of atoms in numbers corresponding to spherical shell closing of the valence electrons.[21] For protein-stabilized AuNCs, studies have reported that most of the gold resides as clusters of 8 or 25 atoms within the protein, with the size of the AuNCs being tunable as a function of reaction conditions.[13–15] Unlike gold nanoparticles, AuNCs do not display LSPR but luminesce at different wavelengths according to their size, which is useful as an optical

[a]*Ugelstad Laboratory, Department of Chemical Engineering, Norwegian University of Science and Technology (NTNU), N-7491 Trondheim, Norway. E-mail: lystvet@chemeng.ntnu.no; glomm@nt.ntnu.no; Tel: (+47) 73550325*
[b]*Department of Chemical Engineering, Osaka Prefecture University, 1-1 Gakuen-cho, Sakai, 5998531 Osaka, Japan*
[c]*Department of Molecular Biology, University of Bergen, Thormøhlensgt 55 90, 5008 Bergen, Norway*

 This journal is © The Royal Society of Chemistry 2013

marker.[14,21,22] Recently, Shiang *et al.* published a review on fluorescent properties of gold and silver nanoclusters.[17]

While a number of studies conclude that conjugation of proteins to nanomaterials such as gold nanoparticles may result in partial unfolding of the protein,[9–11,23] there is a need for systematic studies on how nanomaterials can be used to induce controlled unfolding of the protein with concomitant monitoring of the effect on protein function, such as enzymatic activity or ligand transport.

Earlier studies of protein–AuNCs have mainly focused on the synthesis of the gold nanoclusters and their system-dependent properties.[13–15] Chen *et al.* showed in a newly published article that lysozyme modified with gold nanoclusters of 8 atoms (Au_8) can be used for detection of glutathione (GSH) down to ~20 nM,[16] but to the best of our knowledge no study has been published on the effect of nanocluster formation on protein conformation and how this in turn affects protein function. Nor has anyone studied how the synthesis of gold nanoclusters within the protein will affect proteins with different properties, such as size, isoelectric point and conformation, and stability.

In this study, AuNCs and AuNPs of varying sizes are made within three different proteins; bovine serum albumin (BSA), bovine alpha-lactalbumin (BLA), and chicken egg white lysozyme (LYZ) by varying the concentrations of gold precursor and reducing agent, and the concentration ratios between these two reactants. The proteins were selected so as to allow for a large variety with respect to variables such as size, isoelectric point (pI) and conformational stability. Using dynamic light scattering, we found the hydrodynamic radii of BSA, BLA and LYZ to be approximately 7 nm, 4 nm and 3 nm, respectively, under the experimental conditions used here. BSA is a readily available reference protein with the same pI as the much smaller BLA. This leads to comparable charge density matching between negatively charged amino acid residues and Au^{3+} and opens for protein size-dependent variations in gold nanocluster stabilization. LYZ is a classical rigid protein of the same size as BLA, but with a different pI, which allows for studying how protein charge affects gold nanocluster formation and stabilization. In addition, LYZ also provides correlation of perturbation by NC modification and concomitant protein function *via* a simple activity assay by measuring transmittance as LYZ digests the cell walls of *Micrococcus lysodeikticus* bacteria.[24] The rate of increase in transmittance reflects the activity of the LYZ–AuNCs compared to native LYZ. In this study, sodium borohydride ($NaBH_4$) was used as the reducing agent because it cannot stabilize AuNCs or AuNPs by itself, implying that all gold nanoconstructs formed must be protein-stabilized. The fast reaction rate of $NaBH_4$ also avoids any competition from gold nanoclusters formed within the protein using amino acid residues such as tyrosine as reducing agents.[15] Native proteins, proteins with only reducing agent added, and proteins with both gold precursor and reducing agent were subjected to a palette of photophysical measuring techniques to investigate gold nanoconstructs formed, as well as conformational changes in the protein–gold nanoconstructs. Circular dichroism (CD) was used for further evaluation of changes in conformation, while scanning (transmission) electron microscopy (STEM) was used for size and dispersity studies of the gold nanoconstructs.

By varying the reaction conditions, protein–gold nanoconstructs can be tuned from single proteins functionalized with nanoclusters (small (~Au_8) and/or large (~Au_{25+}) depending on the protein) to protein-stabilized AuNPs, with all the protein systems displaying conformational tunability. Since the optical properties change when going from nanoclusters to nanoparticles,[22] this enables the creation of biomarkers with a wide range of optical signatures, from luminescence to LSPR. The size variation achieved also led to tunability of LYZ function. Consequently, the protein-stabilized gold nanoconstructs studied here allow for gradual tuning of protein conformation and protein function, as well as simultaneous inclusion of a built-in optical marker.

Experimental methods and materials

Bovine serum albumin (BSA), chicken egg white lysozyme (LYZ), bovine α-lactalbumin Type I (BLA), sodium borohydride ($NaBH_4$), and freeze dried *Micrococcus lysodeikticus* cell walls were purchased from Sigma Aldrich. Hydrogen tetrachloroaurate(III)·$3H_2O$ (TCAA) was purchased from Acros organics. Di-potassium hydrogen phosphate (K_2HPO_4) and potassium di-hydrogen phosphate (KH_2PO_4), were purchased from Merck. A phosphate buffer was made by mixing K_2HPO_4 (50 mM) with KH_2PO_4 (50 mM) until pH 7.4.

Proteins (BSA 67 kDa, BLA 14.2 kDa, LYZ 14.3 kDa) were dissolved in Milli-Q water to make up 25 μM protein stock solutions. TCAA (74 mg, 0.2 mmol) was dissolved in Milli-Q water (18.8 ml) to make a stock solution (10 mM). The TCAA solution was then diluted with Milli-Q water to 3, 1, 0.5 and 0.25 mM. $NaBH_4$ (13.1 mg, 0.35 mmol) was dissolved in ice cold Milli-Q water (34.63 ml) to make a 10 mM stock solution, which was diluted to 5 and 1 mM with ice cold Milli-Q water. The $NaBH_4$ solutions were used shortly after their preparation. To make the nanoclusters, protein (3 ml, 25 μM), TCAA (3 ml, variable concentration) and $NaBH_4$ (600 μl, variable concentration) were mixed. The solutions changed color immediately. After two hours the solutions were dialyzed (cut off ~12 kDa) in Milli-Q water (300 ml) for two hours, and then dialyzed further in phosphate buffer (300 ml) in order to ensure that the pH conditions were identical upon characterization. Table 1 show the different solutions made. We tried to use the same TCAA concentration for BLA as for BSA but this led to flocculation and precipitation, which is why the TCAA concentration is lower for BLA and LYZ than for BSA. Controls wherein TCAA was added to the protein and immediately removed *via* dialysis did not yield any measurable differences as compared to protein-only samples.

UV-visible spectroscopy in the range 190–1100 nm was measured using a Shimadzu UV-2401PC spectrophotometer.

Table 1 Each sample was made up of protein, TCAA (conc. in mM given in table), and $NaBH_4$ (conc. in mM given in table). The comment refers to the color after two hours. Au = gold, R = reducing agent, L = low, M = medium, H = high

Protein	Sample	[TCAA]	[$NaBH_4$]	Comment
BSA	BSA	0	0	Clear
	BSA–R_H	0	10	Clear
	BSA–Au_LR_L	1	1	Greyish brown
	BSA–Au_LR_M	1	5	Greyish brown, slightly pink
	BSA–Au_LR_H	1	10	Pale greyish brown (most brown)
	BSA–Au_HR_L	3	1	Purple
	BSA–Au_HR_M	3	5	Dark purple
	BSA–Au_HR_H	3	10	Dark purple
BLA	BLA	0	0	Clear
	BLA–R_H	0	10	Clear
	BLA–Au_LR_L	0.25	1	Orange, slightly pinkish grey
	BLA–Au_LR_M	0.25	5	Orange, slightly grey
	BLA–Au_LR_H	0.25	10	Orange, slightly grey
	BLA–Au_HR_L	0.5	1	Darker greyish orange
	BLA–Au_HR_M	0.5	5	Darker greyish orange
	BLA–Au_HR_H	0.5	10	Darker greyish orange
LYZ	LYZ	0	0	Clear
	LYZ–R_L	0	1	Clear
	LYZ–R_M	0	5	Clear
	LYZ–R_H	0	10	Clear
	LYZ–Au_LR_L	0.25	1	Grey
	LYZ–Au_LR_M	0.25	5	Grey
	LYZ–Au_HR_L	0.25	10	Grey
	LYZ–Au_HR_L	0.5	1	Greyish purple
	LYZ–Au_HR_M	0.5	5	Greyish purple
	LYZ–Au_HR_H	0.5	10	Greyish purple

The software used was UVprobe2.10. UV-vis was measured both on the sample directly after dialysis (protein concentration ~11.4 μM), and after further dilution with phosphate buffer (protein concentration ~2.3 μM). Protein concentration was calculated, assuming no or negligible loss of protein in the dialysis process, as the MWCO of the dialysis tubes used was well below the molecular weight of the proteins studied here.

Scanning (transmission) electron microscopy (STEM) images were acquired in bright-field STEM mode using a Hitachi S-5500 electron microscope operating at a 30 kV accelerating voltage. TEM grids were prepared by placing a drop (10 μL) of the gold nanoparticle solution on a Formvar carbon coated copper grid (Electron Microscopy Sciences) and allowing the solvent to evaporate at room temperature, prior to imaging.

Steady-state fluorescence was measured on the diluted samples (2.3 μM protein) using a Fluorolog-3 HORIBA Jobin Yvon apparatus. The excitation wavelengths used were λ_{ex} = 295 nm (slit 5 for BLA and LYZ, slit 3 for BSA), λ_{ex} = 370 nm, slit 5, and λ_{ex} = 450 nm, slit 10.

Time correlated single photon counting (TCSPC) was performed using the same instrument as for steady-state fluorescence. There were two major sets of lifetimes, one for the protein itself and one for the nanoclusters inside the protein. The conditions for measuring protein lifetimes were light-emitting diodes (LEDs) with wavelength 280 nm, λ_{em} 360 nm, bandpass 14.5 nm, and for the nanocluster the conditions were LED 370,[14] λ_{em} 460 nm, bandpass 14.5 nm. These measurements were also performed on the 2.3 μM solutions. The choice of emission wavelength for gold nanoclusters was based on a combination of the results from our steady-state measurements and from the work by Guével *et al.*,[14] which show that when excited at 370 nm small gold nanoclusters (Au_8) emit at 450 nm, while larger gold nanoclusters (Au_{25}) emit at 685 nm.

Circular dichroism (CD) measurements were conducted on an Olis DSM 1000CD apparatus, the lamp power supply was a LPS-220B from Photon Technology International, the user interface was an Olis online instrument system, and the software was OLIS GlobalWorks. A 10 mm cuvette, a grid of 2400 lines/mm, a slit width of 6.32 mm, a scan range from 290 nm to 200 nm, and an increment number of 720 was used. Each sample was scanned three times. The protein concentration in the samples containing BLA and LYZ was 2.3 μM, but the BSA-containing samples were diluted to 0.26 μM to get an acceptable signal. The phosphate buffer was used as a blank. TCAA in the buffer was measured under the same conditions to exclude contribution to the CD signal intensity from the gold precursor.

A *Micrococcus* test was performed to study the lysozyme activity using the same instrumentation as for the UV-vis measurements. The reference cell contained a *Micrococcus lysodeikticus* solution (0.5 g l^{-1}) in phosphate buffer (50 mM, pH 6.2). The sample cell was filled with 750 μl of the *Micrococcus* solution, and the two cells were heated to 30 °C before lysozyme (20 μl, 10 μM) was added to the sample cell. The solution was mixed quickly using a 200 μl pipette before measurements began. The transmittance measurements start at 100% and then increase. This is because the solution becomes less turbid as the cell walls are digested.

Results and discussion

The following sections are divided into (1) the photophysical properties of the gold nanoconstructs, (2) properties of BSA, BLA and LYZ relative to the native proteins, and finally (3) the resulting changes in protein function, as exemplified by an activity study of LYZ and LYZ–gold nanoconstructs. While the photophysical properties of gold nanoclusters are of inherent interest in biomedical labelling, the main focus of this article is how incorporation of gold nanoclusters into proteins can be tuned to give rise to different nanoconstructs with tunable optical properties as well as tunable protein conformation and function.

The term ''gold nanoconstructs'' here either refers to protein-stabilized gold nanoclusters, protein-stabilized gold nanoparticles, or a mixture of these. For each protein one high concentration of gold ions (Au_H) and one low concentration (Au_L) was employed. Au_L (0.25 mM) and Au_H (0.5 mM) are identical for BLA and LYZ, while higher concentrations were employed for BSA (Au_H = 3 mM, Au_L = 1 mM). Three different concentrations of the reducing agent were combined with each gold ion concentration, one high (R_H), one medium (R_M), and one low (R_L). R_H, R_M and R_L are the same for all the

 This journal is © The Royal Society of Chemistry 2013

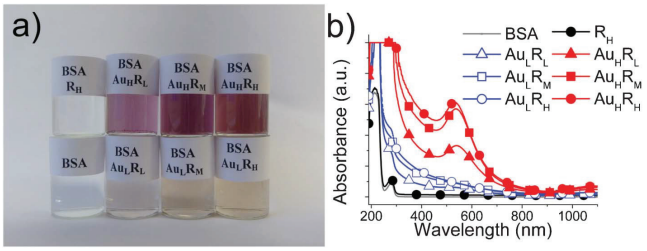

Fig. 1 (a) Picture of the different BSA–gold nanoclusters samples studied. (b) UV-vis spectra for the corresponding solutions. Here the abbreviations denote the following; Au = gold, R = reducing agent, L, M, H = low, medium and high concentrations, respectively.

protein-systems studied here. Following modification, all the systems were dissolved under identical solvent conditions, thus avoiding artefacts emanating from solvatochromism. For a complete description of the experimental conditions and concentrations, the reader is referred to the Materials and methods section.

(1) Photophysical properties of the gold nanoconstructs are tunable

The photophysical properties for all proteins and protein–gold constructs used here display similar trends. In order to minimize redundancies in the presented data, BSA was chosen as an example for UV and STEM results.

Immediately after mixing of the reagents, the solutions attained color, as shown in Fig. 1 for the BSA systems, together with the UV-vis spectra.

Fig. 1a reveals that the solutions containing only protein or protein and reducing agent were clear, while the solutions containing BSA and a low concentration of TCAA (*i.e.* Au_L in Fig. 1a) were weakly tinted. At higher TCAA concentrations (*i.e.* Au_H in Fig. 1a) the BSA containing solutions turned to a deeper shade of red. In Fig. 1b the band at 280 nm is distorted by a scattering contribution, which indicates the presence of multimeric gold following reduction and dialysis. Increasing the TCAA concentration resulted in an increased production of AuNPs associated with the proteins, as revealed by the concentration dependent absorbance between 300 and 500 nm. For the highest TCAA concentration we also see a localized surface plasmon resonance (LSPR) band at ~530 nm, indicating the formation of gold nanoparticles with diameters >3 nm (~1300 atoms).[22] As $NaBH_4$ does not act as a passivating ligand, these nanoparticles are likely stabilized by multiple proteins, forming multivalent protein–AuNP constructs. The LSPR position is related to nanoparticle diameter within the framework of Mie–Drude theory, with the LSPR position shifting towards higher wavelengths with increasing nanoparticle diameter (for a theoretical treatment, see *e.g.* Franzen[25] or Mulvaney[26–28]). For the BSA–gold nanoconstruct samples, both LSPR position and intensity varied with the reducing agent concentration used, as: BSA–Au_HR_L: λ_{max} = 537 nm, BSA–Au_HR_M: λ_{max} = 534 nm, and BSA–Au_HR_H: λ_{max} = 529 nm. Here, the LSPR position appears to be inversely correlated with the concentration of the reducing agent, indicating that the lowest reducing agent concentration resulted in the largest nanoparticles, which is in agreement with what has generally been observed for the formation of colloidal gold.[29] For BLA and LYZ, the observed UV-vis lineshapes were not as evidently dependent on the concentration of the reducing agent as for BSA (data not shown). Rather, systematic differences were observed as the concentration of the gold precursor varied. Unlike other common reducing agents such as citric or ascorbic acid, $NaBH_4$ does not impart any electrostatic or steric stability on the gold nanoparticles created, so the particles will rapidly form large aggregates, and precipitate out of solution. As the protein–gold nanoconstructs described here were found to be stable on a timescale of ~weeks, the gold nanostructures formed must be strongly associated with the protein—either embedded as nanoclusters within single proteins, or as single nanoparticles coated with a protein layer.

The UV-vis measurements indicate that the synthetic protocol used allows for a gradual transition between protein–AuNCs and protein-stabilized AuNPs. For the latter, a reducing agent-dependent size difference in the gold nanoparticles/-clusters was inferred. In order to verify these observations, the protein–gold nanoconstructs used here were investigated using STEM, as illustrated in Fig. 2 for BSA–Au systems. The particles must be larger than 3 nm for observation with the STEM instrument used in this study, and no such particles could be observed in any of the samples with low concentrations of gold precursor.

Fig. 2a shows a STEM image of the BSA sample that contained the highest gold concentration and the lowest amount of reducing agent (BSA–Au_HR_L), while Fig. 2b shows the same gold precursor concentration but the highest reducing agent concentration (BSA–Au_HR_H). The STEM observations are in agreement with the UV-vis measurements presented above (Fig. 1b), revealing that the presence of a well-defined LSPR band can be used to distinguish between formation of AuNCs and AuNPs. However, while a well-defined LSPR confirms the presence of AuNPs, it does not confirm or deny the co-presence of AuNCs associated with the protein corona. The BSA–Au_HR_L sample was found to contain particles in the size range from 5 nm to 15 nm and revealed highly

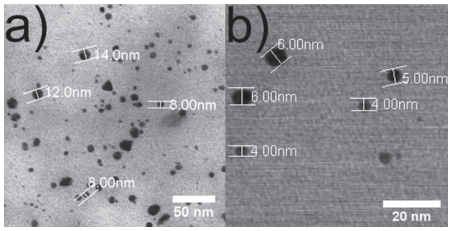

Fig. 2 STEM images of BSA-stabilized gold nanoparticles. (a) BSA–Au constructs with high concentration of TCAA and low amount of reducing agent (BSA–Au_HR_L), (b) BSA–Au constructs with high amount of gold precursor and high concentration of $NaBH_4$ (BSA–Au_HR_H). The samples were made with $NaBH_4$ being present for two hours.

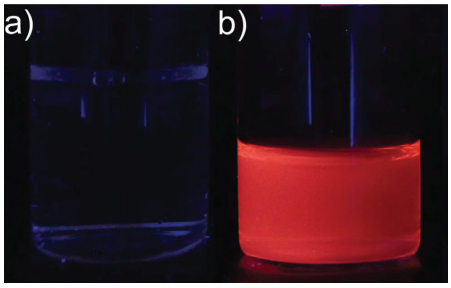

Fig. 3 (a) BSA in buffer, (b) BSA–gold nanoclusters. UV-light used was λ = 365 nm.

polydisperse constructs (Fig. 2a), where most of the particles were >7 nm in size. The suspension containing BSA–Au_HR_H revealed particles in the range from 3 nm to 9 nm, with the majority of the particles having a diameter of 6 $\pm$ 2 nm in size (Fig. 2b). The trend that higher amounts of reducing agent results in smaller, quite monodisperse gold nanoparticles, while lower concentrations of $NaBH_4$ yield larger, polydisperse particles was also observed for BLA and LYZ. This is also in agreement with the LSPR position as discussed above, indicating that UV-vis can be used to distinguish between AuNCs and AuNPs, as well as qualitatively rank particle size for the latter. Gold nanoparticles were only observed in samples made with high gold precursor concentrations. Consequently, the samples in this study that do not display a well-defined LSPR or show nanoparticles in the STEM images likely contain gold nanoclusters only. On the other hand, the samples where both LSPR and STEM reveal nanoparticles might also contain an unknown number of protein-embedded AuNCs. Moreover, as the diameter of AuNPs formed typically exceeds the size of the proteins used, the protein : AuNP ratio must be greater than one, whereas the opposite must hold for the systems where only AuNCs can be observed by spectroscopy. In turn, the fact that we observe stable protein–AuNPs suggests that sequestration, reduction and protection of gold species likely occur close to the external surface of the proteins, with subsequent protein unfolding exposing internal residues, depending on reaction conditions and conformational flexibility.

UV-vis and STEM measurements allow for the distinction between nanoclusters and nanoparticles, but provide very little specific information on the nature of the AuNCs. As AuNCs are comparable in size to the electron de Broglie wavelength at the Fermi level (~0.5 nm for Au), they exhibit molecular-like behavior, including discrete electronic states and size-dependent luminescence.[14,15,21] Earlier studies by Xie[15] and Schneider[14] have concluded that formation of AuNCs in BSA typically results in blue-emitting (~450 nm) small AuNCs (Au_8) or red-emitting (~650 nm) large AuNCs (Au_{25}). Irradiation with UV light at λ = 365 nm leads to excitation of both sets of magic number AuNCs, enabling the identification of small and large NCs, as well as a linear combination thereof.[13] When irradiated with UV light at λ = 365 nm, samples with only protein, as well as samples containing protein-stabilized gold nanoparticles, do not reveal any detectable color upon irradiation, while samples with protein-gold nanoclusters luminesce, as shown for BSA and BSA-AuNCs in Fig. 3 below, revealing the presence of magic number Au nanoclusters. The absence of detectable luminescence from the AuNP-containing solutions can be attributed to either (i) no AuNCs coexisting with AuNPs, (ii) the fraction of nanoclusters in the AuNP-containing samples being too small to provide visible luminescence, (iii) only Au_8 NCs coexisting with AuNPs, with concomitant quenching of luminescence *via* $Au_8 \rightarrow$ LSPR energy transfer, or a combination of these. In order to investigate the photophysical properties of the AuNCs, the emission profiles of the systems were investigated using steady-state fluorescence.

When excited at λ_{ex} = 350–390 nm, earlier studies have concluded that small protein-stabilized gold nanoclusters (Au_8) emit at λ_{em} ~ 450 nm, while larger nanoclusters (Au_{25}) show emission at λ_{em} ~ 685 nm.[14] Nanoclusters with magic numbers between 8 and 25 (11, 13, 18 and 22) are likely to emit somewhere in between. This fact was used to further investigate the AuNCs formed in BSA, BLA and LYZ (Fig. 4).

Steady-state emission profiles for proteins, proteins with reducing agent and protein–gold nanoconstructs are shown in Fig. 4. In the presence of gold (Fig. 4b–d), the intensity is significantly higher at 450 nm as compared to the native proteins (Fig. 4a), indicating the presence of small nanoclusters (~8 Au atoms).[14] The emission intensity increases with gold concentration until gold nanoparticles are formed. In general the emission at ~450 nm from the protein–gold nanoparticles was lower than for emission from the protein–gold nanoclusters. This is because AuNPs are not luminescent and due to Förster energy transfer they quench the fluorescence from AuNCs. The Förster quenching is most clear for the BSA stabilized gold nanoparticles (Fig. 4b) as the high TCAA concentration yields BSA-stabilized AuNPs and the low gold precursor concentration yields BSA-stabilized AuNCs. For BLA- and LYZ-stabilized gold constructs there is a more fluent transition from AuNCs to AuNPs. This can partly be caused by the concentration of gold precursor being higher in the BSA

 This journal is © The Royal Society of Chemistry 2013

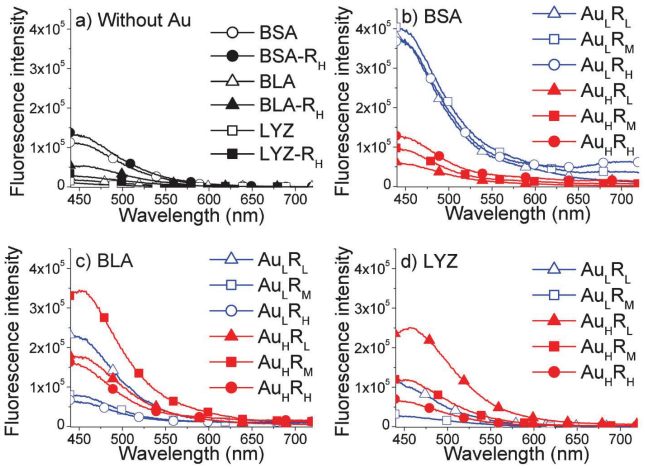

Fig. 4 Steady-state fluorescence of proteins and protein–gold constructs. λ_{ex} = 370 nm. Au = gold precursor (TCAA), R = reducing agent ($NaBH_4$), L, M, H = Low, Medium and High concentrations, respectively.

samples than for the other two proteins. BSA is also the only protein that exhibits bimodal distribution, as sample BSA–Au_LR_H has emission maxima at both ~450 nm and ~700 nm, indicating the presence of both small and large protein–gold nanoclusters.[15] The λ_{em} of gold nanoclusters increases with cluster size, and in the emission wavelength range observed here the clusters are likely to consist of a magical number of atoms between 8 and 25 (11, 13, 18 and 22). To simplify the discussion, the small gold nanoclusters are qualitatively set to Au_8 and the large ones to Au_{25}. This is also in agreement with the previous results for BSA–AuNCs published by Xie *et al.*[15] The results from the steady-state λ_{ex} = 370 nm measurements reveal that the protein–gold nanoconstructs can be tuned from small protein–gold nanoclusters to protein-stabilized gold nanoparticles for all of the proteins in this study. Additionally, BSA allows for tuning from small to large nanoclusters, likely due to the larger size of the protein, or an optimal combination of size, isoelectric point and conformational flexibility. When AuNPs are formed, they are likely to coexist with AuNCs, but due to the low concentration of AuNCs, energy transfer from the luminescence of Au_8 to the LSPR of AuNPs, or a combination of these two, the AuNCs do not provide observable luminescence in these samples. Sample LYZ–Au_LR_H was removed from the dataset before measuring steady-state fluorescence, due to observable instability within the timeframe of the data collection (~1 week).

UV, STEM and steady-state fluorescence measurements reveal that by varying the gold precursor concentration it is possible to vary the size of the gold constructs formed from small clusters, larger clusters and up to plasmonic nanoparticles. For UV as well as for steady-state fluorescence (λ_{ex} = 370 nm) the differences between gold nanoclusters and gold nanoparticles are most clear for BSA, while the differences were less prominent for BLA and LYZ. Thus, the synthetic protocol, wherein proteins are exposed to TCAA and $NaBH_4$, is a good general procedure for the formation of protein-stabilized nanoclusters and nanoparticles. However, the concentration ratios of reducing agent and gold precursor to polypeptide must be adjusted for the individual protein with respect to size, pI and stability.

(2) Protein conformation can be tuned using gold nanostructures

Tryptophan (Trp) is an environmentally sensitive intrinsic fluorophore frequently used to monitor conformational changes, including protein unfolding.[30] Changes in the local environment of a protein, such as increased solvent exposure following partial unfolding, is typically accompanied by a shift of the emission maximum towards longer wavelengths and/or a decrease in emission intensity. Whereas red-shifts of the emission profile can be directly attributed to partial protein unfolding, interpreting changes in emission intensity can be more ambiguous. However, the UV-vis results for the protein–gold nanoconstructs studied here (Fig. 1b) reveal that the gold nanoclusters absorb around 350 nm, enabling quenching of Trp emission *via* energy transfer into the AuNCs. Consequently, the changes in Trp emission profile make it possible to follow conformational changes in a protein as well as the presence of gold nanoconstructs using steady-state Trp fluorescence (Fig. 5). Here the excitation wavelength λ_{ex} = 295 nm.

The Trp emission profiles depicted in Fig. 5a, c and d reveal a decrease in intensity for all proteins upon addition of reducing agent, with the magnitude of the decrease being

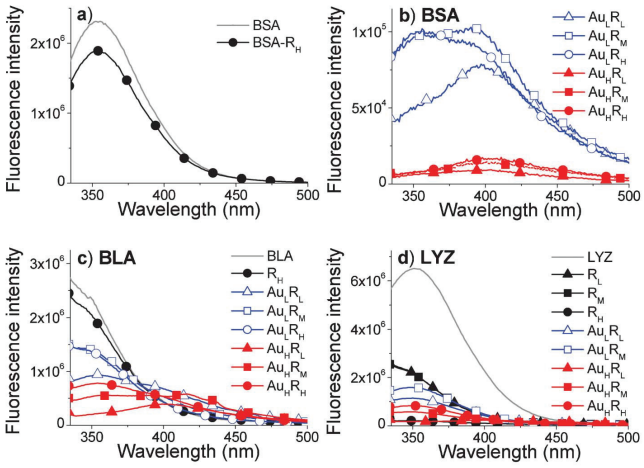

Fig. 5 Steady-state fluorescence of proteins and protein–gold constructs. λ_{ex} = 295, Au = gold precursor (TCAA), R = reducing agent, L, M, H = low, medium and high concentrations, respectively.

highly protein dependent. This decrease in intensity is probably due to quenching from increased solvent exposure of Trp, as $NaBH_4$ partially denatures the proteins. Upon addition of the highest amount of reducing agent (R_H), Trp emission intensity was mostly maintained for BSA and BLA, whereas all Trp emission was quenched in the case of LYZ. This can likely be attributed to the difference in pI of the proteins used. While BSA and BLA both have pIs below 5, the pI of LYZ is 10.8, enabling effective charge density matching between the overall cationic LYZ and the reducing agent. Thus, LYZ is more exposed to attack from BH_4^- than the other proteins investigated here. Interestingly, Fig. 5d reveals the same amount of emission intensity decrease compared to the native protein for addition of low and medium $NaBH_4$ concentrations, whereas the high amount of $NaBH_4$ led to complete quenching of LYZ Trp emission. Fig. 5d also reveals that while the intensity was reduced to almost zero at R_H, intensity was only reduced by 1/3 at R_M or R_L. This can likely be linked to unfolding of the protein.[11] $NaBH_4$ can reduce aldehydes, ketones, thiolesters and imines, but it cannot reduce carboxylates or esters.[31] This means that amino acids susceptible to attack by $NaBH_4$ are basic forms of histidine (His) and arginine (Arg), which are imines. A reduction of the imine in His would require a ring opening, which is very unlikely. However, the imine (guadinium group to be exact) in Arg can be susceptible to attack by $NaBH_4$. Comparing the amino acid sequences of BSA, BLA and LYZ, the Arg contents are 4.3%, 0.8% and 10.8% for BSA, BLA and LYZ, respectively. Thus, we attribute the strong effect of $NaBH_4$ on LYZ to reduction of Arg residues.

From the UV-measurements of BLA and LYZ (data not shown), differences in the absorption profile due to the gold precursor concentration were obvious, while varying the $NaBH_4$ concentration seemed to have little effect on the absorbance properties. From the Trp fluorescence in Fig. 5c and d, an intensity variation, dependent both on the gold precursor concentration and the concentration of the reducing agent, is evident. The intensity changes can be due to both increased protein unfolding and energy transfer to gold nanoconstructs. Despite differences in the degree of Trp emission lineshape distortion, all the three proteins here followed the same trend: the magnitude of fluorescence quenching was found to be proportional to the concentration of gold precursor. Furthermore, the difference between Au_H and Au_L was larger for BSA than for the two other proteins. This is probably due to the higher (3 ×) TCAA concentration in BSA–Au_H as compared to BSA–Au_L, whereas for the BLA and LYZ samples the TCAA concentration was doubled. Conversely, with the exception of the BSA–Au_L suspensions, the fluorescence intensity was found to be inversely proportional to the concentration of the reducing agent. The Trp fluorescence was quenched more at R_L than at R_H, likely due to energy transfer to gold nanostructures. Owing to the high extinction cross-sections associated with LSPR, gold nanoparticles are vastly more efficient acceptors for Förster energy transfer than gold nanoclusters. As expected, the samples with the most depleted Trp emission in Fig. 5 contain AuNPs, as determined *via* UV-vis, STEM and steady-state λ_{ex} = 370 nm.

The reduction in Trp emission intensity can also be partially caused by conformational changes, a hypothesis that is strengthened by the fact that Trp emission is also red shifted for all the proteins; a typical sign of conformational change as Trp is more exposed to solvent.[30,32] In the case of BSA, there seem to be two Trp populations for the nanocluster-containing

 This journal is © The Royal Society of Chemistry 2013

samples (Fig. 5b), while only one population is evident for the samples containing gold nanoparticles. Again, this is likely attributable to the more efficient energy transfer for the systems containing gold nanoparticles. Moreover, as both the emission profiles from multimeric gold (Fig. 4) and the Trp emission profiles (Fig. 5) reveal protein dependent variations, despite otherwise similar reaction conditions, the observed effects likely emanate from the properties of the proteins used. BSA allows for a wide range of tunability with respect to Au size, varying from small clusters to larger clusters and finally AuNPs stabilized by multiple proteins, while BLA allows for significant tunability of protein structure (provided the gold concentration is not too high). Conversely, LYZ displays a bimodal behavior, where it is difficult to tune both Au size and protein conformation, with the resulting nanoconstructs exhibiting limited stability.

From STEM, λ_{ex} = 370 nm results (Fig. 4) and Trp emission (Fig. 5) low $NaBH_4$ concentrations (R_L) yield larger AuNCs (and indeed AuNPs) than R_H, with the increased size of the gold constructs resulting in a higher degree of unfolding. Fluorescence lifetime measurements (time-correlated single photon counting (TCSPC), Table 2) were used to further investigate the local Trp environment.[10,11,30] No distinct lifetimes attributable to the gold nanostructures could be detected upon excitation at 280 nm for any of the systems studied here.

As the proteins used here contain different amounts of Trp residues (BSA = 3 Trp, BLA = 3 Trp, and LYZ = 5 Trp), interpretation of the TCPSC results with respect to comparison of proteins is intricate. With the exception of BSA–Au_H, a bimodal fitting was found to provide the best overall fit for the fluorescence decay profiles of the samples studied here, yielding one "short" ($T1$) and one "long" ($T2$) lifetime, with corresponding relative populations $B1$ and $B2$, respectively. For the samples BSA–Au_HR_L and BSA–Au_HR_M, the short lifetime $T1$ was found to be outside the range of the LED used, *i.e.* faster than the repetition rate. We attribute this reduction of the short lifetime to a combination of efficient quenching from the gold nanoparticles formed, as well as unfolding of the protein.[10,11] Overall, formation of gold nanostructures within BSA results in reduction of the short lifetime ($T1$), and a large increase of the short lifetime population ($B1$) as compared to the native protein, indicating changes in Trp environment following formation of gold nanoconstructs. With the exception of a single sample (BSA–Au_HR_M), the long lifetime ($T2$) also decreased upon the introduction of gold. Specifically, the population shifts towards shorter lifetimes, and a reduction in lifetimes indicates either quenching from increased Trp exposure to water, energy transfer to gold (either NCs or NPs), or a combination of the two.

All the gold-modified BLA samples (Table 2) reveal a decrease in the short lifetime population ($B1$) and a corresponding increase in the long lifetime population ($B2$). No significant changes in the short lifetime ($T1$) of the BLA systems could be detected within the estimated uncertainties. However, the long lifetime ($T2$) displayed variation towards longer (particularly BLA–Au_HR_L) and shorter (BLA–Au_LR_M and BLA–Au_HR_H) lifetimes compared to the native protein, without any obvious trend with respect to TCAA or $NaBH_4$ concentration. In general, an increase in the long lifetime, and particularly its population ($T2$ and $B2$, respectively), indicate that the Trp residues are more protected from quenchers—hydroxyl or other—following formation of gold nanoconstructs. The gold-modified LYZ samples generally reveal the same overall trend as for BSA, albeit with a much stronger dependence on the reducing agent, as discussed above.

BSA contains three Trp residues, where $T1$ and $T2$ (with populations $B1$ and $B2$, respectively) can be attributed to the external and buried Trp residues, respectively.[30] As such, changes either in lifetime or the associated population can be rationalized *via* increased solvent exposure emanating from protein unfolding and/or from energy transfer to the gold nanoconstructs.[11] However, as both BLA and LYZ contain several Trp residues (three and five for BLA and LYZ, respectively) with less well-defined spatial distribution of the fluorophores, interpretation of TCSPC data for BLA and LYZ is more complex. In the case of BLA, the overall trend of a relative increase in the long lifetime population suggests a change in protein conformation, with the apparent lack of trend with respect to $B1$ and $B2$ values as a function of either TCAA or $NaBH_4$ concentrations perhaps being attributable to a gradual distortion of protein structure, which is in agreement with the steady-state Trp emission results displayed in Fig. 5. As the BLA systems reveal a gradual transition from NCs to NPs, the TCSPC results could emanate from a varying size and number of gold nanoconstructs associated with BLA for different concentrations of precursor and reducing agent. Overall, the trend for LYZ is somewhat similar to what was found for BSA, with the caveat that interaction with the reducing agent only

Table 2 Fluorescence lifetimes and corresponding populations of protein, protein–AuNPs and protein–AuNCs. T = lifetimes in nanoseconds (ns), B = populations in %, λ_{ex} = 280 nm, λ_{em} = 360 nm

	$T1$ (ns)	$B1$ (%)	$T2$ (ns)	$B2$ (%)
BSA	4.7 ± 0.2	40 ± 1	7.5 ± 0.1	60 ± 1
BSA–R_H	4.1 ± 0.1	36 ± 1	7.5 ± 0.1	64 ± 1
BSA–Au_LR_L	0.9 ± 0.1	72 ± 1	5.1 ± 0.1	28 ± 1
BSA–Au_LR_M	1.3 ± 0.1	66 ± 1	5.5 ± 0.1	34 ± 1
BSA–Au_LR_H	1.3 ± 0.1	50 ± 1	5.9 ± 0.1	50 ± 1
BSA–Au_HR_L	0.3 ± 0.1[a]	57 ± 1	5.9 ± 0.1	43 ± 1
BSA–Au_HR_M	0.6 ± 0.1[a]	62 ± 1	7.5 ± 0.1	38 ± 1
BSA–Au_HR_H	0.9 ± 0.1	67 ± 1	7.0 ± 0.1	33 ± 1
BLA	0.9 ± 0.1	93 ± 1	5.2 ± 0.1	7 ± 1
BLA–R_H	0.9 ± 0.1	88 ± 1	5.5 ± 0.1	12 ± 1
BLA–Au_LR_L	1.1 ± 0.1	67 ± 1	5.3 ± 0.1	33 ± 1
BLA–Au_LR_M	1.0 ± 0.1	77 ± 1	4.8 ± 0.1	23 ± 1
BLA–Au_LR_H	1.0 ± 0.1	75 ± 1	5.3 ± 0.1	25 ± 1
BLA–Au_HR_L	0.9 ± 0.1	66 ± 1	7.5 ± 0.1	34 ± 1
BLA–Au_HR_M	1.1 ± 0.1	67 ± 1	5.2 ± 0.1	33 ± 1
BLA–Au_HR_H	1.1 ± 0.1	64 ± 1	4.6 ± 0.1	36 ± 1
LYZ	1.5 ± 0.1	70 ± 1	3.5 ± 0.1	30 ± 1
LYZ–R_L	0.9 ± 0.1	91 ± 1	6.9 ± 0.1	9 ± 1
LYZ–R_M	1.0 ± 0.1	90 ± 1	6.9 ± 0.1	10 ± 1
LYZ–R_H	1.8 ± 0.1	42 ± 1	11.6 ± 0.1	58 ± 1
LYZ–Au_LR_L	1.6 ± 0.1	84 ± 1	6.6 ± 0.1	16 ± 1
LYZ–Au_LR_M	1.7 ± 0.1	86 ± 1	6.6 ± 0.1	14 ± 1
LYZ–Au_HR_L	1.1 ± 0.1	64 ± 1	11.6 ± 0.1	36 ± 1
LYZ–Au_HR_M	1.4 ± 0.1	81 ± 1	8.4 ± 0.1	19 ± 1
LYZ–Au_HR_H	1.5 ± 0.1	84 ± 1	8.0 ± 0.1	16 ± 1

[a] Outside the range of the LED used.

has a more pronounced effect on Trp emission than the formation of gold nanoconstructs. This is in agreement with the steady-state observations in Fig. 5d, where it was evident that LYZ is very vulnerable to addition of $NaBH_4$. From Table 2 it can be seen that when a small amount of $NaBH_4$ is added to LYZ the short lifetime goes down and its population increases dramatically (from ~70% to 90%). Both the absolute value of the fluorescence lifetimes and their corresponding populations are sensitive to the surrounding chemical environment such as the presence of quenchers. Upon exposure to a hydroxyl quencher, the fluorescence lifetime can be expected to decrease. Moreover, as the measured signal is a composite of contributions from buried as well as exposed Trp residues, an increase in the population of the short lifetime can be attributed to increased exposure to solvent for all the Trp residues in the polypeptide chain. Taken together, a decrease in the absolute value of the short lifetime as well as an increase in its relative population indicate that the surface Trps are more exposed to water and that the protein has partially unfolded. The long lifetime also increases, so it might be that the structural changes upon reduction of surface amino acids has led to a shielding of buried Trp residues (there are 5 Trp in LYZ). An increase from R_L to R_M had little influence on the lifetimes and populations, which is in agreement with the Trp steady-state emission intensities shown in Fig. 5d. However, at R_H the short lifetime almost doubles, its population is dramatically reduced from ~90% to ~40%, the long lifetime is almost doubled and its population increases from ~10% to ~60%. The increase in the population of the long lifetime as well as in both lifetimes indicates that all the Trp residues are more shielded from quenching. The most parsimonious explanation for the pronounced effect of the reducing agent is that the unfolding of LYZ is so severe that denaturation and subsequent aggregation occurs, trapping Trp within larger flocks and shielding them from water. An aggregation due to excessive protein unfolding induced by high amounts of $NaBH_4$ could also explain why LYZ–Au_LR_H precipitated early in the study. The LYZ–Au_HR_H system remained stable within the timeframe of these experiments (~2 weeks), likely due to stabilization imparted by the gold nanoparticles formed.

Fluorescence measurements gave some indication about structural changes in the protein, but for a more thorough examination of structural changes, circular dichroism measurements were performed. Changes in intensity and lineshape indicate structural changes in the protein, as shown in Fig. 6 for BSA, Fig. 7 for BLA and in Fig. 8 for LYZ. At this point the LYZ–Au_HR_L sample was also removed from the dataset due to precipitation. For CD, as well as for the TCSPC, the addition of reducing agent seems to affect BLA a bit more than BSA, while LYZ is most severely altered by $NaBH_4$. To exclude any effects from gold, CD was measured using the same concentration of TCAA as in the synthesis of the gold nanoclusters. There were no contributions to the CD signal from the TCAA.

To rule out the possibility of changes due to attenuation of the signal by gold, the relationship between signal intensity at 200 nm and 222 nm was studied for all samples (see Fig. 6d, 7d and 8d). The 200 nm/222 nm ratio varies in a manner not

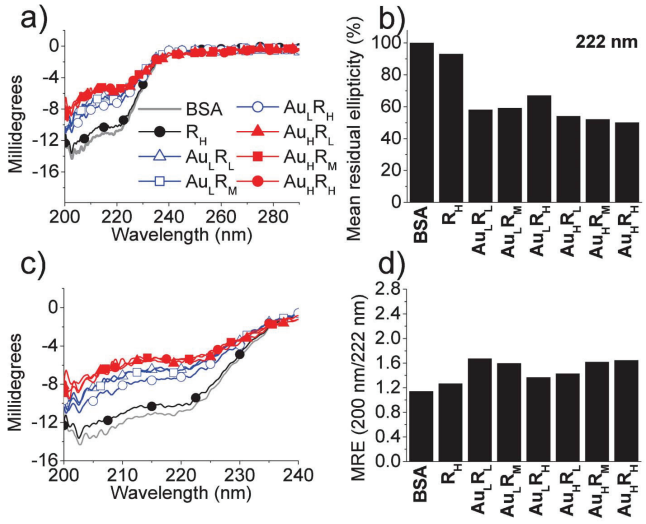

Fig. 6 (a) CD of samples containing BSA. (b) Mean residual ellipticity of samples containing BSA at 222 nm. Au = gold, R = reducing agent, L = low amount, M = medium amount, H = high amount. (c) Magnified section of (a). (d) Relationship between mean residual ellipticity (MRE) at 200 nm and 222 nm.

 This journal is © The Royal Society of Chemistry 2013

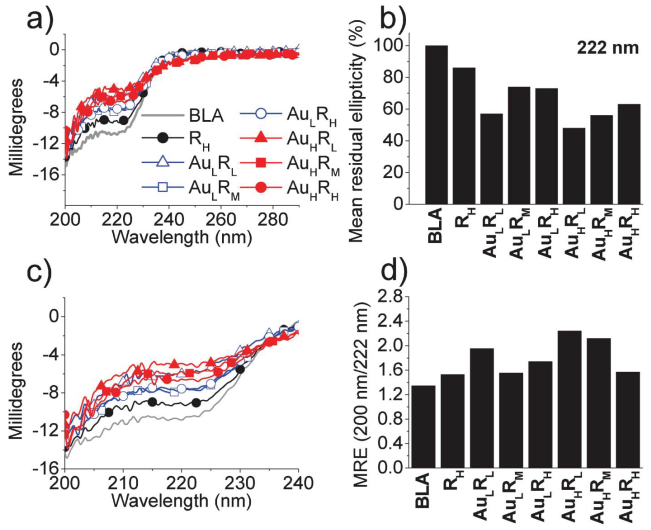

Fig. 7 (a) CD of BLA samples. (b) Mean residual ellipticity of samples containing BLA at 222 nm. Au = gold, R = reducing agent, L = low amount, M = medium amount, H = high amount. (c) Magnified section of (a). (d) Relationship between mean residual ellipticity (MRE) at 200 nm and 222 nm.

directly correlated to the concentration of the gold precursor or the corresponding absorbance at these wavelengths (Fig. 1). Thus, the spectral changes are likely due to changes in the protein, not attenuation of the signal caused by the presence of gold.

As for UV (Fig. 1) and the fluorescence studies (Fig. 4, 5 and Table 2) the CD data in Fig. 6 show that only a small change in intensity occurred when reducing agent was added to BSA. The change was larger when small amounts of gold precursor were also added, and even more so when the TCAA concentration was higher. This confirms that $NaBH_4$ by itself has some, but little, effect on BSA, and by varying the gold precursor concentration it is possible to gradually change the protein conformation with respect to the secondary structure content. The bar chart in Fig. 6b indicates that the variation in reducing agent concentration within each set of gold concentrations has some effect on the structure of BSA. The BSA–Au_LR_H sample stands out with a mean residual ellipticity closer to the native protein than any other sample where gold is added; thus more of the original structure is probably intact. From several of the other techniques used we have seen that the highest concentration of reducing agent gave the smallest nanoclusters. Small clusters give a high curvature, and allow the protein to unfold less.[9,33,34]

The main trends in the CD measurements are similar for BLA (Fig. 7) as for BSA (Fig. 6) considering that $NaBH_4$ has a small effect on the signal intensity, and that addition of a gold precursor changes the intensity more. For BSA all the samples with high gold concentration had a more reduced signal, compared to native protein, than samples with lower TCAA concentration (Fig. 6b), but for BLA there seems to be an overlap in signal reduction between high and low gold precursor concentration (Fig. 7b). This probably means that $NaBH_4$ has some, but not high influence on the BLA structure and that formation of gold nanoclusters and gold nanoparticles changes the structure further. Moreover, it seems to be a gradual transition between nanocluster and nanoparticle formation within BLA, contrasting with the behavior of LYZ. This may reflect a higher tunability of the BLA structure.

At this point also sample LYZ–Au_HR_L is removed from the dataset, due to the high degree of flocculation. Small tendencies to flocculation were also observed in samples LYZ–Au_LR_L and LYZ–Au_HR_M. Just like for the steady-state measurements (Fig. 5), Fig. 8a shows that a small addition of $NaBH_4$ changed the intensity of the signal slightly and that adding a medium amount of $NaBH_4$ gave no difference in results. But when the high amount of reducing agent was added, the signal was completely quenched. For LYZ the mean residual ellipticity is more similar to the native protein when high amounts of gold precursor are used than low. This is the exact opposite of BSA and BLA; however the difference is quite small. This deviation might be caused by an onset of flocculation in the system. The CD results point in the same direction as the previous results; high amounts of $NaBH_4$ completely perturb the LYZ structure, but when gold nanoconstructs are formed within the protein this partially stabilizes the structure.

From the CD results and TCSPC we have seen that the effect of the reducing agent on the protein increases in the order BSA

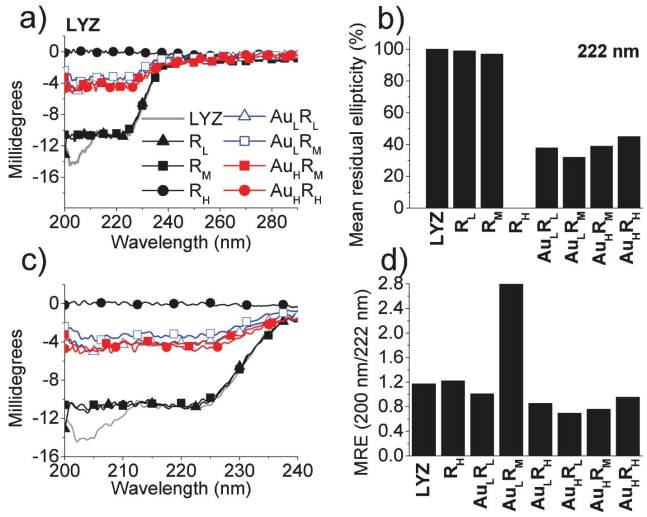

Fig. 8 (a) CD of LYZ samples. (b) Mean residual ellipticity of samples containing LYZ at 222 nm. Au = gold, R = reducing agent, L = low amount, M = medium amount, H = high amount. (c) Magnified section of (a). (d) Relationship between mean residual ellipticity (MRE) at 200 nm and 222 nm.

< BLA < LYZ, and CD also showed that there is a gradual loss of alpha helical motifs (reduction in mean residual ellipticity at 222 nm) as gold nanoconstructs are formed. The change was most gradual for BLA. This is also seen by the fact that BSA and LYZ have separated regions in CD and steady-state λ_{ex} = 295 nm fluorescence experiments for nanocluster and nanoparticle containing proteins, while there is an overlap between the two regions for BLA. Lysozyme is the least tunable, meaning that the effect of $NaBH_4$ is more crucial to the unfolding of the protein than is the formation of gold nanoconstructs.

BLA and LYZ are of equal size and overall fold, so the large differences between them might be caused by the differences in their pI. As mentioned earlier LYZ (pI = 10.5) is more likely to electrostatically interact with $NaBH_4$ than BLA (pI = 4.5), and can therefore interact more efficiently. LYZ is also a very rigid protein compared to BLA[35] and the low flexibility makes it difficult to stabilize when unfolding agents are introduced. Considerations regarding conformational flexibility can also be used to explain why BSA is less altered than BLA. BSA and BLA have equal pI, but BSA is almost five times larger than BLA, and has three semi-independent but similar domains that can each respond to a change that is local on the protein size scale.[32]

The CD results as well as fluorescence show that the formation of gold nanoconstructs stabilizes the structure of LYZ for a while, so that $NaBH_4$ completely destroys the protein conformation. Over time the LYZ–gold nanoclusters aggregate and precipitate. For this reason it seems that the gold nanoclusters are formed on the surface of the protein, and over time the clusters collide and form gold nanoparticles instead. The aggregation can then be a combined result of hydrophobic interactions between exposed amino acids in LYZ as it has partially unfolded, and crosslink between gold nanoclusters from different proteins colliding and forming a gold nanoparticle bridge.

(3) Protein–gold nanoconstructs display tunable functional retention

Protein function, such as enzymatic activity, is known to be closely linked to the protein structure, and so any conformational changes might compromise or otherwise affect the functionality. In this study, all observables indicate that $NaBH_4$ alters the LYZ structure, while formation of gold nanoconstructs allows for at least partial retention of the native structure (see Fig. 5 and 8). Moreover, it is clearly shown that protein–gold nanoclusters behave differently from the individual components, demonstrating emergent properties of the protein-gold systems, which might be of tremendous use within biomedicine. LYZ digestion of *Micrococcus lysodeikticus* cell walls was used to compare the enzyme activity of modified LYZ with that of the native protein (Fig. 9). Thus, correlating information on the conformational changes to LYZ enzyme activity enables a measure of how much the modification has affected the structure–function relationship. The transmittance for the measurements depicted in Fig. 9 was set to 100% for the cell wall suspended in buffer, as described in the materials and methods section. As LYZ or LYZ–gold nanoconstructs are added, the cell walls are digested and the

 This journal is © The Royal Society of Chemistry 2013

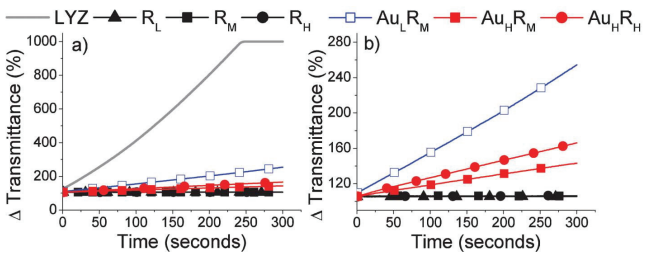

Fig. 9 Cell wall digestion activity of lysozyme, lysozyme with $NaBH_4$ and lysozyme–gold nanoconstructs at pH 6.2 and 30 °C. The change in transmittance starts at 100% and the transmittance increase means that *Micrococcus lysodeikticus* cell walls are digested. (a) All results, (b) the dataset for the native protein is removed.

suspension becomes more transparent, resulting in increased transmittance.

From the kinetic profiles displayed in Fig. 9a, the increase in transmittance over time is larger when native LYZ is used to digest the cell walls than when modified LYZ is used, indicating that the enzymatic activity of native LYZ is higher than for the modified samples studied here. Fig. 9b reveals that the cell wall digesting activity of modified LYZ varies with the concentration of gold precursor and reducing agent. While steady-state measurements (Fig. 5) and CD measurements (Fig. 8) showed that only the highest concentrations of $NaBH_4$ resulted in severe loss of structural domains for LYZ, Fig. 9b reveals that introduction of $NaBH_4$ results in complete loss of substrate digesting activity, irrespective of the concentration of the reducing agent. Interestingly, LYZ with both reducing agent and gold precursor added is able to change the transmittance, and thus has cell wall digesting properties. Samples LYZ–Au_HR_H and LYZ–Au_HR_M retain approximately 6% $\pm$ 1% and 4% $\pm$ 1%, respectively, of LYZ cell wall digesting activity, whereas sample LYZ–Au_LR_M retains as much as 14% $\pm$ 1% enzyme activity as compared to native LYZ. To exclude any destructive effects from TCAA on the *Micrococcus lysodeikticus* cell wall, the activity test was performed with different TCAA concentrations as well (data not shown). None of the TCAA concentrations used here had any measurable effect on the cell walls. These results imply that gold nanoclusters to some extent are able to stabilize LYZ, and just as it was possible to tune LYZ conformation by varying the gold precursor and reducing agent concentrations it is possible to tune LYZ enzyme activity.

In the Trp steady-state section it was implied that the high amount of arginine could explain why the LYZ structure is more vulnerable to $NaBH_4$ than the other two proteins. The amino acids Glu35 and Asp52 are critical for LYZ activity, but the amino acids Arg62, Tyr63, Arg101 and Ala107 are also a part of the active site.[36] Thus, two Args are directly involved in the active site of LYZ and additionally there is Arg108 next to Ala107 and Arg50 close to Asp52. The density of arginine in the active site, or very close to amino acids that are in the active site, is very high. This strengthens the hypothesis about Arg being the key to why $NaBH_4$ is so harsh on the LYZ structure and activity compared to BSA and BLA.

Conclusion

The steady-state and time-resolved fluorescence using both the gold covalent modifications and tryptophan residues as probes, as well as CD, suggests that the metal and protein components of the constructs have a mutual influence on each other. UV-vis, STEM, and the fluorescence measurements show that it is possible to controllably functionalize single proteins with gold nanoclusters and also stabilizing gold nanoparticles by multiple proteins, as well as controlling the transition between these using one single synthetic protocol. Our results show that the approach is versatile; by varying the gold precursor concentration it is possible to tune all the way from protein–gold nanoclusters to protein–gold nanoparticles, and by simultaneously changing the reducing agent concentration the size and polydispersity of both kinds of constructs can be tuned. As an effect of the different construct sizes, the protein structures are affected to different extents, as shown by steady-state λ_{ex} = 295 nm and CD measurements. Of BSA, BLA and LYZ, BLA is the protein that opens for the best tunability, while LYZ gets the most disrupted. $NaBH_4$ alone has quite a severe effect on the LYZ structure and enzymatic activity. The effect of $NaBH_4$ is, interestingly, reduced as the embedded nanoclusters and nanoparticles stabilize the protein. LYZ–gold nanoconstructs were a lot less stable than for the other two proteins, probably due to the rigid structure of LYZ and its high Arg content. Strategies for modifying proteins with AuNCs and AuNPs must thus balance the disruptive and stabilizing effect the modification has on the modified protein's structure and solubility, respectively. The protein fold is significantly loosened, although not enough to abolish all activity in the case of LYZ. Additionally, physical blocking of active sites from the gold species might have attributed to the reduced activity. Although the function of BLA and BSA was not assayed, it is reasonable to assume that these proteins may also be prepared with covalent cluster or particle modification in a manner that allows retention of at least part of their function. The spectroscopic data suggest an incremental perturbation of the protein fold, and it may be that this feature could be used to kinetically lock proteins in folding

intermediates that would otherwise not be thermodynamically stable and amenable to investigation. The spectroscopic data presented here suggest that this possibility is strongest for BLA, which in support of this has been shown to have a marginal folding barrier.[35] Such a possibility would be of high relevance for the general study of folding intermediates and particle-associated states in particular, both problems being relatively inaccessible to normal techniques.[35,37–39] In addition to the fundamental importance of studying partially folded protein states, such states are implicated in many detrimental diseases such as Alzheimer's and Parkinson's disease.[35] For instance, β-amyloid plaque and its more cytotoxic precursor annular oligomers, are formed from marginally stable proteins that are perturbed either by mutation, oxidation or interference with an interface, such as a lipid membrane or monolayer.[40,41] The presence of the gold modification could, in addition to its role as a fluorescence reporter of the local environment, ensure that a non-native protein state could be explored by steady-state techniques, which cannot ordinarily be employed due to its short lifetime in the absence of noble-metal clusters.

Acknowledgements

The authors acknowledge the Department of Chemical Engineering, NTNU, for financial support. Wilhelm R. Glomm and Sondre Volden acknowledge financial support from the Research Council of Norway (NFR). STEM measurements were performed at the NTNU NanoLab (Grantnumber 81601100).

References

1 S. Rana, Y.-C. Yeh and V. M. Rotello, Engineering the Nanoparticle–Protein Interface: Applications and Possibilities, *Curr. Opin. Chem. Biol.*, 2010(14), 828–834.
2 M. De, P. S. Ghosh and V. M. Rotello, Applications of Nanoparticles in Biology, *Adv. Mater.*, 2008, **20**, 4225–4241.
3 W. P. Faulk and G. M. Taylor, Immunocolloid Method for Electron Microscope, *Immunochemistry*, 1971, **8**(11), 1081–1083.
4 C. Feldherr, D. Akin, T. Littlewood and M. Stewart, The Molecular Mechanism of Translocation through the Nuclear Pore Complex is Highly Conserved, *J. Cell Sci.*, 2002, **115**(14), 2997–3005.
5 C. M. Feldherr and D. Akin, The Permeability of the Nuclear-Envelope in Dividing and Nondividing Cell-Cultures, *J. Cell Biol.*, 1990, **111**(1), 1–8.
6 W. R. Glomm, Functionalized Gold Nanoparticles for Applications in Bionanotechnology, *J. Dispersion Sci. Technol.*, 2005, **26**(3), 389–414.
7 B. Krisch, C. Buchholz, R. Mentlein and A. Turzynski, Visualization of Neuropeptide-Binding Sites on Individual Telencephalic Neurons of Rat, *Cell Tissue Res.*, 1993, **272**(3), 523–531.
8 B. L. Wang, L. Scopsi, M. H. Nielsen and L. I. Larsson, Simplified Purification and Testing of Colloidal Gold Probes, *Histochemistry*, 1985, **83**(2), 109–115.
9 R. S. Kane and A. D. Stroock, Nanobiotechnology: Protein-Nanomaterial Interactions, *Biotechnol. Prog.*, 2007, **23**(2), 316–319.
10 S. M. Lystvet, S. Volden, Ø. Halskau and W. R. Glomm, Immobilization onto Gold Nanoparticles Alters Alpha-Lactalbumin Interaction with Pure and Mixed Phospholipid Monolayers, *Soft Matter*, 2011, **7**(24), 11501–11509.
11 S. M. Lystvet, S. Volden, M. Yasuda, Ø. Halskau and W. R. Glomm, Emergent Membrane-Affecting Properties of BSA–Gold Nanoparticle Constructs, *Nanoscale*, 2011, **3**(4), 1788–1797.
12 S. Volden, A.-L. Kjøniksen, K. Zhu, J. Genzer, B. Nyström and W. R. Glomm, Temperature-Dependent Optical Properties of Gold Nanoparticles Coated with a Charged Diblock Copolymer and an Uncharged Triblock Copolymer, *ACS Nano*, 2010, **4**(2), 1187–1201.
13 X. L. Guével, N. Daum and M. Schneider, Synthesis and Characterization of Human Transferrin-stabilized gold nanoclusters, *Nanotechnology*, 2011, **22**(27), 275103/1–275103/7.
14 X. L. Guével, B. Hötzer, G. Jung, K. Hollemeyer, V. Trouillet and M. Schneider, Formation of Fluorescent Metal (Au,Ag) Nanoclusters Capped in Bovine Serum Albumin Followed by Fluorescence and Spectroscopy, *J. Phys. Chem. C*, 2011, **115**, 10955–10963.
15 J. Xie, Y. Zheng and J. Y. Ying, Protein-Directed Synthesis of Highly Fluorescent Gold Nanoclusters, *J. Am. Chem. Soc.*, 2009, **131**, 888–889.
16 T. H. Chen and W. L. Tseng, (Lysozyme Type VI)-Stabilized Au8 Clusters: Synthesis Mechanism and Application for Sensing of Glutathione in a Single Drop of Blood, *Small*, 2012, **8**(12), 1912–1919.
17 Y. C. Shiang, C. C. Huang, W. Y. Chen, P. C. Chen and H. T. Chang, Fluorescent gold and silver nanoclusters for the analysis of biopolymers and cell imaging, *J. Mater. Chem.*, 2012, **22**(26), 12972–12982.
18 S. Volden, S. M. Lystvet, Ø. Halskau and W. R. Glomm, General applicable procedure for in situ formation of fluorescent protein–gold nanoconstructs, *RSC Adv.*, 2012, **2**(31), 11704–11711.
19 L. Berti and G. A. Burley, Nucleic acid and nucleotide-mediated synthesis of inorganic nanoparticles, *Nat. Nanotechnol.*, 2008, **3**(2), 81–87.
20 D. L. Feldheim and B. E. Eaton, Selectionof biomolecules capable of mediating the formation of nanocrystals, *ACS Nano*, 2007, **1**(3), 154–159.
21 W. A. de Heer, The Physics of Simple Metal Clusters: Experimental Aspects and Simple Models, *Rev. Mod. Phys.*, 1993, **65**(3), 611–676.
22 S. Link, A. Beeby, S. FitzGerald, M. A. El-Sayed, T. G. Schaaff and R. L. Whetten, Visible to Infrared Luminescence from a 28-Atom Gold Cluster, *J. Phys. Chem. B*, 2002, **106**(13), 3410–3415.
23 Ø. Halskau, S. Volden, A. C. Calvo, A. Martinez and W. R. Glomm, Adsorption and Bioactivity of Tyrosine Hydroxylase on Gold Surfaces and Nanoparticles, *Protein Pept. Lett.*, 2010, **17**(11), 1376–82.
24 D. Shugar, The Measurement of Lysozyme Activity and the Ultra-Violet Inactivation of Lysozyme, *BBA*, 1952, **8**(0), 302–309.

 This journal is © The Royal Society of Chemistry 2013

25 S. Franzen, Surface Plasmon Polaritons and Screened Plasma Absorption in Indium Tin Oxide Compared to Silver and Gold, *J. Phys. Chem. C*, 2008, **112**(15), 6027–6032.
26 P. Mulvaney, Surface Plasmon Spectroscopy of Nanosized Metal Particles, *Langmuir*, 1996, **12**, 788–800.
27 A. C. Templeton, J. J. Pietron, R. W. Murray and P. Mulvaney, Solvent Refractive Index and Core Charge Influences on the Surface Plasmon Absorbance and Alkanethiolate Monolayer-Protected Gold Clusters, *J. Phys. Chem. B*, 2000, **104**, 564–570.
28 T. Ung, M. Giersig, D. Dunstan and P. Mulvaney, Spectroelectrochemistry of Colloidal Silver, *Langmuir*, 1997, **13**(6), 1773–1782.
29 J. Turkevich, Colloidal Gold. Part I, *Gold Bull.*, 1985, **18**(3), 86–91.
30 J. R. Lakowicz, *Principles of Fluorescence Spectroscopy*. Springer, New York, 2006.
31 T. W. G. Solomons and C. B. Fryhle, *Organic Chemistry*, 8th edn, John Wiley & Sons, Inc., USA, 2004.
32 D. Togashi, A. Ryder and D. O'Shaughnessy, Monitoring Local Unfolding of Bovine Serum Albumin During Denaturation Using Steady-State and Time-Resolved Fluorescence Spectroscopy, *J. Fluoresc.*, 2010, **20**(2), 441–452.
33 M. Lundqvist, I. Sethson and B. H. Jonsson, Protein Adsorption onto Silica Nanoparticles: Conformational Changes Depend on the Particles' Curvature and Protein Stability, *Langmuir*, 2004, **20**(24), 10639–10647.
34 P. Roach, D. Farrar and C. C. Perry, Surface Tailoring for Controlled Protein Adsorption: Effect of Topography at the Nanometer Scale and Chemistry, *J. Am. Chem. Soc.*, 2006, **128**(12), 3939–3945.
35 Ø. Halskau, R. Perez-Jimenez, B. Ibarra-Molero, J. Underhaug, V. Muñoz, A. Martinez and J. M. Sanchez-Ruiz, Large-scale Modulation of Thermodynamic Protein Folding Barriers Linked to Electrostatics, *Proc. Natl. Acad. Sci. U. S. A.*, 2008, **105**(25), 8625–8630.
36 J. M. Berg,L. T. John and L. Stryer,*Biochemistry*, 5th edn, W. H. Freeman and Company, New York, 2001.
37 S. Nabuurs, A. Westphal and C. van Mierlo, Noncooperative Formation of the Off-Pathway Molten Globule During Folding of the Alpha-Beta Parallel Protein Apoflavodoxin, *J. Am. Chem. Soc.*, 2009, **131**(7), 2739–2746.
38 M. F. M. Engel, A. Visser and C. P. M. van Mierlo, Conformation and Orientation of a Protein Folding Intermediate Trapped by Adsorption, *Proc. Natl. Acad. Sci. U. S. A.*, 2004, **101**(31), 11316–11321.
39 Ø. Halskau, N. Å. Frøystein, A. Muga and A. Martínez, The Membrane-bound Conformation of a-Lactalbumin Studied by NMR-monitored 1H Exchange, *J. Mol. Biol.*, 2002, **321**(1), 99–110.
40 J. Fantini and N. Yahi, Molecular Insights into Amyloid Regulation by Membrane Cholesterol and Sphingolipids: Common Mechanisms in Neurodegenerative Diseases, *Expert Rev. Mol. Med.*, 2010, **12**, e27.
41 P. Thomas and M. A. Fenech, Review of Genome Mutation andAlzheimer's disease, *Mutagenesis*, 2007, **22**(1), 15–33.

Paper IV

Generally applicable procedure for *in situ* formation of fluorescent protein-gold nanoconstructs

View Online / Journal Homepage / Table of Contents for this issue
Dynamic Article Links

RSC Advances

Cite this: *RSC Advances*, 2012, **2**, 11704–11711

www.rsc.org/advances

PAPER

Generally applicable procedure for *in situ* formation of fluorescent protein-gold nanoconstructs

Sondre Volden,[a] Sina M. Lystvet,[a] Øyvind Halskau[b] and Wilhelm R. Glomm*[a]

Received 13th August 2012, Accepted 28th September 2012
DOI: 10.1039/c2ra21931j

Small noble metal nanoclusters can be formed *in situ* by direct reduction and stabilization of a metal precursor by biomolecules such as proteins. Considering the diversity in amino acid composition of proteins, and hence their reductive ability, a general method for synthesis of gold nanoclusters using proteins is presented here. A range of proteins (bovine serum albumin, fibrinogen, α-lactalbumin, lysozyme, cytochrome *c*, myoglobin, β-lactoglobulin and α-chymotrypsin) have been studied, based on size, isoelectric point, flexibility and 3-dimensional structure. Results show protein-gold nanoconstructs with complex protein-specific photophysical properties. The effect on the 3-dimensional conformation of the proteins upon formation of gold nanoclusters and/or nanoparticles within the protein structure is also shown to be highly protein-dependent. A general mechanism for the formation of protein-gold nanoconstructs is proposed, based on charge density matching, yielding a high local concentration of the metal precursor on the protein structure which in turn can nucleate, grow and be stabilized by amino acid residues in the protein.

Introduction

Protein-stabilized fluorescent gold and silver nanoclusters (NCs) of subnanometer size have attracted a great deal of interest, owing to their potential use in a wide range of applications such as sensing,[1] biolabeling and imaging,[2–4] and even as enzyme mimics.[5] Unlike gold and silver nanoparticles, NCs are fluorescent, and do not exhibit localized surface plasmon resonance (LSPR) or the surface chemistry of the bulk metal. The NCs are typically of sizes comparable to the Fermi wavelength (~0.5 nm for Ag and Au) and display molecular-like, size-dependent fluorescence likely due to the transition between discrete molecule-like electronic states. Absorption and emission properties of the NCs can be described as a function of the number of atoms N as $E_{Fermi}/N^{1/3}$ according to the Jellium energy scaling law.[6]

Recently, Xie *et al.*[7] reported a one-pot, ''green'' synthetic route for the preparation of Au NCs using the intrinsic reduction potential of bovine serum albumin (BSA) at physiological temperature and basic conditions (pH > 10). The resulting Au NCs were found to consist mostly of 25 gold atoms (Au_{25}), with red emission (λ_{max} = 640 nm) and a quantum yield of ~6%. Since this seminal paper, other authors have reported AuNC formation using a similar biomineralization-inspired procedure using BSA[3,5,8] as well as other proteins such as transferrin, apoferritin,[4] and horseradish peroxidase.[1] Modifications to the original synthesis procedure typically involve the addition of a reducing agent such as ascorbic acid[2,3,8] in order to trigger nucleation of NCs at lower protein concentrations than initially reported. Procedures relying on the addition of an extrinsic reducing agent (hereafter referred to as ''extrinsic'' protocols) also offer the advantage of short reaction times and negligible competition from amino acid residue-induced reduction of the metal precursor, leading to a well-defined reduction and growth mechanism. Conversely, biomineralization-inspired synthetic procedures (hereafter referred to as ''intrinsic'' protocols) rely solely on the reduction potential of amino acid residues in the polypeptide chain under the reaction conditions (pH, temperature). Here, tyrosine[7] and histidine[4] have been proposed as the amino acids responsible for reduction of gold precursor in BSA and apoferritin, respectively.

As the amino acid composition varies greatly between proteins, the capacity to produce nanoclusters as well as the nature of the produced nanoclusters is expected to be protein-dependent. Here, we present a generally applicable synthetic procedure for *in situ* modification of proteins with gold nanoclusters, yielding protein-AuNCs and AuNPs with tuneable complex fluorescence. A small library of eight proteins of different molecular weights, charge properties and conformational flexibilities has been utilized, showing that nanocluster/nanoparticle formation, as well as the accompanying conformational changes and photophysical properties, are highly protein-dependent. As both the stability and function of the final protein-gold construct depend critically on the degree of change in protein conformation as well as the characteristics of the gold

[a]*Ugelstad Laboratory, Department of Chemical Engineering, Norwegian University of Science and Technology (NTNU), N-7491 Trondheim, Norway. E-mail: glomm@nt.ntnu.no; Tel: (+47) 735594158*
[b]*Department of Molecular Biology, University of Bergen, Thormøhlensgt 55 90, 5008 Bergen, Norway*

 This journal is © The Royal Society of Chemistry 2012

View Online

nanoclusters, the results obtained here can be used for the rational design of materials for a wide range of applications, including catalysis, bio-sensing and -labeling, as well as for imaging purposes. We also present a general mechanism for the *in situ* nanocluster formation, which could be beneficial for research in the aforementioned areas.

Materials and methods

Materials and solutions

Bovine serum albumin (BSA), bovine milk α-lactalbumin type I (BLA, >85%), (horse heart) myoglobin (Mb, >90%), (chicken egg white) lysozyme (Lyz), bovine pancreas α-chymotrypsin (CTR), bovine plasma fibrinogen (Fib) and bovine milk β-lactoglobulin (BLG) were purchased from Sigma. Bovine heart cytochrome *c* (Cyt, >95%) was purchased from BioChemika, and hydrogen tetrachloroaurate (TCAA) was purchased from Acros.

PBS-buffer was made by mixing two solutions; i) K_2HPO_4 (50 mM) and KCl (150 mM) and ii) KH_2PO_4 (50 mM) and KCl (150 mM), until pH was 7.4. Protein-nanoclusters were made by mixing protein (0.746 mM, 1 ml, 37 °C) with TCAA (10 mM, 1 ml, 37 °C). After stirring for 2 min NaOH (1 M, 100 μl, 37 °C) was added.[7] After one week at 37 °C, the nanocluster solutions were dialyzed against PBS (400 ml) for about 60 h, using a membrane with a molecular weight cut-off of 12.4 kDa. After measuring UV-vis, the solutions were diluted with PBS to 3.6 μM for UV-vis and fluorescence measurements. Stock solutions of native protein were made by dissolving protein in PBS to 25 μM. For UV-vis and steady-state measurements the protein stock solutions were diluted to 3.6 μM using PBS-buffer.

UV-Visible spectroscopy

UV-vis spectra were collected using a Shimadzu UV-2401PC spectrophotometer, over the wavelength range of 190–1100 nm. The path length of the quartz cuvettes used was 2 mm.

Fluorescence

The fluorescence measurements were performed on a Fluorolog-3 HORIBA Jobin Yvon apparatus. For the steady-state measurements, excitation was done at λ = 295 nm (slit width = 3 nm), λ = 370 nm (slit width = 5 nm) and λ = 495 nm (slit width = 10 nm) in order to probe the emission contributions from tryptophan (Trp), AuNCs (Au_8 and Au_{25}) and large AuNCs (Au_{25}), respectively. Time-correlated single photon counting (TCSPC) emission measurements to probe the local environment of Trp residues was done using excitation at λ = 280 nm as previously described.[9]

Circular dichroism (CD)

Measurements were conducted at room temperature on an Olis DSM 1000CD apparatus. The lamp power supply was a LPS-220B from Photon Technology International, the user interface was an Olis online instrument system, and the software was OLIS GlobalWorks. The 300 μL cuvette had a path-length of 1 mm, the grid was 2400 lines/mm, slit width was 6.32 mm, the scan range was from 290 nm to 200 nm, and the increment number was 720. Each sample was scanned three times. The concentration of BSA, BSA NC, CTR, and CTR NC was 5 μM, for Fib and Fib NC the concentration was 2.5 μM, and for BLA, BLA NC, Lyz, Lyz NC, Cyt *c*, Cyt *c* NC, Mb, Mb NC, BLG and BLG NC the concentration was 25.4 μM. The buffer was used as blank.

Results and discussion

In this study, a single-step procedure for the synthesis of protein-stabilized gold nanoclusters was investigated for a small library of eight proteins, chosen on the basis of the following. Bovine serum albumin (BSA) is much studied as an important constituent of blood. Albumin is a carrier protein responsible for transport of thyroid and fat-soluble hormones *via* the bloodstream,[10] and is also involved in other physiological functions such as control of serum osmotic pressure and pH buffering.[11] Fibrinogen (Fib) is part of the final step of the blood clotting cascade, wherein Fib is converted into fibrin by the protolytic enzyme thrombin.[12] Fib is made up of three globular units connected by two rod regions, each of which consists of triple-stranded α-helical coiled coils. Bovine α-lactalbumin (BLA) and lysozyme (Lyz) are homologous proteins with similar tertiary structures and primary sequence identities of approximately 35%.[13–15] Apart from biological function, BLA and Lyz differ with respect to their folding and calcium binding properties. Notably, BLA has the ability to form a stable molten globule and can strongly bind Ca^{2+},[16] whereas no such stable state or metal binding has been reported for (chicken egg white) Lyz. Cytochrome *c* (Cyt *c*) shuttles electrons between the two membrane-associated protein complexes cytochrome *c* reductase and cytochrome *c* oxidase inside the inner mitochondrial membrane and participates in mitochondrial production of ATP. Molten globule states of Cyt *c* have been reported under various conditions both at interfaces and in bulk.[17–22] Myoglobin (Mb) is a monomeric heme-binding protein involved in oxygen-carrying and can be found in muscle and blood cells. Mb is known to form a stable molten globule state in the absence of its heme group under moderately low pH conditions.[23] β-Lactoglobulin (BLG) is a globular milk protein which binds small ligands including palmitic and oleic acids.[24,25] Unlike the other major whey protein BLA, the exact biological function of BLG has yet to be elucidated. BLG forms an eight-stranded, antiparallel β-barrel with a three-turn α-helix on the outer surface and a ninth β-strand flanking the first strand.[24] The main ligand-binding site is located within the central cavity of the protein. The proteolytic enzyme α-chymotrypsin (CTR) participates in the breakdown of proteins in the digestive system of mammals and other organisms.[12] Specifically, CTR cleaves peptide bonds selectively on the carboxyl-terminal side of large hydrophobic amino acids such as tryptophan, tyrosine, phenylalanine and methionine.

A summary of the molecular properties of the proteins used in this study is shown in Table 1. By using the same synthesis procedure for the eight proteins studied here, we can probe the effects of protein size, overall protein charge (as determined by their isoelectric point; pI), conformational flexibility as well as the occurrence of specific amino acid residues on the ability to reduce and stabilize gold nanostructures – both subnanometer clusters and nanoparticles.

View Online

Table 1 Molecular properties of the proteins used in this study

Protein	Abbreviation	Molecular weight (kDa)	pI
Bovine serum albumin	BSA	67.0	4.7–4.9
Bovine plasma fibrinogen	Fib	340.0	N/A
Bovine milk holo α-lactalbumin (type I)	BLA	14.2	4.5
Chicken egg white lysozyme	Lyz	14.3	10.5
Bovine heart cytochrome *c*	Cyt *c*	12.4	10.1
Horse heart myoglobin	Mb	17.2	6.8–7.0
Bovine milk β-lactoglobulin	BLG	18.0	3.5–5.2
Bovine pancreas α-chymotrypsin	CTR	25.0	8.8

The results will be presented in the following order 1) photophysical properties of the gold nanoclusters, 2) effect of nanocluster/nanoparticle formation on protein conformation, and 3) a suggested mechanism for protein-directed intrinsic synthesis of gold nanoclusters.

Photophysical properties of gold nanoclusters are highly protein-dependent

Following incubation at 37 °C for one week with gold precursor (tetrachloroauric acid; TCAA), the solutions changed color from light yellow (TCAA) to yellow, brown or dark red, according to the nature of the gold structures present and depending on the protein in question. Upon excitation with UV light (λ_{ex} = 365 nm), most of the incubated solutions display an intense red photoluminescence, with the intensity and hue being protein-dependent, and varying from orange to purple (see Fig. 1), indicating formation of gold nanoclusters.[7] Two of the proteins – β-lactoglobulin (BLG) and cytochrome *c* (Cyt *c*) – emitted a much weaker blue or purple fluorescence, which could be due to aromatic amino acid side groups (tryptophan, tyrosine and phenylalanine), or low concentrations of gold nanoclusters in the final product (not shown).

UV-vis spectra of the protein-AuNCs as well as the respective native proteins are shown in Fig. 2. For all the systems studied here, the spectra of the protein-AuNCs differ significantly from the native proteins both with respect to lineshape and intensity. Incorporation of gold nanoclusters results in a broad absorption below ~400 nm which significantly distort or hide the 280 nm absorption band of the proteins. This can be attributed to scattering contributions upon formation of supramolecular gold nanoconstructs, with the resulting lineshape being highly protein-dependent. For Cyt *c* and Mb (Fig. 2, lower left panel), the absorption band at ~410 nm is also blue-shifted and weakened, indicating that *in situ* formation of gold nanostructures distorts the environment surrounding the heme groups.

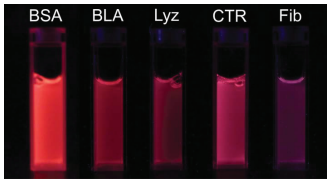

Fig. 1 Photograph of aqueous solutions for five of the proteins used here (concentration 35.5 mM) upon excitation at λ_{ex} = 365 nm.

Three of the proteins studied here – BLA, Cyt *c* and BLG – display strong absorbance in the 520–550 nm region upon incorporation of gold. This feature is consistent with localized surface plasmon resonance (LSPR), revealing that AuNPs of diameters larger than 3 nm are present upon incorporation of gold in BLA, Cyt *c* and BLG (see *e.g.* Glomm[26] and references therein). As the three proteins in question have similar or smaller dimensions to the AuNPs formed (for example, the dimensions of BLA are approximately 4 nm × 3 nm × 3 nm), and the samples remained stable in solution, the systems formed are likely to be AuNPs stabilized by multiple proteins. Thus, under otherwise identical experimental conditions, the protein used determines the resulting gold nanostructure, from nanoclusters embedded in single proteins to gold nanoparticles stabilized by multiple proteins.

From the observation that the protein-AuNCs formed display fluorescence upon excitation with UV light (see Fig. 1 for an illustration for BLA), there is no clear separation between proteins supporting AuNCs or AuNPs, respectively. Rather, the three protein-gold systems displaying LSPR likely contain AuNCs as well. In order to investigate this, we measured steady-state fluorescence upon excitation of the gold nanostructures at 370 nm and 495 nm (Fig. 3 and 4, respectively). Excitation wavelengths were chosen in order to distinguish between blue-emitting small (Au_8) and red-emitting larger (Au_{25}) AuNCs, respectively.[2,8]

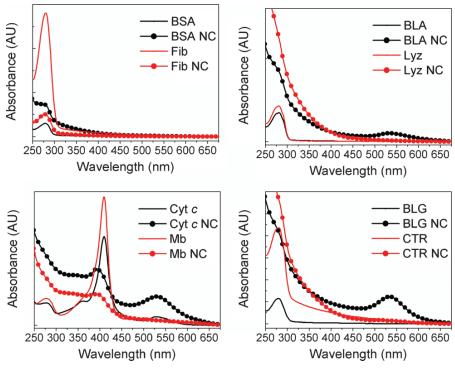

Fig. 2 UV-vis spectra of the proteins and protein-AuNCs used in this study. For all spectra, protein concentration was 3.6 mM.

 This journal is © The Royal Society of Chemistry 2012

View Online

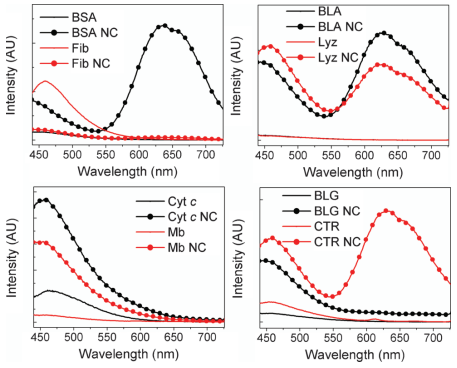

Fig. 3 Fluorescence spectra of proteins and protein-nanoclusters upon excitation at 370 nm. Protein concentration was 3.6 mM for all samples (in the top right panel, BLA and Lyz are completely overlapping).

Steady-state fluorescence spectra of the proteins and protein-AuNCs upon excitation at 370 nm are shown in Fig. 3. The excitation wavelength used for the spectra in Fig. 3 corresponds to what was used to obtain the photograph in Fig. 1. All emission profiles of the protein-AuNCs are markedly different from those of the native proteins, confirming that the reaction has occurred between the metal precursor and the proteins. As was found for the UV-vis results above, emission lineshape and intensity is highly protein-dependent despite otherwise identical reaction conditions. With the exception of Fib NC, all the protein-AuNCs display clearly defined emission maxima around 450 nm, where the emission intensity far exceeds that of the native protein. The emission at 450 nm has been reported to emanate from small nanoclusters reported to consist of ~8 atoms[2,8] – hereafter referred to as "small AuNCs". Four of the proteins studied – BSA, BLA, Lyz and CTR – also produce protein-AuNCs with a clearly defined second (bimodal) emission maximum between 625 and 675 nm, which has been reported to correspond to larger AuNCs reported to consist of ~25 atoms,[2,7,8] hereafter referred to as "large AuNCs". Additionally, the emission of BLG is significantly higher than baseline levels above 600 nm, possibly indicating the presence of large AuNCs. In order to rank the proteins according to their capacity for forming small or large AuNCs, the ratio between emission intensities at 650 nm and 450 nm (I_{650}/I_{450}) upon excitation at 370 nm for each protein-AuNC system, as well as the type of gold nanostructure formed, have been listed in Table 2. Here, the relative population of large AuNCs increases with increasing values of I_{650}/I_{450}. From Table 2 as well as from Fig. 3, it is evident that the proteins' capacity for forming large AuNCs can be listed in increasing order as (BLG) $\ll$ Lyz $<$ BLA $\leqslant$ CTR $\ll$ BSA. From the UV-vis results (Fig. 2) and the steady-state emission spectra upon excitation at 370 nm (Fig. 3), the three protein-AuNC systems found to contain AuNPs – BLA, Cyt *c* and BLG – also contain small, blue-emitting AuNCs. Among the eight proteins studied here, BLA NC and possibly BLG NC are the only protein-AuNC systems where small and large AuNCs are represented in addition to AuNPs. We have recently shown that the conformation of BLA can be tuned/unfolded more gradually than its homologue Lyz *via* incorporation of gold nanostructures using an extrinsic reducing agent. This observation is likely to be related to the greater conformational flexibility, which in turn is linked to its marginal folding barrier and stable molten globule. The behaviour may bear a semblance to the phenomenon of HAMLET, where multiple oleic acid molecules hold the anticancer HAMLET complex in a molten globule state, which can thereby interact effectively with cellular and artificial membranes and affect their morphology and integrity significantly.[27,28] The relevance with respect to NC modifications may be that these provide an alternative way of loosening the fold and providing an increased affinity and effect on the lipid membrane. Initial studies suggest that BLA NC is indeed cytotoxic.

In order to further characterize the large AuNCs, we measured the steady-state emission upon excitation at higher wavelengths, where the emission properties of the large AuNCs are expected to dominate the emission properties of the small AuNCs. Steady-state fluorescence spectra of the proteins and protein-AuNCs upon excitation at 495 nm are shown in Fig. 4. Comparing the emission profiles in Fig. 3 and 4, it is evident that a clearly

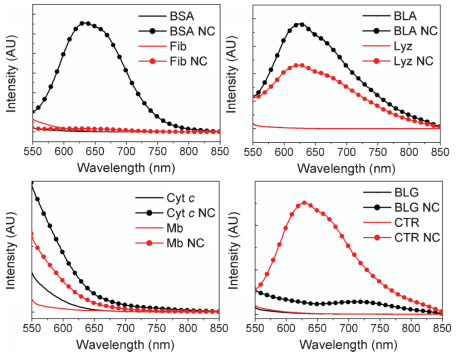

Fig. 4 Fluorescence spectra of proteins and protein-nanoclusters upon excitation at 495 nm. Protein concentration was kept constant at 3.6 μM (in the top right panel, BLA and Lyz are completely overlapping).

Table 2 Gold nanostructures formed for the different protein-AuNC systems studied here

Protein-AuNC	I_{650}/I_{450}	Gold nanostructure(s) formed[a]
BSA NC	3.00	Small AuNCs, Large AuNCs
Fib NC	0.24	N/A
BLA NC	1.24	Small AuNCs, Large AuNCs, AuNPs
Lyz NC	0.72	Small AuNCs, Large AuNCs
Cyt *c* NC	0.04	Small AuNCs, AuNPs
Mb NC	0.04	Small AuNCs
BLG NC	0.13	Small AuNCs, Large AuNCs, AuNPs
CTR NC	1.25	Small AuNCs, Large AuNCs

[a] Small AuNCs and large AuNCs denote Au_8 and Au_{25}, respectively. AuNPs denotes gold nanoparticles >3 nm displaying localized surface plasmon resonance (Fig. 2), stabilized by multiple proteins.

View Online

defined bimodal emission band around 650 nm exists for BSA NC, BLA NC, Lyz NC and CTR NC, with the relative intensities between the systems being identical to what was found for excitation at 370 nm (Fig. 3), confirming the presence of large AuNCs in these proteins. Additionally, excitation at 495 nm reveals a similar emission band for BLG NC, albeit at significantly lower intensities, indicating the presence of large AuNCs for this system as well. Thus, the proteins' capacity for forming large AuNCs can be listed in increasing order as BLG $\ll$ Lyz $<$ BLA $\leqslant$ CTR $\ll$ BSA.

Formation of gold nanoclusters induces highly protein-dependent conformational changes

Tryptophan (Trp) is an intrinsic fluorophore frequently used to monitor changes in the local protein environment such as unfolding.[29] Partial unfolding of a protein and a concomitant increase in solvent exposure is typically accompanied by a shift of the emission maximum towards longer wavelengths and/or a decrease in emission intensity. Whereas red-shifts of the emission profile can often be directly attributed to partial protein unfolding, interpreting changes in emission intensity can be more ambiguous. However, the UV-vis results for the protein-AuNCs studied here (Fig. 2) reveal that the gold NCs absorb around 350 nm, enabling quenching of Trp emission *via* distance-dependent energy transfer into the AuNCs. Consequently, the changes in Trp emission profile make it possible to follow conformational changes in a protein as well as the presence of gold nanoconstructs using steady-state Trp fluorescence (Fig. 5). The excitation wavelength λ_{ex} used was 295 nm.

The Trp emission profiles depicted in Fig. 5 reveal a decrease in Trp emission intensity compared to the native protein for all the protein-AuNC systems studied here, with the most severe relative intensity decrease being observed for BSA NC. Another common feature for all the protein-AuNC systems studied here is a red-shift, *i.e.* a shift towards longer wavelengths, of the Trp emission relative to the native protein, with the smallest red-shifts observed for the two largest proteins studied here, BSA and Fib (Fig. 5, upper left panel). For the two heme-containing proteins used here, Cyt *c* and Mb (Fig. 5, lower left panel) the red-shift is manifested by a large (>50 nm) red-shift of the secondary emission peak at 350 nm upon incorporation of AuNCs. While energy transfer into the AuNC band (as seen from the UV-vis spectra in Fig. 2) could contribute to the quenching of the Trp emission intensity, this mechanism cannot account for the observed red-shift of the emission maxima. Moreover, there is no clear correlation between the absorption intensity at $\sim$350 nm and the distortions in the corresponding Trp emission spectra for the different systems. Thus, we conclude that the quenched and red-shifted Trp emission indicates partial unfolding of the protein upon functionalization with AuNCs.

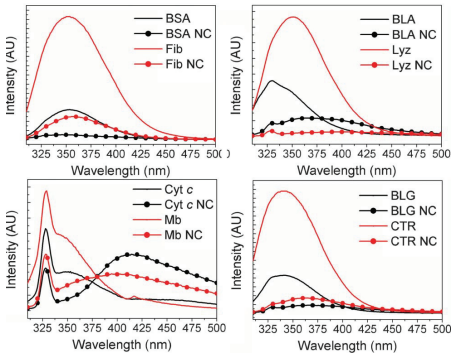

Fig. 5 Trp emission spectra of proteins and protein-nanoclusters upon excitation at 295 nm. Protein concentration was 3.6 μM for all samples.

In order to further probe the local Trp environment, fluorescence lifetime measurements (time-correlated single photon counting (TCSPC), Table 3) were performed for all proteins and protein-AuNC systems. While the excitation wavelength λ_{ex} = 280 nm excites all three intrinsic fluorophores in the proteins, Trp will still be the main contributor to the emission lifetime profile due to a significantly higher quantum yield as compared to tyrosine and phenylalanine.[29] No distinct lifetimes attributable to the AuNCs could be detected upon excitation at 280 nm for any of the systems studied here.

As the proteins used here contain different amounts of Trp residues, interpretation of the TCPSC results with respect to comparison of proteins is intricate. A bimodal fitting was found to provide the best overall fit for the fluorescence decay profiles of the samples studied here, yielding one "short" (t_1) and one "long" (t_2) lifetime, with corresponding relative populations B_1 and B_2, respectively. The lifetimes and populations listed in Table 3 show that the Trp fluorescence profiles, *i.e.* both lifetimes and populations, were altered upon incorporation of AuNCs for all the systems studied here, indicating changes in the Trp environment following formation of gold nanoconstructs. No single trend with respect to shifts in either lifetimes or populations could be detected for the entire dataset, revealing that the impact of AuNC formation on the chemical environment surrounding Trp residues is very protein-dependent. Additionally, differences in the number of Trp residues as well as their position and orientation relative to the NC modifications for the proteins studied here likely play a significant role. Formation of gold nanostructures within the proteins results in reduction of the short lifetime (t_1) as compared to the native protein for five of the systems studied here (BSA NC, Fib NC, Lyz NC, Cyt *c* NC, CTR NC). Three of these systems (BSA NC, Fib NC and Cyt *c* NC) also reveal population shifts towards shorter lifetimes, indicating either quenching from increased Trp exposure to water, energy transfer to gold (either NCs or NPs), or a combination of these effects. The largest observable changes in the Trp fluorescence lifetime profile upon formation of gold nanoconstructs was observed for the two milk proteins included in the dataset; BLA and BLG. Interestingly, BLA and BLG also display the same changes in Trp fluorescence lifetimes (Table 3); little or no changes in t_1, a significant reduction of t_2, and a large shift in population towards the longest lifetime for both proteins. Specifically, whereas the population is heavily shifted towards the short lifetime for both native proteins (94% and 85% for BLA and BLG, respectively), the AuNC-modified protein systems reveal an approximately even distribution of the two populations (B_1 for BLA NC and BLG NC are 50% and 55%, respectively).

 This journal is © The Royal Society of Chemistry 2012

View Online

Table 3 Fluorescence lifetimes and the corresponding populations for the proteins and protein-AuNCs used in this study. t = lifetimes in nanoseconds (ns), B = populations in %. λ_{ex} = 280 nm, λ_{em} = 360 nm. The ratio of mean residual ellipticities MRE_{200}/MRE_{222} for the same systems are listed in the rightmost column

Protein	System	t_1 (ns)	B_1 (%)	t_2 (ns)	B_2 (%)	MRE_{200}/MRE_{222}
BSA	Native	5.0 ± 0.2	46.5 ± 0.1	7.5 ± 0.1	53.5 ± 0.1	1.6
	NC	1.35 ± 0.02	48.7 ± 0.1	5.19 ± 0.03	51.3 ± 0.1	3.2
Fib	Native	2.30 ± 0.04	41.8 ± 0.1	7.99 ± 0.03	58.2 ± 0.1	1.8
	NC	1.63 ± 0.04	45.6 ± 0.1	5.01 ± 0.03	54.4 ± 0.1	5.3
BLA	Native	0.9 ± 0.1	93.8 ± 0.1	4.5 ± 0.1	6.2 ± 0.1	3.7
	NC	0.90 ± 0.02	49.7 ± 0.1	4.27 ± 0.03	50.3 ± 0.1	10.8
Lyz	Native	1.52 ± 0.03	69.5 ± 0.1	3.67 ± 0.04	30.1 ± 0.1	1.4
	NC	0.6 ± 0.1	70.0 ± 0.1	4.1 ± 0.8	30.0 ± 0.1	13.5
Cyt *c*	Native	2.15 ± 0.04	60.8 ± 0.1	7.8 ± 0.1	39.2 ± 0.1	3.4
	NC	0.6 ± 0.1	68.8 ± 0.1	5.8 ± 0.1	31.2 ± 0.1	13.3
Mb	Native	0.3 ± 0.2	55.2 ± 0.1	4.6 ± 0.1	44.8 ± 0.1	2.0
	NC	0.7 ± 0.1	62.1 ± 0.1	4.2 ± 0.1	37.9 ± 0.1	6.1
BLG	Native	1.25 ± 0.01	85.4 ± 0.1	5.1 ± 0.1	14.6 ± 0.1	0.2
	NC	1.30 ± 0.03	55.4 ± 0.1	4.24 ± 0.03	44.6 ± 0.1	8.3
CTR	Native	1.09 ± 0.02	53.2 ± 0.1	3.94 ± 0.03	46.8 ± 0.1	8.8
	NC	0.85 ± 0.02	47.6 ± 0.1	3.87 ± 0.03	52.4 ± 0.1	−31.0[a]

[a] No discernible secondary structure could be detected using CD upon modification with AuNCs.

As such, the fluorescence results illustrate that the effect of AuNC formation on the microenvironment surrounding the Trp residues – such as the degree of unfolding and NC modifications in close proximity– is highly protein-dependent.

For a more thorough investigation of the effect of AuNC formation on protein secondary structure, circular dichroism measurements were performed (Fig. 6). Here, changes in intensity and lineshape compared to the native protein indicate conformational changes. To rule out the possibility of changes due to attenuation of the signal by gold, the relationship between signal intensity at 200 nm and 222 nm was studied for all samples (Table 3). The 200 nm/222 nm ratio varies in a manner not directly correlated to the concentration of gold precursor or the corresponding absorbance at these wavelengths (Fig. 2). Thus, the spectral changes are likely due to changes in the protein, not attenuation of the signal caused by the presence of gold.

From the CD results presented in Fig. 6, all the AuNC-containing systems display large differences as compared to the native proteins with respect to intensity and lineshape, indicating conformational changes upon incorporation of the gold

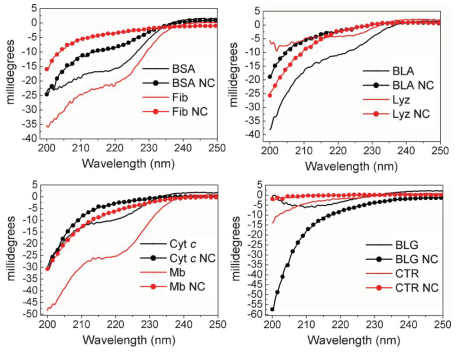

Fig. 6 CD traces of the protein and protein-AuNCs studied here.

nanoconstructs. With the exception of BLG, incorporation of AuNCs resulted in a relative decrease of alpha-helical motifs (*i.e.* mean residual ellipticity at 222 nm) compared to the native protein for the systems studied here. For two of the proteins – Lyz and BLG – incorporation of AuNCs resulted in a significant transition from alpha-helical motifs to other secondary structures (mostly random coils as seen from the increased signal at ~200 nm), compared to the native protein. The values of the ratios between signal intensity at 200 nm and 222 nm (MRE_{200}/MRE_{222}, Table 3) were found to increase by more than a factor of two upon incorporation of AuNCs for all the systems studied here, further indicating that the changes in lineshapes and signal intensities, documented by the fluorescence intensities, are due to changes in protein conformation rather than attenuation of the signal from the presence of gold. No apparent trend with respect to the nature of the gold nanoconstructs formed (*i.e.* small or large AuNCs or AuNPs) could be identified from either Trp emission or CD data, revealing that the effect of incorporation of gold on the degree of conformational change is mainly protein-dependent. As the stability and indeed function of the protein-gold nanoconstruct for any intended application is highly dependent on the structural changes of the protein shell, the results presented here show that care must be taken to understand the nanocluster formation on a protein-specific basis. In order to be able to predict the final properties – both with respect to nanocluster population and protein conformation – for a given protein, there is a need for a general mechanism.

Protein-mediated gold nanocluster formation can be attributed to a general mechanism

Earlier biomineralization-inspired studies have pointed to single amino acid residues being responsible for reduction and nucleation of Au^{3+}, tyrosine (Tyr) in the case of BSA,[7] and histidine (His) in the case of apoferritin.[4] While Tyr is known to have a high, albeit strongly pH-dependent redox potential[7,30] and mixtures of His and $HAuCl_4$ have been shown to reduce Au^{3+} to Au^0 *via* X-ray absorption near-edge structure (XANES),[4] these are either single-protein (in the case of BSA)

View Online

or single amino acid (in the case of His) studies. Additionally, the importance of cysteine (Cys) residues in immobilizing/stabilizing the resulting gold nanoconstructs within the protein *via* covalent Au–S bonds has been reported (see *e.g.* Xie[7] and references therein). Here, we have compared eight different proteins varying in molecular weights, isoelectric points and conformational flexibilities with respect to their capability of forming AuNCs utilizing a single intrinsic, *i.e.* biomineralization-inspired, synthesis procedure. From the findings presented above, the type of gold nanoconstructs formed, the photophysical properties of the AuNCs and the resulting effect on polypeptide conformation are highly protein-dependent. No correlation could be found between the number/percentage of Tyr and His residues and the propensity for AuNC formation, or for the type of gold nanoconstruct (*i.e.* small and large AuNCs, AuNPs) formed. The small library employed here includes a protein without any Cys residues (Mb), which is capable of formation and stabilization of formation of small AuNCs, showing that Cys residues are not necessary for stabilization of the gold nanoconstructs.

Based on the strong protein-dependence, as opposed to single amino acid residue-dependence, of AuNC formation observed here, we propose that the general protein-templated gold nanoconstruct nucleation and growth can be explained *via* a general mechanism. Our proposed mechanism is adapted from Berti and Burley's postulated mechanism for nucleic acid and nucleotide-mediated synthesis of inorganic nanoparticles,[31] and Feldheim and Eaton's SELEX model for biomolecule-mediated crystal formation,[32] and consists of the following four steps:

Step 1: Nucleation. Charge density matching between Au^{3+} and negatively charged amino acid residues yields high local metal concentrations, providing the necessary microenvironment for triggering the nucleation event. Nucleation occurs *via* reduction of the gold precursor from surrounding amino acid residues with a sufficiently high redox potential, including Tyr, Trp and His. The combination of initial charge density matching and the local presence of amino acid residues with a sufficient redox potential implies that the nucleation event is highly protein-dependent. As this step requires interaction between a water-soluble metal precursor and polar amino acid residues, initiation likely occurs close to the external protein surface.

Step 2: Growth. Small nuclei formed close to the protein surface are capped by anionic amino acid residues, and grow either (i) from influx of Au^{3+} ions as determined by charge density matching with negatively charged amino acid residues in the immediate vicinity, eventually leading to overlapping clusters, (ii) from partial unfolding of the polypeptide chain leading to close contact between adjacent nuclei and subsequent aggregation, (iii) collisions between proteins leading to contact between exposed nuclei, or (iv) a combination of (i)–(iii). Here, the growth is limited by the available amount of metal precursor relative to the protein concentration for all the growth mechanisms. Additionally, limitations in steps (i)–(iii) are highly protein-dependent. Specifically, mechanisms (i)–(iii) are dependent on the size and proximity of large patches of charged amino acid residues for sequestration of Au^{3+}, mechanism (ii) depends on the conformational flexibility of the polypeptide chain, and mechanism (iii) depends on the charge density surrounding the nucleation sites and the proximity of the nuclei to the surrounding aqueous environment.

Step 3: Termination. Termination can occur *via* depletion of metal precursor from the bulk phase, but more importantly *via* capping from anionic amino acid residues in the case of mechanisms (i) and (ii), whereby the surrounding polypeptide chain acts as a stabilizing electrostatic shell, or *via* a combination of electrostatic and steric (*i.e.* electrosteric) capping in the case of mechanism (iii), where single nanoparticles are stabilized by multiple proteins. Upon reaching a critical size, the electrosteric barrier for bringing clusters into close proximity becomes too large to overcome, thus preventing further growth.

Step 4: Passivation and solubilization. The capping ligands – either amino acid residues or proteins depending on the size and nature of the gold nanoconstructs – suppress defect surface states by forming covalent bonds (such as in the case of Cys), or simply forming complexes with empty orbitals and dangling bonds. Integration into single proteins or capping by multiple proteins provides the presence of a hydrophilic corona and enables dispersion in aqueous solution. Limitations to the stability in an aqueous environment are then linked to the degree of protein unfolding following nanoconstruct formation, as unfolding is accompanied by exposure of hydrophobic amino acid residues, leading to an increased sticking probability and concomitant propensity for protein aggregate formation.

The general mechanism suggested here accounts for the highly protein-dependent AuNC formation in that local negative charge, availability of electron-donors and the local stability of the secondary structure and overall flexibility of the fold determines where clusters form and when formation is terminated, as well as their effect on the protein. The mechanism is also in agreement with existing literature for comparable systems.[31,32]

Conclusion

In this work a small library of eight proteins of different molecular weights, charge properties and conformational flexibilities has been studied with respect to their ability to form gold nanoconstructs using a single intrinsic, *i.e.* biomineralization-inspired, synthetic procedure wherein no extrinsic reducing agent was added. The type of gold nanostructure formed, the photophysical properties of the protein-gold constructs as well as the accompanying conformational changes were found to be highly protein-dependent. Using a combination of UV-vis spectroscopy and steady-state fluorescence measurements, we identified the three primary sets of gold nanoconstructs formed as fluorescent clusters of $\sim$8 and $\sim$25 atoms (small and large AuNCs, respectively) and nanoparticles (AuNPs) of diameters $>$3 nm displaying localized surface plasmon resonance (LSPR), with all three structures occurring within the same system for the two milk proteins studied here, BLA and BLG (see Table 2). We also present a general mechanism for the *in situ* nanocluster formation, based on nucleation, growth, termination and stabilization/solubilization events. As such, this work represents a contribution to the general understanding of how the protein shell as well as the size and properties of nanoclusters can be tuned to manipulate conformation and stability of the resulting

 This journal is © The Royal Society of Chemistry 2012

View Online

nanomaterial, and how labelling with plasmonic and fluorescent nano-species can enable easier biolabeling and tracking in biological systems.

Acknowledgements

The authors acknowledge the Department of Chemical Engineering, NTNU, for financial support. Wilhelm R. Glomm and Sondre Volden acknowledge financial support from the Research Council of Norway (NFR) within the FRINAT program, project number 177556/V30.

References

1 F. Wen, Y. H. Dong, L. Feng, S. Wang, S. C. Zhang and X. R. Zhang, *Anal. Chem.*, 2011, **83**, 1193.
2 X. Le Guevel, N. Daum and M. Schneider, *Nanotechnology*, 2011, **22**, 7.
3 A. Retnakumari, J. Jayasimhan, P. Chandran, D. Menon, S. Nair, U. Mony and M. Koyakutty, *Nanotechnology*, 2011, **22**, 11.
4 C. J. Sun, H. Yang, Y. Yuan, X. Tian, L. M. Wang, Y. Guo, L. Xu, J. L. Lei, N. Gao, G. J. Anderson, X. J. Liang, C. Y. Chen, Y. L. Zhao and G. J. Nie, *J. Am. Chem. Soc.*, 2011, **133**, 8617.
5 X. X. Wang, Q. Wu, Z. Shan and Q. M. Huang, *Biosens. Bioelectron.*, 2011, **26**, 3614.
6 J. Zheng, C. W. Zhang and R. M. Dickson, *Phys. Rev. Lett.*, 2004, **93**, 4.
7 J. P. Xie, Y. G. Zheng and J. Y. Ying, *J. Am. Chem. Soc.*, 2009, **131**, 888.
8 X. Le Guevel, B. Hotzer, G. Jung, K. Hollemeyer, V. Trouillet and M. Schneider, *J. Phys. Chem. C*, 2011, **115**, 10955.
9 S. M. Lystvet, S. Volden, M. Yasuda, O. Halskau and W. R. Glomm, *Nanoscale*, 2011, **3**, 1788.
10 H. Lodish, A. Berk, P. Matsudaira, C. A. Kaiser, M. Krieger, M. P. Scott, S. L. Zipursky and J. Darnell, *Molecular Cell Biology*, 5th ed., W. H. Freeman and Company, New York, 2003.
11 V. N. Uversky, N. V. Narizhneva, T. V. Ivanova and A. Y. Tomashevski, *Biochemistry*, 1997, **36**, 13638.
12 J. M. Berg, J. L. Tymoczko and L. Stryer, *Biochemistry*, 5 ed., W. H. Freeman and Company, New York, 2002.
13 A. V. Agasoster, O. Halskau, E. Fuglebakk, N. A. Froystein, A. Muga, H. Holmsen and A. Martinez, *J. Biol. Chem.*, 2003, **278**, 21790.
14 A. C. W. Pike, K. Brew and K. R. Acharya, *Structure*, 1996, **4**, 691.
15 S. Sugai, M. Ikeguchi, in *Advances in Biophysics, Vol 30, 1994*, Japan Scientific Soc Press, Tokyo, 1994, vol. **30**, p 37.
16 E. A. Permyakov and L. J. Berliner, *FEBS Lett.*, 2000, **473**, 269.
17 P. Hildebrandt and M. Stockburger, *Biochemistry*, 1989, **28**, 6710.
18 V. E. Bychkova, A. E. Dujsekina, S. I. Klenin, E. I. Tiktopulo, V. N. Uversky and O. B. Ptitsyn, *Biochemistry*, 1996, **35**, 6058.
19 A. A. Moosavi-Movahedi, J. Chamani, Y. Goto and G. H. Hakimelahi, *J. Biochem.*, 2003, **133**, 93.
20 A. Muga, H. H. Mantsch and W. K. Surewicz, *Biochemistry*, 1991, **30**, 7219.
21 P. J. R. Spooner and A. Watts, *Biochemistry*, 1990, **30**, 3880.
22 P. J. R. Spooner and A. Watts, *Biochemistry*, 1990, **30**, 3871.
23 Y. V. Griko and P. L. Privalov, *J. Mol. Biol.*, 1994, **235**, 1318.
24 G. Kontopidis, G. Holt and L. Sawyer, *J. Dairy Sci.*, 2004, **87**, 785.
25 S. E. Permyakov, E. L. Knyazeva, L. M. Khasanova, R. S. Fadeev, A. P. Zhadan, H. Roche-Hakansson, A. P. Hakansson, V. S. Akatov and E. A. Permyakov, *Biol. Chem.*, 2012, **393**, 85.
26 W. R. Glomm, *J. Dispersion Sci. Technol.*, 2005, **26**, 389.
27 A. K. Mossberg, M. Puchades, O. Halskau, A. Baumann, I. Lanekoff, Y. X. Chao, A. Martinez, C. Svanborg and R. Karlsson, *PLoS One*, 2010, **5**, 10.
28 A. Baumann, A. U. Gjerde, M. Ying, C. Svanborg, H. Holmsen, W. R. Glomm, A. Martinez and O. Halskau, *J. Mol. Biol.*, 2012, **418**, 90.
29 J. R. Lakowicz, *Principles of Fluorescence Spectroscopy*, Springer, New York, 2006.
30 A. Harriman, *J. Phys. Chem.*, 1987, **91**, 6102.
31 L. Berti and G. A. Burley, *Nat. Nanotechnol.*, 2008, **3**, 81.
32 D. L. Feldheim and B. E. Eaton, *ACS Nano*, 2007, **1**, 154.

Paper V

Anticancer activity from gold-alpha-lactalbumin nanoconstructs?

Is not included due to copyright